NANYANG TECHNOLOGICAL UNIVERSITY
SINGAPORE

DESYMMETRISATION OF 1,3-DIOLS AND THEIR DIACETATES UNDER ENZYMATIC HETEROGENEOUS CATALYSIS AND SYNTHESIS OF 1,3-DIOLS UNDER CONTINUOUS FLOW CONDITIONS

VARSHA SIRI PAMARTHY

SCHOOL OF CHEMICAL AND BIOMEDICAL ENGINEERING

2019

HETEROGENEOUS CATALYSIS VARSHA SIRI PAMARTHY 2019

DESYMMETRISATION OF 1,3-DIOLS AND THEIR DIACETATES UNDER ENZYMATIC HETEROGENEOUS CATALYSIS AND SYNTHESIS OF 1,3-DIOLS UNDER CONTINUOUS FLOW CONDITIONS

VARSHA SIRI PAMARTHY

VARSHA SIRI PAMARTHY

SCHOOL OF CHEMICAL AND BIOMEDICAL ENGINEERING

A thesis submitted to the Nanyang Technological University in

partial fulfilment of the requirement for the degree of

Doctor of Philosophy

2019

DESYMMETRISATION OF 1,3-DIOLS AND THEIR DIACETATES UNDER ENZYMATIC HETEROGENEOUS CATALYSIS AND SYNTHESIS OF 1,3-DIOLS UNDER CONTINUOUS FLOW CONDITIONS

VARSHA SIRI PAMARTHY

VARSHA SIRI PAMARTHY

SCHOOL OF CHEMICAL AND BIOMEDICAL ENGINEERING

A thesis submitted to the Nanyang Technological University in

partial fulfilment of the requirement for the degree of

Doctor of Philosophy

2019

Statement of Originality

I hereby certify that the work embodied in this thesis is the result of original research, is free of plagiarised materials, and has not been submitted for a higher degree to any other University or Institution.

05-06-2019 ……

Date

…… Varsha Siri Pamarthy

Supervisor Declaration Statement

I have reviewed the content and presentation style of this thesis and declare it is free of plagiarism and of sufficient grammatical clarity to be examined. To the best of my knowledge, the research and writing are those of the candidate except as acknowledged in the Author Attribution Statement. I confirm that the investigations were conducted in accord with the ethics policies and integrity standards of Nanyang Technological University and that the research data are presented honestly and without prejudice.

05-06-2019

. . . . . .

Date

. . . . . .

Assoc. Prof. Zaher Judeh

Authorship Attribution Statement

This thesis **does not** contain any materials from papers published in peer-reviewed journals or from papers accepted at conferences in which I am listed as an author.

05-06-2019
…….
Date


……
Varsha Siri Pamarthy

Acknowledgements

I would like to express my heartfelt gratitude to the following people who have supported me so far:

Associate Professor Zaher Judeh, my supervisor, for his patience, encouragement and understanding.

Associate Professor Zhiping Lai for permitting me to work at KAUST and kindly allowing me to use the facilities in his lab.

Associate Professor Kuo-Wei Huang Andy, KAUST, for advising me on several organic chemistry reactions.

Associate Professor Saif Khan, NUS, for allowing me to visit his lab and introducing me to the practical aspects of flow reactors.

Associate Professor Lee Jong-Min and Associate Professor Roderick Wayland Bates, members of my Thesis Advisory Committee, for their valuable suggestions and guidance.

Dr. Khong Duc Thinh who has helped me since the first day I began working in the lab and has helped proofread my thesis despite his busy schedule.

Dr. Swapan Kumar Das, former post-doctoral researcher in Prof. Lai's lab, for teaching me procedures for synthesis of CTPP-1 and helping me characterise several other samples using SEM and BET.

Mr. Dogancan Karan and Dr. Yap Swee Kun from Prof. Saif's group for teaching me the basic set-up of a flow reactor.

Mdm. Gan Chew Mei, Jessica, Dr. Ong Teng Teng, Rachel, Mr. Teo Chea Boon and Dr. Wang Xiujuan from SCBE for their technical help. I would also like to

thank Dr. Tay Yee Yan from FACTS, NTU for his help in performing TEM imaging for the magnetic nanoparticles I synthesised.

Dr. Sudipta Chatterjee, Kathy Wong, Ong Li Lin, Dr. Tatina Madhu Babu, Dr. Mallikharjuna Rao Lambu, Shuddhodana and Dr. Surabhi Devaraj for their support and help in lab.

Members of Prof. Lai's group and Prof. Huang's group for all their help.

School of Chemical and Biomedical Engineering, NTU and Nanyang Technological University for the generous research scholarship and facilities.

My friends for their encouragement and support.

Most importantly, my family, especially my parents and my sister, for believing in me and offering their unconditional love and support.

Table of Contents

Abstract

Piperidones are present in many biologically important compounds. One of the key steps in the synthesis of one such piperidone, *N*-benzyl-5-methoxypiperidone, is the desymmetrisation of 1,3-diol, *N*-Benzyl-5-hydroxy-4-(hydroxymethyl)pentanamide or 1,3-diacetate, *N*-Benzyl-5-acetoxy-4-(acetoxymethyl)pentanamide, which provide access to the (*R*)- and (*S*)-enantiomers of the piperidone, respectively. The main aim of this thesis is to develop a flow process to perform synthesis and desymmetrisation of the 1,3-diol.

Lipase AK from *Pseudomonas fluorescens* was immobilised by cross-linking using glutaraldehyde on (3-aminopropyl)triethoxysilane functionalised Fe_3O_4 magnetic nanoparticles and silica nanospheres (KCC-1), and by physical adsorption on covalent triazine-piperazine linked polymer (CTPP-1). Desymmetrisation of 1,3-diol in batch conditions using free lipase AK provided the (*R*)-monoacetate in up to 93% yield and 92% *ee* while catalysis of the same reaction by immobilised lipase AK provided the monoacetate in up to 98% yield and 93% *ee* in 9 h respectively. Under batch conditions, hydrolysis of 1,3-diacetate offered the (*S*)-monoacetate in up to 54% yield and 93% *ee*, and 57% yield and 93% *ee*, in 24 h each, when free lipase AK and immobilised lipase AK were used as the catalysts correspondingly. Amongst the investigated immobilised lipase AK, lipase AK immobilised on Fe_3O_4 magnetic nanoparticles were found to be the most suitable catalysts for the desymmetrisation reactions as they not only provided the monoacetates in relatively high yields but were also easily separable and maintained their activity up to five reaction cycles.

Since flow reactors are not only energy efficient but also offer improved mixing control and high interfacial area for biphasic reactions, a semi-continuous synthesis of 1,3-diol was developed. Desymmetrisation of 1,3-diol in flow provided the (*R*)-monoacetate in up to 73% yield and 93% *ee*. The flow reactor for the hydrolysis of 1,3-diacetate gave the (*S*)-monoacetate product in up to 81% yield and 95% *ee*, a marked improvement from 57% yield and 93% *ee* obtained using a batch process.

List of abbreviations

^{1}H NMR	Proton nuclear magnetic resonance
^{13}C NMR	Carbon-13 nuclear magnetic resonance
Å	Angstrom
Ac	Acetyl
APTES	(3-Aminopropyl)triethoxysilane
BET	Brunauer, Emmett and Teller surface area analysis
BJH	Barrett-Joyner-Halenda analysis
Bn	Benzyl
br	Broad (NMR spectroscopy)
°C	Degree Celsius
cm^{-1}	Wavenumber
CTPP-1	Covalent triazine-piperazine linked polymer
CTPP1-iAK	Amano lipase AK immobilised on CTPP-1
δ	Chemical shift in parts per million downfield from tetramethylsilane
d	Doublet (NMR spectroscopy)
DBU	1,8-Diazabicyclo[5.4.0]undec-7-ene
DCM	Dichloromethane
dd	Doublet of doublet (NMR spectroscopy)
DMAP	*N*,*N*-Dimethylaminopyridine
DMF	*N*,*N*-Dimethylformamide
EA	Ethyl acetate

EDC	1-Ethyl-3-(3-dimethylaminopropyl)carbodiimide
ee	Enantiomeric excess
eq	Equivalent
ESI-MS	Electrospray Ionisation Mass Spectroscopy
Et	Ethyl
Et_3N	Triethylamine
FT-IR	Fourier Transform infrared spectroscopy
g	Gram
h	Hour
Hex	Hexane
HPLC	High Performance liquid chromatography
Hz	Hertz
IPA	Isopropyl alcohol
J	Coupling constant (in NMR spectroscopy)
KCC-1	KAUST Catalysis Centre-1 silica nanoparticles
KCC1-iAK	Amano lipase AK immobilised through covalent binding using glutaraldehyde on APTES coated KCC-1 nanoparticles
m	Multiplet (NMR spectroscopy)
m/*z*	Mass/charge
min	Minute
mmol	Millimole
MNP	Fe_3O_4 magnetic nanoparticles functionalised with APTES

MNP-iAK	Amano lipase AK immobilised through covalent binding using glutaraldehyde on APTES coated MNP
MTBE	*tert*-Butyl methyl ether
PFL	*Pseudomonas fluorescens* lipase
PMP	Polymethylpentene
pNPP	p-Nitrophenyl Phosphate
ppm	Parts per million
rt	Room temperature
SEM	Scanning electron microscopy
STP	Standard temperature and pressure
t	Triplet (NMR spectroscopy)
t-Bu	*tert*-Butyl
TEM	Transmission electron microscopy
TFA	Trifluoroacetic acid
THF	Tetrahydrofuran
TLC	Thin layer chromatography
UV-vis	Ultraviolet-visible
XRD	X-ray powder diffraction

Chapter I Introduction

1. Chirality

In chemistry, chirality is a property of asymmetry found in molecules that have non-superimposable mirror images. It is most often caused by the presence of a carbon atom, which is attached to four different molecules. Such a carbon atom is also called an asymmetric carbon atom or stereogenic centre. An example of a chiral compound is the amino acid Alanine, which exists in two forms, (*S*)-alanine and (*R*)-alanine (Figure 1).

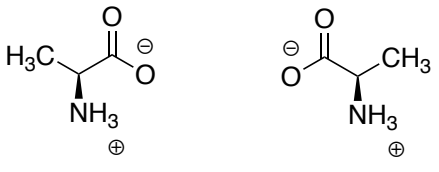

(*S*)-alanine **1** (*R*)-alanine **2**

Figure 1: Example of enantiomers – (*S*)-alanine and (*R*)-alanine

(*S*)-alanine **1** and (*R*)-alanine **2** are enantiomers since they are non-superimposable mirror images of each other. Enantiomers possess identical physical and chemical properties in an achiral (non-chiral) environment but differ in certain chemical and physical properties in a chiral environment, such as living system. When both the enantiomers of a compound are present in 50:50 ratio, such a mixture of enantiomers is called a racemic mixture or racemate. It is often observed that while one of the enantiomers possesses favourable properties, the other enantiomer might have none, or have undesirable side effects. This is particularly dangerous in the food and pharmaceutical industries. An example is thalidomide, which was administered to pregnant women in Europe to treat

morning sickness, due to its sedative and anti-nausea properties. It was initially synthesised as a racemate but was subsequently found to be highly neurotoxic and teratogenic. Studies later proved that the toxic side effects of thalidomide were found only in one of its enantiomers, (*S*)-thalidomide.[1]

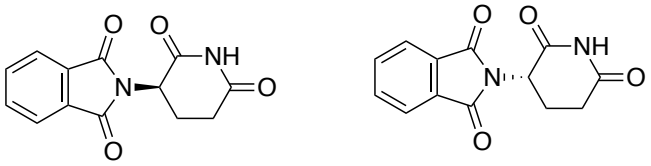

(*R*)-thalidomide
3

(*S*)-thalidomide
4

Figure 2: Enantiomers of thalidomide – examples of chiral molecules[1]

This illustrates the importance of synthesis of enantiopure compounds, especially in the pharmaceutical industry. As such, except one, all the chiral drugs approved by the FDA in the year 2015 were enantiopure compounds.[2]

Enantiopure, or single enantiomer compounds can be synthesised by three major methods – chiral pool, kinetic resolution and asymmetric synthesis.

1.1 Strategies to synthesise enantiopure compounds

Chiral pool is a group of naturally occurring chiral molecules such as amino acids, alkaloids, carbohydrates, vitamins, etc. that can be used as catalysts, modifiers or ligands in organic syntheses.[3] Nature has provided several of these compounds in abundance. Chiral pool synthesis refers to the synthesis of an enantiopure compound from an existing enantiopure starting material obtained from the chiral pool. During the course of the synthesis reactions, the chirality, which is obtained from the enantiopure starting material, is preserved. Enantiopure compounds can therefore be obtained from this chiral pool, especially if their synthesis in laboratory is complex and expensive. However,

for those compounds which are not available in abundance, other methods such as chiral resolution and asymmetric synthesis are necessary.[4]

Chiral resolution is the separation of a racemic mixture into its enantiomers through specific techniques such as chiral column chromatography[5] and kinetic resolution.[6] In the absence of a chiral environment, enantiomers possess similar physicochemical properties , thus rendering orthodox separation strategies such as flash chromatography and recrystallisation useless. In a chiral environment, the distinct physical properties of the enantiomers can be exploited using methods mentioned earlier such as kinetic resolution, chiral column chromatography and diastereoselective recrystallisation, to separate them. The major disadvantage of this method, however, is that the maximum yield of the desired enantiopure compound that can be obtained is just 50%.[7]

Asymmetric synthesis refers to the synthesis of an enantiopure product starting with one or more prochiral materials. Enantioselective induction in asymmetric synthesis can be achieved *via* use of (i) chiral reagent (ii) chiral auxiliary or (iii) chiral catalyst.

In the first strategy, asymmetric synthesis using chiral reagent refers to a method where a stoichiometric amount of chiral, non-racemic reagent is consumed to induce the enantioselectivity on the chiral product. Though this is a convenient approach since neither the substrate nor the product need chemical manipulation, the available reagents suffer from lack of generality and low level of stereoselectivity.

In the second approach, asymmetric synthesis using a chiral auxiliary refers to a method where a prochiral substrate is attached to a chiral, non-racemic group

called chiral auxiliary leading to enantiomerically pure product. However, major drawbacks of this approach are that stoichiometric amounts of chiral auxiliary are required, and synthetic manipulations of product and substrate are necessary. The third approach, asymmetric synthesis using a chiral catalyst, employs the use of a chiral, non-racemic catalyst while the reagent is achiral, and substrate is prochiral. The major advantage of this method is that only catalytic amounts of the chiral catalyst are required which have obvious economic and practical advantages.[4, 7]

Asymmetric synthesis can theoretically afford up to 100% yield of enantiopure product in comparison to kinetic resolution, which only gives a maximum yield of 50%.[4, 7] In addition, asymmetric synthesis appears to be more practical for obtaining enantiopure compounds since it utilizes non-chiral starting materials, which are more economical and accessible in comparison to chiral pool synthesis approach. Asymmetric synthesis also allows diversification of the enantiopure compound since it permits manipulation during the synthesis, unlike kinetic resolution which yields only a final enantiopure product.[4, 7]

Catalytic asymmetric synthesis or asymmetric catalysis refers to the use of a chiral catalyst to produce a desired diastereoisomer from a chiral compound. It can be achieved using either homogeneous or heterogeneous catalysts. Homogeneous catalysis involves reactions where the catalyst and the reactants are in the same phase. Conversely, in heterogeneous catalysis, the catalyst is insoluble in the reaction solvent or the catalyst and the reactants are in different phases. While chiral homogeneous catalysis is very common in asymmetric synthesis, it is only suitable for small scale or laboratory synthesis. On the

industrial scale, recyclability and separation of the chiral catalyst is not only practical but also economically imperative. Homogeneous catalysis is therefore not suitable for industrial application since it does not permit separation or reuse of the catalyst. Also, most of the homogeneous catalysis processes involve use of trace amounts of soluble heavy metal ions that would remain even after purification which in itself an expensive and rigorous process. This is harmful especially in the food and pharmaceutical industries. On the other hand, chiral heterogeneous catalysis, though not as common, has several advantages including scalability to industrial scale, ease of separation of catalyst and its recycle and reuse.[8] Enzymes are a special category of catalysts, which possess characteristics of both homogeneous and heterogeneous catalysis and are therefore attractive catalysts for our application. Lipase is one of the most commonly used enzymes due to its stability in organic solvents in comparison to other enzymes.[9]

2. Lipase

Enzymes have been extensively used in academia [10] and industry,[11] especially for application in organic reactions. Enzymes as biocatalysts are preferred in asymmetric reactions compared to those catalyzed by chemical catalysts, because they are environmentally friendly, do not require the use of toxic solvents or cofactors[12] and possess high chemo-, regio-, and stereoselectivity.[11] Side reactions that normally occur such as racemisation, rearrangement, etc. are avoided when reactions are catalysed by enzymes due to the mild conditions the enzymes typically require. Some of the most commonly used enzymes in the industry are proteases, cellulases, lipases, amylases and pectinases.[13] Of these,

lipases have gained special interest due to their stability even in non-aqueous environments.[14] This stability is probably provided by water molecules bound to the enzyme which provide conformational flexibility for catalysis. Anhydrous solvents in which water is exclusively removed would lead to denaturation of lipase while excess water would lead to high conformational mobility.[15] Lipase can be further stabilised either by modifying its structure to increase its resistance to non-conventional media or by modifying the solvent environment. Some disadvantages of using lipases include the risk of product contamination due to the difficulty in separating lipase from the reaction medium, as well as possible aggregation in the presence of hydrophobic organic solvents.[16] Since it is not always possible to modify the solvent environment, immobilisation is one of the easiest and convenient alternatives to modify the structure of lipase to enhance its stability in organic solvents, as it not only provides rigidity, thus preventing the unfolding of lipase, but also protects the active site from deformation. In addition, the immobilisation of lipase on supporting materials permits recyclability and continuous operations in both aqueous and non-aqueous environments, thus circumventing the problems of product contamination as well as enzyme aggregation.[17, 18] In order to choose an optimum support for the immobilisation of lipase, it is important to understand its structure and mechanism of catalytic action.

3. Structure and mechanism of action of lipase

Lipases are a class of esterases that catalyse both transesterification and hydrolysis reactions. Structurally, most of the lipases contain a helical

oligopeptide chain that covers the most important region of the lipase – its active site. This chain is often termed a 'Lid'. Depending on whether the active site is covered by the lid or not, the lipase is said to be in its closed or open form respectively.[19] The opening and closing of the lid depends on how the residues forming it interact with the reaction medium. In the presence of water, lipase tends towards the closed form, although, technically it is in an equilibrium between the open and closed forms. On encountering a hydrophobic surface, this equilibrium shifts towards the open form, a phenomenon called interfacial activation.[19] The desired chemical reaction takes place when the open form of the lipase allows the substrate to bind to the active site. The active site of the lipase is home to a set of three amino acids called the catalytic triad, which comprise of an acid, a base and a nucleophile. In most of the lipases, these amino acids are Serine (nucleophile), Histidine (base) and Aspartic acid (acid). This catalytic triad functions *via* a charge-relay system. Although these amino acids are not located close to each other in the primary structure of the lipase, they are brought close together upon folding of the enzyme which is a result of electrostatic interactions with the reaction medium. So, it is inferred that in order to initiate catalytic activity, it is very important to choose a reaction medium and in case of immobilised enzymes, also the right support, which allows the lipase to remain flexible enough to fold as a result, allowing the catalytic triad to remain in an active form. When the substrate approaches the active site, the acid residue (Aspartic acid), due to the negative charge on its oxygen atom, polarises the base (Histidine), whose ring undergoes an alteration in its electronic configuration, increasing the pKa of the imidazole nitrogen. The nitrogen from the base

deprotonates the nucleophile residue (Serine). This creates a highly reactive alkoxide ion on the Serine residue which launches a nucleophilic attack on the ester carbonyl of the substrate leading to molecular rearrangement in the substrate. A negatively charged tetrahedral intermediate is formed, which is stabilised by the oxyanion hole comprising of positively charged amino acid residues. The histidine base then donates a proton to the leaving group and subsequently extracts a proton from the water or acyl substrate. Depending on whether the acyl-enzyme intermediate is attacked by an acyl substrate or by the OH- ions from water as a substrate, the lipase catalyses esterification and hydrolysis reactions correspondingly.[20] The mechanism of catalytic action by lipase is illustrated in Scheme 1.

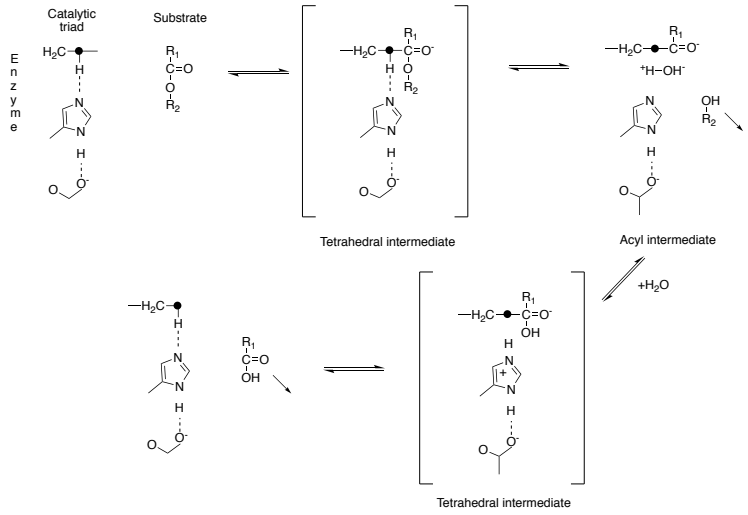

Scheme 1: Nucleophilic attack on the ester carbonyl by the catalytic triad where the dot indicates the nucleophile atom and R_1 and R_2 are alkyl groups. Modified and reprinted with permission from (Dodson, G., & Wlodawer, A. (1998). Catalytic triads and their relatives. Trends in Biochemical Sciences, 23(9), 347-352).Copyright (1998) Elsevier Ltd.)

4. Immobilisation of lipase on supporting materials and its applications

Lipases are not soluble in organic solvents due to which, in their free form, they are susceptible to precipitation and agglomeration, causing inactivation of the enzyme.[9] A convenient method to prevent this loss of activity is by immobilising the enzyme on suitable support materials for stabilisation.[21] There are several other advantages in performing immobilisation of lipase which include convenience in handling of the lipase, ease of separation thereby preventing product contamination, efficient recycle of the enzyme which is economically beneficial, possibility of use in continuous reactions, [22] ease of using different reactor configurations, [23, 24] reduced enzyme inhibition, improved enzyme selectivity and specificity.[25, 26] Immobilisation also enables safe handling of the enzyme since it cannot penetrate the skin preventing allergies.[27] Nevertheless, if the choice of support material were incorrect, immobilisation would lead to inactivity of the lipase due to its interaction with the support which might cause its denaturation, blockage of the active site of the lipase preventing enzyme-substrate interaction, [22-26, 28] and diffusion problems.[29, 30] Most commonly used support materials for immobilisation of lipases include synthetic organic polymers such as Eupergit® C, [31-33] porous acrylic resins such as Amberlite XAD-7, [22] Novozym 435™, [34] biopolymers such as DEAE-Sephadex, [35, 36] agarose, chitosan, starch, cellulose, [37] hydrogels such as polyvinyl alcohol (PVA), [38] polydimethylsiloxane (PDMS), [39] inorganic supports such as zeolites, [40, 41] mesoporous silica, [42-44] alumina, silica, [45] and smart polymers such as poly-*N*-isopropylacrylamide (polyNIPAM).[46]

Immobilisation of lipase can be performed using the one of the following methods:

(i) Adsorption: Adsorption of lipase on the support material takes place through hydrophobic, dipole-dipole, van der Waals interactions or hydrogen bonding. However, due to the relatively weak binding, the enzyme can possibly leach from the support material, which would result in lower activity and loss of enzyme.[47]

(ii) Entrapment: Lipase can be localised within a porous matrix made up of gel or fibres which protects the lipase from harsh solvents, shear stresses, etc. that can cause lipase inactivation.[47]

(iii) Covalent Bonding: Lipase is bound to the immobilisation support *via* covalent bonding. This is a stronger bond compared to the interactions taking place between lipase and support during physical adsorption. As such, the possibility of reduced lipase activity as a result of leaching is minimal in the case of covalent bonding as the bonding restricts conformational mobility of the lipase.[47] Nevertheless, if the functional groups in the active site of the lipase undergo covalent modification, it can lead to inactivation of the enzyme. Therefore, immobilisation is sometimes performed in the presence of substrates or their analogues which bind reversibly to the important functional groups in the active site, thus preventing them from forming covalent bonds with the immobilisation supports.[9] Another method of improving the stability of lipase on the support is to functionalise the support material prior to covalent bonding. Increasing hydrophobicity

of the surface of the lipase has also shown to improve its activity upon immobilisation.[48]

(iv) Cross-linking: Cross-linking involves the attachment of lipase to other lipase molecules by a cross-linking reagent thus doing away with an immobilisation support. However, since it is not easy to control the level of cross-linking of the lipases, it is difficult to ensure the activity of the resulting cross-linked enzyme is retained.[47]

Immobilised lipase has been used to catalyse asymmetric reactions due to its high regio- and enantioselectivity, ease of separation, requirement of mild reaction conditions and environmental compatibility.[49]

The first report of immobilisation of an enzyme was by Nelson and Griffin in 1916, who immobilised invertase on charcoal and aluminum hydroxide for inversion of 10% cane sugar solution. It was observed that the immobilised invertase retained its catalytic activity. The longer the contact between immobilised enzyme and the cane sugar solution, the greater was the inversion.[50]

Later, Novozymes introduced Novozym 435™, which is a non-specific lipase B from *Candida Antarctica* immobilised on acrylic resin. It has been widely used in organic reactions in the synthesis of optically active compounds from *meso* substrates. For example, Schulze *et al*. reported the application of Novozym 435™ for enantioselective acetylation of 1,3-diol **5** to obtain monoacetate **6** in 81% yield and 98% *ee* (Scheme 2a).[51] Lu *et al*. also used the same enzyme to catalyse the desymmetrisation of silicon-centred diol **7** to afford the monoester product **9** in 98% yield and 78% *ee* (Scheme 2b).[52]

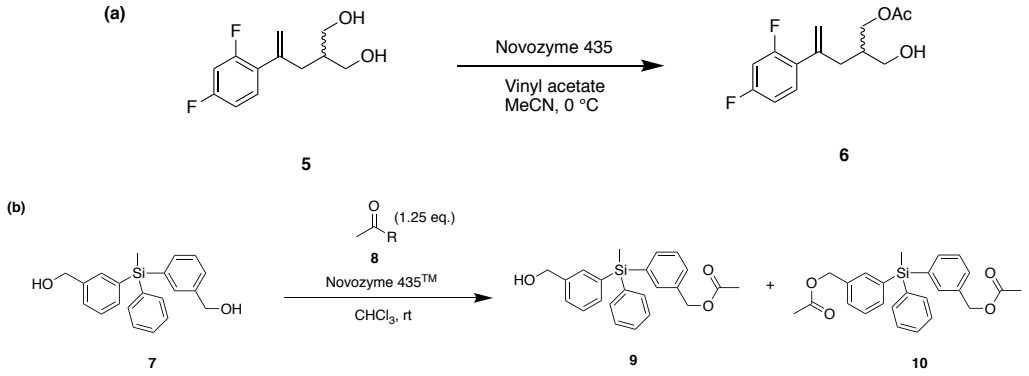

Scheme 2: Desymmetrisation of 1,3-diols using Novozym 435™

Similarly, another commercially available lipase (from *Pseudomonas* sp.), immobilised on Hyflo-Super Celite, also demonstrated great synthetic utility. For example, Tsuji *et al*. reported the effective enzymatic desymmetrisation of 1,3-diol **11** to monoester product (*R*)-**13** in 88% yield and 89% *ee* (Scheme 3).[53] This product was used as a key intermediate in the synthesis of novel immunosuppressants.

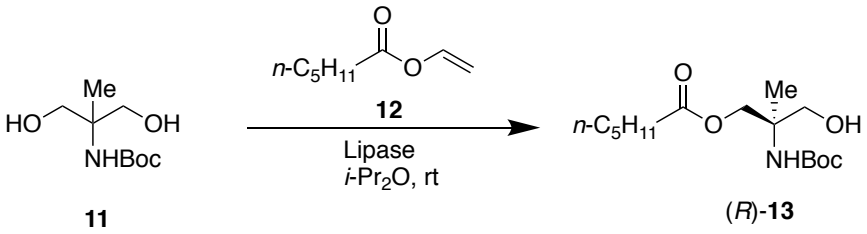

Scheme 3: Desymmetrisation of 1,3-diol 11 using immobilized lipase as catalyst[53]

Lin *et al*. also successfully used Hyflo-Super Celite as support material for immobilisation of porcine pancreas lipase (PPL). This catalyst system was used for the desymmetrisation of various 2-substituted 1,3-propanediols **14** to yield monoester products **15** with a yield of 84% and 94% *ee* (Scheme 4).[54]

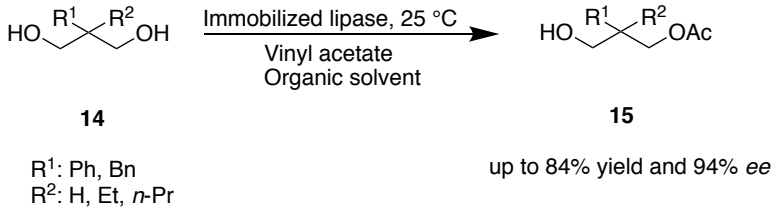

Scheme 4: Immobilised PPL catalysed desymmetrisation of 2-substituted 1,3-propanediols 14[54]

Ceramic was also demonstrated to be an effective catalyst support. Gotor *et al*. have successfully used *Pseudomonas cepacia* lipase (PSL) immobilised on a ceramic support for desymmetrisation of 1,3-propanediamines **16** to the corresponding (*R*)-monocarbamates **18**, which are important building blocks of agrochemicals and pharmaceuticals, with yields between 68% to 72% and 86% to greater than 95% *ee* (Scheme 5).[55]

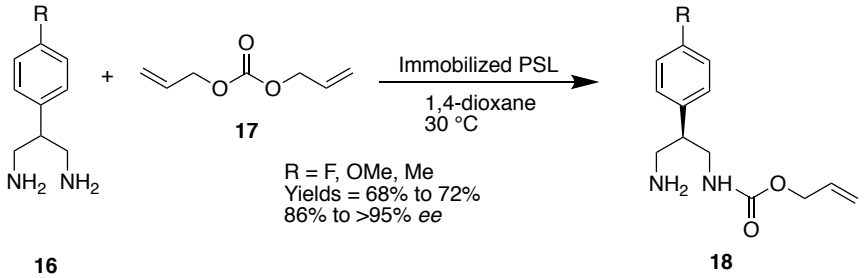

Scheme 5: Enzymatic desymmetrisation of 2-aryl-1,3-propanediamines 16[55]

Patel *et al*. successfully immobilised lipase PCL (from *Bulkhoderia cepacia*) on Accurel polypropylene resin. The resulting immobilised system has been shown to catalyse enantioselective hydrolysis of 1,3-diacetate **19** in 80% yield and 98% *ee*, to afford the monoacetate (±)-**20**, which is a crucial intermediate in the synthesis of Entecavir, a drug approved to treat Hepatitis B (Scheme 6).[56]

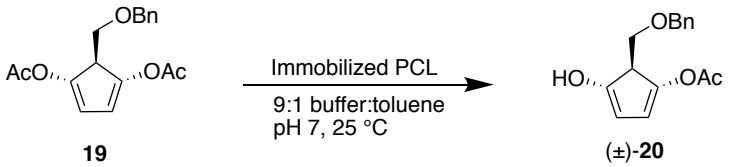

Scheme 6: Enantioselective hydrolysis of diacetate 19 by immobilised PCL[56]

Ozyilmaz *et al*. used *Candida rugosa* lipase immobilised on β-cyclodextrin coated Fe_3O_4 magnetic nanoparticles to catalyse the enantioselective hydrolysis of racemic naproxen methyl esters **21** in an isooctane/aqueous buffer solution to obtain the product **22** in high yield and *ee* (Scheme 7).[57]

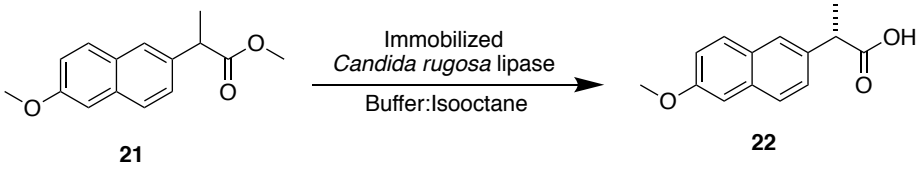

Scheme 7: *Candida rugosa* lipase immobilised on β-cyclodextrin coated Fe_3O_4 magnetic nanoparticles for enantioselective hydrolysis of racemic naproxen methyl esters[57]

It is noted from the existing literature that desymmetrisation of prochiral substrates through immobilised enzymatic heterogeneous catalysis gives enantiopure compounds in high yield and selectivity. In addition, an ideal support material is affordable, inert, strong, stable, offers minimum diffusion limits, can be regenerated, and is sustainable.[58] The support materials used in this research – Fe_3O_4 magnetic nanoparticles, covalent triazine-piperazine linked polymer (CTPP-1) and silica nanoparticles (KCC-1), possess high mechanical and thermal stability, offer high surface to volume ratio for greater lipase binding, and can be easily separated and regenerated. These are characteristics of ideal support materials for immobilisation of lipases. To test this hypothesis, in this research,

lipase immobilised on these three materials were applied in the desymmetrisation of 1,3-propanediol derivatives.

5. Flow Chemistry

In recent years, there is an increased focus on flow chemistry both in academia as well as pharmaceutical industries, due to the numerous advantages it offers over batch chemistry, such as, reduced reaction times, efficient mixing on a small scale, ease of scale-up, improved heat and mass transfer, possibility for in-line monitoring of the reaction process thereby offering better control, lower energy consumption, convenience of performing reactions having unstable intermediates or reagents, enhanced safety, etc.[59-63]

On a laboratory scale, a flow reactor can be conveniently constructed using various components depending on the application. Most often, the reaction 'Vessel' is a reactor coil or a microfluidic chip. The protocol for assembling a laboratory scale reactor has been explained in detail by Britton *et al*.[59] Ideally, the assembled reactor must be portable, easy to use and convenient to construct. Some of the factors determining the components of the reactor include the number of reagents that are used in the reaction, the type of solvent, reaction conditions that need to be maintained such as temperature and pressure, residence time of the reactants, type of catalyst, nature of the reaction - homogeneous or heterogeneous, etc. [59] Depending on the number of reactants and the sequence in which they are added to the reaction, a reactor may contain several mixing modules that aid in mixing of the reactants. Commonly used mixing modules include T-junctions, Y-junctions and cross-junctions. Since each junction has a

particular geometry and volume, it is very important to consider this characteristic while calculating the residence time.[59]

Based on the mechanism of the reaction, the type of catalyst used and its recyclability, convenience of separating the desired product, and solubility of the reactants and/or catalyst in the solvent, different flow systems can be used. The flow systems can have:

(i) all the reactants flowing through the reactor together with a clean product collected at the end without any requirement for further purification steps,[62]

(ii) one of the reactants supported on a solid support such as a polymer and restricted in the reactor, with the remaining reactants flowing through the reactor such that only the pure product remains in the exit stream,[62]

(iii) the reactants as well as a homogeneous catalyst flowing through the reactor together. At the end of the reaction, the product needs to be separated from the catalyst and byproducts if any,[62]

(iv) the catalyst, either in its free form (if insoluble in the reaction solvent), or immobilised on a support material, is constrained in the reactor, while the reactants flow through the reactor. The product is collected at the end without any need for separation from the catalyst, which can be easily recycled and reused.[62]

For instance, uridine diphosphate galactose (UDP-galactose) was synthesised using uridine monophosphate (UMP), galactose, adenosine triphosphate (ATP) and glucose 1-phosphate by Liu *et al*. The three-part biosynthetic pathway

required the use of seven different enzymes (Scheme 8) which were immobilised on nickel agarose beads due to the advantages of enzyme immobilisation and constrained in a column. The reaction mixture was then allowed to flow through the column several times with 50% conversion of UMP to UDP-galactose obtained in 48 h.[64]

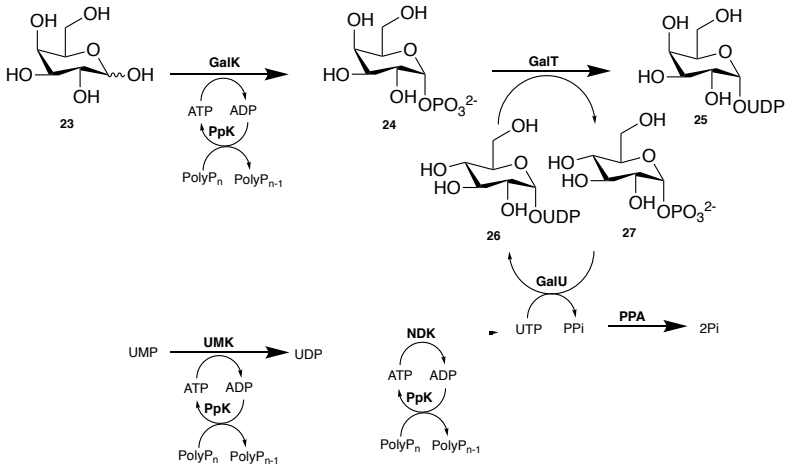

GalK: galactokinase, ATP: adenosine triphosphate, ADP: adenosine diphosphate
PpK: polyphosphate kinase, PolyP: polyphosphate, GalT: galactose 1-phosphate uridyltransferase,
UDP: uridine diphosphate, GalU: UDP-glucose pyrophosphorylase, UTP: uridine triphosphate,
UMP: uridine monophosphate, UMK: uridine monophosphate kinase, PpK: polyphosphate kinase,
NDK: nucleotide diphosphate kinase, PPi: pyrophosphate, Pi: phosphate group

Scheme 8: The three-part biosynthetic pathway for UDP-galactose production as performed by Liu *et al.*[64]

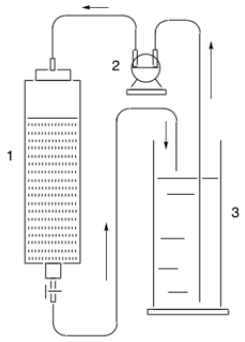

Figure 3: Set-up for the UDP-galactose production as reported by Liu *et al.* (1) column packed with immobilised enzyme beads (2) pump and (3) mixture reservoir[64] (Reprinted with permission from (Liu, Z., *et al.*, Combined biosynthetic pathway for de novo production of UDP-galactose: catalysis with multiple enzymes immobilised on agarose beads.

ChemBioChem, 2002. 3(4): p. 348-355). Copyright (2002) WILEY-VCH Verlag GmbH, Weinheim, Fed. Rep. of Germany)

Similarly, Chen *et al*. synthesised chiral cyanohydrins in high yields (>90%) and selectivity (97->99% *ee*) using defatted almond meal as an enzyme source. The pretreated almond meal was housed in a column through which a mixture of aldehydes and HCN flowed through to provide the cyanohydrins in the product stream (Figure 4).[65]

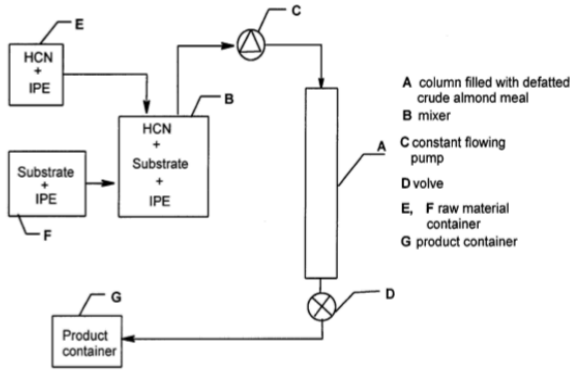

Figure 4: Continuous flow process adapted by Chen *et al.* for the synthesis of cyanohydrins[65] (Reprinted with permission from (Chen, P., *et al*., A practical high through-put continuous process for the synthesis of chiral cyanohydrins. The Journal of Organic Chemistry, 2002. 67(23): p. 8251-8253). Copyright (2002) American Chemical Society)

A continuous total synthesis of rufinamide **30**, an antiseizure medication, was performed by Zhang *et al*. using a copper tubing reactor, with the product collected in 92% overall yield after a residence time of 11 min. Since the reaction involves production of organoazide intermediates, the continuous flow synthesis helped in their in-situ production and consumption, thus improving the overall safety of the reaction.

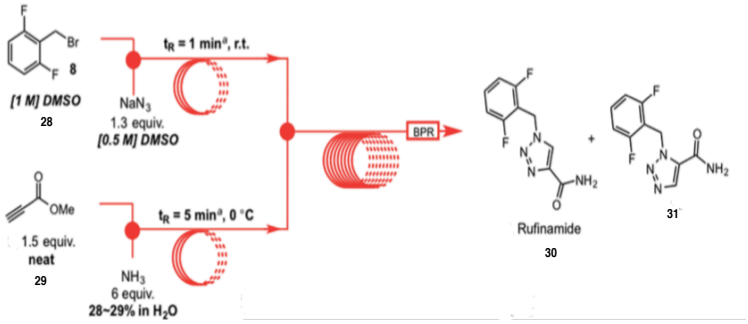

Scheme 9: Reaction scheme used by Zhang *et al*. for the continuous synthesis of rufinamide[66] (Adapted with permission from (Zhang, P., M.G. Russell, and T.F. Jamison, Continuous flow total synthesis of rufinamide. Organic Process Research & Development, 2014. 18(11): p. 1567-1570.). Copyright (2014) American Chemical Society)

Olanzapine **38**, an antipsychotic medication, was synthesised by Hartwig *et al*. *via* continuous flow technology with the aid of inductive heating. For this purpose, they used several reactor modules such as PEEK reactors, glass columns, silica cartridges, and fixed bed reactors containing Pd/C. At the end of the process (Scheme 10)[62], olanzapine was obtained in 83% yield after inductive heating at 85 °C.[67]

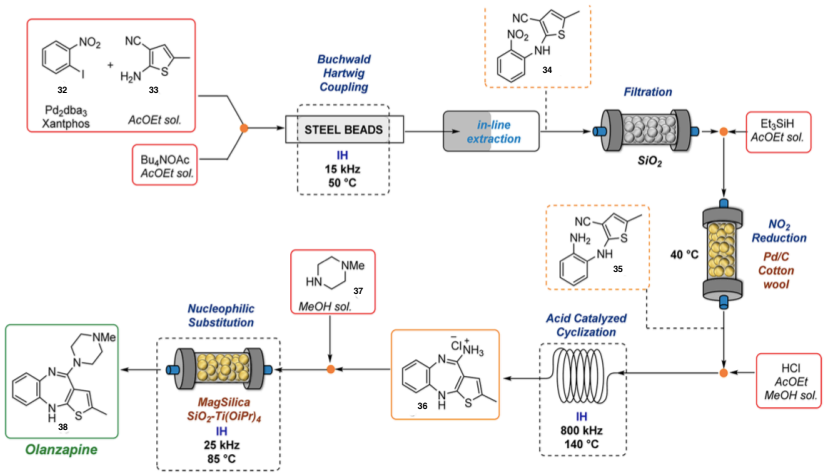

Scheme 10: Flow process used by Hartwig *et al*. for the continuous flow synthesis of olanzapine[67] (Adapted from (Porta, R., M. Benaglia, and A. Puglisi, Flow chemistry: recent developments in the synthesis of

pharmaceutical products. Organic Process Research & Development, 2015. 20(1): p. 2-25.). Copyright (2015) American Chemical Society. Open access article with permission for reuse and copy of the article/adaptions for non-commercial purposes).[62]

As illustrated from the successful synthesis examples listed in this section, continuous flow technology allows synthesis of products quickly, efficiently and safely. While there are certain challenges with the use of flow reactors such as associated high costs, optimisation of the reaction conditions in flow, and handling of solids that are part of the reaction or precipitate during the course of the reaction, most often than not, the issues can be bypassed using appropriate solutions, wherever possible. For example, solid formations can be minimised by using solvents that allow homogeneity and complete dissolution of the solids. If not, the solids can be constrained in a column or reactor, with or without ultrasonication. Often, though the initial investment for the flow reactor set-up is high, on the long run, the costs are offset due to the higher rate of production of the desired compound, reduced energy consumption due to shorter reaction times and nominal reaction conditions, and facile purification of the product, as compared to batch processes.

In this research, synthesis and desymmetrisation of 1,3-diol **52** and the desymmetrisation of 1,3-diacetate **53** were performed using a simple flow reactor comprising of a syringe pump, PTFE reactor tubing and a PEEK T-junction (Chapter IV).

6. Desymmetrization of 1,3-diol in the synthesis of cytisine 42

Our group is interested in the total asymmetric synthesis of cytisine **42** and its derivatives. Cytisine **42** is a tricyclic quinolizidine alkaloid extracted from the seeds of *Cytisus laburnum* and other plants in the *Leguminosae* family.[68, 69] It is a partial agonist to β-2 containing nicotinic acetylcholine receptors (nAChRs), which can influence the cognitive processes in humans.[70, 71] Therefore, it has shown to be a potential therapeutic agent in the treatment of Alzheimer's, [72-74] Parkinson's diseases, [75] schizophrenia, [76, 77] anxiety and depression.[78]

Various total syntheses of cytisine **42** have been reported in literature.[79] Reviews indicate three common intermediates in the total synthesis – tetrahydroquinolizinones, [80, 81] piperidines[82-85] and piperidones.[86, 87] Our group is particularly interested in chiral piperidone **39** (Scheme 16) because it is a versatile building block that can also be used in the total syntheses of other valuable biologically active products such as varenicline **43**, [88, 89] paroxetine **41**, [90] deplancheine **46** [90] and tacamonine **45**[90] (Scheme 16). Despite its versatility and relevance, reports of synthesis of enantiopure piperidone **39** are currently limited.

Maruoka *et al*. performed the first reported synthesis of enantiopure piperidone **39** (Scheme 11).[91] Asymmetric conjugate addition of aldehyde **80** to methylenemalonate **81** using axially chiral aminodiol **82** as an organocatalyst, induced enantioselectivity, and provided chiral adduct **83**. *O*-benzylated piperidone (*S*)-**84** was obtained by the intramolecular cyclization of **83** in TFA/toluene. The piperidone (*S*)-**84** was subsequently *O*-benzylated through

hydrogenation catalysed by Pd/C in acetic acid to give the piperidone (*S*)-**39** in 88% *ee*.

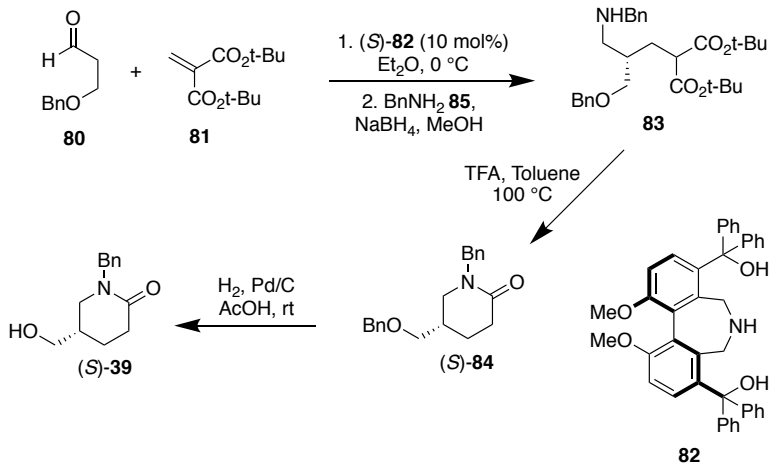

Scheme 11: Synthesis of piperidone (*S*)-39 from enantioselective conjugate addition of aldehyde 80 to methylenemalonate 81

Samarat *et al*.[92] (Scheme 12) reported the synthesis of piperidone **39** using a different approach. Michael addition and cyclization between benzylamine **85** and dimethyl 2-methylenepentanedioate **86** provided racemic ester *rac*-**87** in 82% yield, which was reduced using $LiAlH_4$ or $LiBH_4$ to provide the piperidone *rac*-**39** in 71-89% yield.[87, 93]

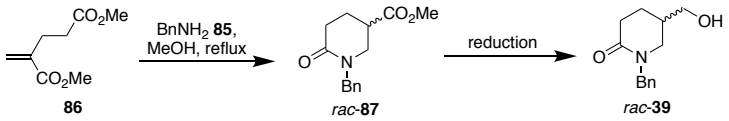

Scheme 12: Synthesis of piperidone 39 from benzylamine 85 and methylenepentanedioate 86[92]

Gallagher *et al.* reported the asymmetric synthesis of piperidone (*R*)-**39** in the total synthesis of cytisine **42**.[86] Aza-annulation reaction of benzylamine **85**, acryloyl chloride **88**, and methyl propiolate **89** provided *N*-heterocyclic product

90 which was hydrogenated using Pd/C as the catalyst to afford the racemic ester *rac*-**87** in 53% yield. Kinetic resolution of the ester *rac*-**87** using α-chymotrypsin gave enantiopure (*R*)-**87** in 42% yield and greater than 98% *ee*.[94] Reduction of (*R*)-**87** gave the corresponding piperidone (*R*)-**39** in 16% overall yield (Scheme 13).

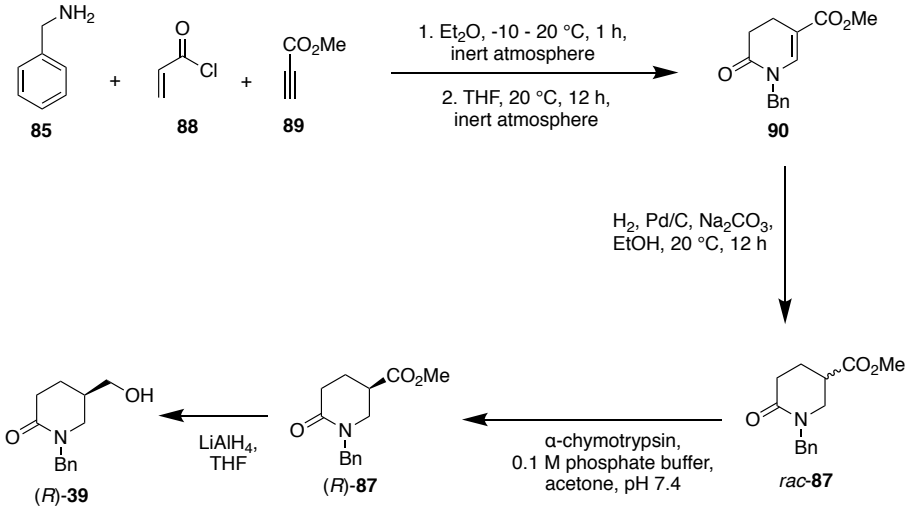

Scheme 13: Enzymatic resolution of racemic ester *rac*-87 to (*R*)-87 and synthesis of piperidone (*R*)-39

Takasu *et al*.[90] reported an approach for the synthesis of piperidone **93** analogues of ester **87** *via* double Michael addition between α,β-unsaturated amide **91** and methyl acrylate **92**. Using this approach, 3-substituted amides **91a, 91b and 91d** gave the piperidones **93a, 93b** and **93d** respectively. However, the reaction of *N*-benzylacrylamide which was expected to give *rac*-**87** as a product was not promising and homodimer **93c** was obtained in approximately 70% yield upon cyclization of **91c** (Scheme 14).

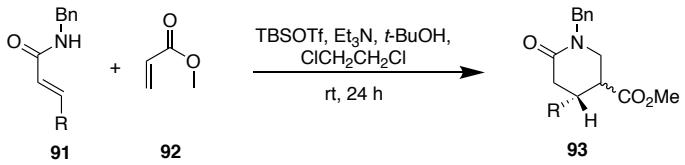

	R		Yield (%)
91a	4-MeOPh	**93a**	52
91b	4-F-Ph	**93b**	59
91c	H	**93c**	0
91d	$(CH_2)_2OTBS$	**93d**	66

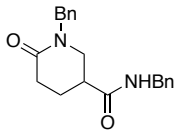

93c

Scheme 14: Synthesis of substituted piperidones 93 by double Michael addition of acrylamide 91 and methyl acrylate 92

Kim *et al.* reported the enantioselective synthesis of a piperidone (*S*)-**99** which is structurally analogous to piperidone **39**.[95] Asymmetric monoalkylation of malonamide ester **94** bromoalkene **95** catalysed by chiral phase transfer catalyst **96**[96] (1 mol%) introduced enantioselectivity to piperidone **97**. The monoalkylated product **98** was obtained in 95% yield and was converted to piperidone (*S*)-**39** in 35% overall yield after seven steps.

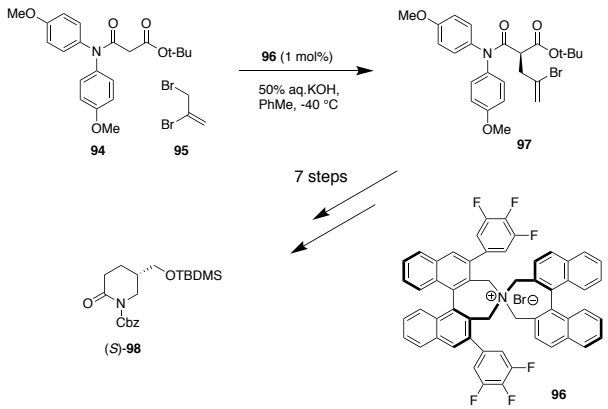

Scheme 15: Synthesis of piperidone (*S*)-98 using asymmetric phase-transfer catalytic monoalkylation of malonamide ester 94 with bromoalkene 95[96]

As discussed, due to limited reports on the enantioselective synthesis of piperidone **39**, there is an urgent need to develop new strategies for the facile and economical synthesis of both enantiomers of piperidone **39**. Enantiopure piperidone **39** would provide an easy approach to the synthesis of many valuable products (Scheme 16).

We have developed a chemo-enzymatic approach for the synthesis of chiral piperidone **39** (Scheme 17) using *tert*-butyl acrylate **47**, and dimethyl malonate **48** as the starting material.[97] The key step in this synthetic route is the enzymatic desymmetrisation of diol **52** and diacetate **53**. Using only lipase AK, we have demonstrated that both enantiomeric products (*R*)-**54** and (*S*)-**54** monoacetates can be prepared effectively with 93% *ee*.[97]

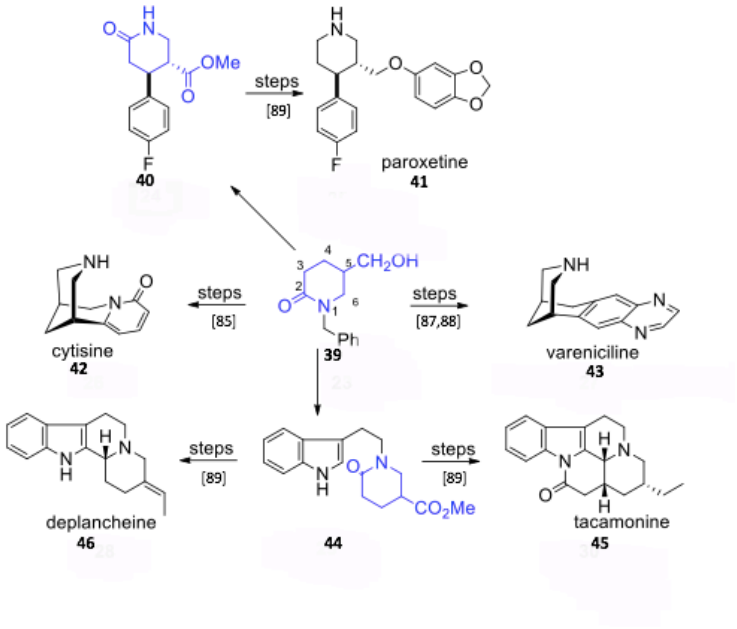

Scheme 16: Synthesis of important biologically active compounds from chiral piperidone 39

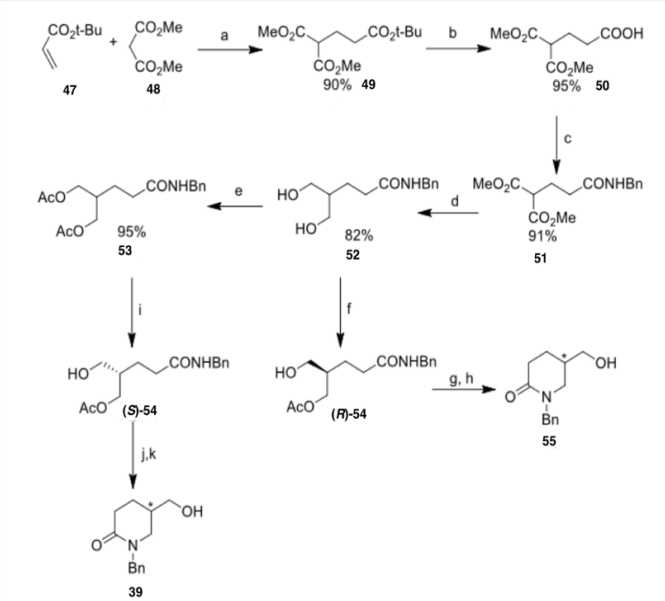

Scheme 17: Chemo-enzymatic approach for the synthesis of chiral piperidone 39 [97]

Although lipases are present in several organisms and can be used for catalysis, microbial lipases are particularly attractive because they do not need any coenzymes.[9] Since diol **52** is a synthetic substrate, in order to identify the optimal lipase for the acetylation of diol **52**, we attempted its desymmetrisation with vinyl acetate in THF using different lipases that have been used extensively in the desymmetrisation of 1,3-diol substrates. The lipases used were lipase AK from *Pseudomonas fluorescens*, lipase PS from *Burkholderia cepacia*, lipase G from *Penicillium camemberti*, CAL-B from *Candida antartica*, lipase A from *Aspergillus niger*, lipase M from *Mucor javanicus*, CCL from *Candida rugosa* and PPL (porcine pancreas lipase). However, except lipases AK, lipase PS, CAL-B and CCL, none of the other lipases succeeded in converting the diol **52** to the monoacetate (*R*)-**54**.

Table 1: Screening of lipases for the enantioselective acetylation of diol 52[a][97]

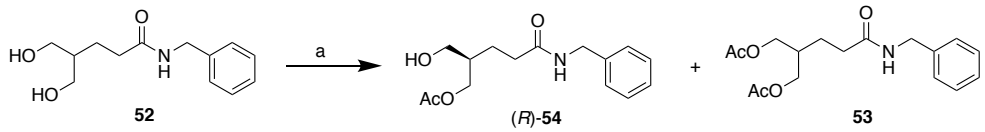

Reagents and conditions: (a) lipase, vinyl acetate, MS 4 Å, THF, r.t.

Entry	Lipase	Time (h)	Monoacetate (*R*)-**54**		Diacetate **53**
			Yield[b] (%)	*ee*[c] (%)	Yield[b] (%)
1	Lipase PS	21	91	75	4
2	Lipase AK	1	85	87	10
3	CAL-B	21	46	0	4
4	CCL	21	17	14	0

[a] Conditions: diol **52** (0.2 mmol), lipases (150 mg/mmol diol **52**), vinyl acetate (10.0 equiv.), molecular sieves (4 Å, 10 mg), THF (3.125 ml), room temp.[b]Isolated yield. [c] Measured by HPLC: Chiralpak AD-H (hexane/*i*PrOH, 95:5), 0.9 ml/min, 254 nm, t_1 = 46.3 min, t_2 = 49.8 min.

Monoacetate (*R*)-**54** was formed in high isolated yields (91% and 85%) and enantioselectivities (75% *ee* and 87% *ee*) only when the acetylation of diol **52** was catalysed by lipases PS and AK respectively (Table 1, Entries 1 and 2). Lipase AK was chosen as the catalyst to perform further desymmetrisation of diol **52** and its diacetate **53** because it provided monoacetate (*R*)-**54** in high isolated yield (85%) and enantioselectivity (87%) in a short reaction time (one hour) (Table 1, Entry 2) compared to other lipases (Table 1).[97] Lipase AK is an alkaline lipase obtained from the Gram-negative, rod-shaped bacterium *Pseudomonas fluorescens* AK102.[98]

Since lipases display the same prochiral selectivity for acetylation and hydrolysis, desymmetrisation of diacetate **53** in phosphate buffer solution was also performed using lipase AK. However, monoacetate (*S*)-**54** was obtained with a maximum yield and enantioselectivity of 54% and 91% *ee* respectively.[97]

The use of immobilised lipase AK is expected to improve its stability and therefore enhance its catalytic ability. In addition, immobilisation also offers significant purification and recycling advantages. In this work, the desymmetrisation of diol **52** and diacetate **53** will be performed using immobilised lipase AK to get a heterogeneous catalytic perspective.

Although flow reactors have been used to perform asymmetric reactions,[99] to the best of our knowledge, the use of flow reactors to perform the desymmetrisation of 1,3-diols or their diacetates have not been well investigated. We seek to fill this gap through this thesis by performing the synthesis and desymmetrisation of diol **52** and hydrolysis of diacetate **53** using a continuous flow process.

7. Research Objectives and Significance

The main objective of this research is to develop an effective continuous flow process for the synthesis of diol **52** and its desymmetrisation through enzymatic heterogeneous catalysis.

While batch reactions are associated with disadvantages such as unequal reactant and temperature distributions, flow reactors offer high surface to volume ratio, improved mass and heat transfer and hence enhanced operational safety, [99] high selectivity and conversion in a short period of time, possess well defined reaction times, operate at steady state and form laminar flow, which permits greater control of reactants in addition to increased reproducibility.[100-103] However, a disadvantage of flow reactors at the laboratory scale is the inability to synthesise large quantities of products. This disadvantage can be overcome by using

multiple parallel reaction structures, a process called scale-out or numbering up.[104]

Another objective of this research is to identify suitable support materials and optimum conditions for the immobilization of lipase AK, for application in the desymmetrisation of diol **52** and diacetate **53**. With optimum immobilisation, there will be reduced enzyme inhibition, improved enzyme selectivity and specificity, [28, 105] enzyme reuse, [9] ease of product purification, [9] improvement in process economy, [9] stabilisation of enzyme in organic media, [25, 26] convenient handling, [22] sustainability, [27] and improved energy efficiency.[27] Nevertheless, immobilisation may cause diffusion limitations and enzyme inactivation.[9] Hence, it is all the more important to identify suitable support materials for each particular application.

As discussed previously in section 4, the enzymatic desymmetrisation of diol **52** and diacetate **53** to produce the corresponding monoacetates (*R*)-**54** and (*S*)-**54**, will lead to a facile method of synthesis of chiral piperidone **39**. Chiral piperidones are embedded in several biologically important compounds such as cytisine **42**, varenicline **43**, paroxetine **41**, deplancheine **46** and tacamonine **45**. Cytisine **42**, a member of the lupin alkaloids, possesses partial agonist activity to α4β2 nAChRs. Therefore, they are promising therapeutics in the treatment of central nervous disorders such as Parkinson's and Alzheimer's diseases.

8. Research methodologies

Monoacetates (*R*)-**54** and (*S*)-**54** can be produced by the acetylation of diol **52** and hydrolysis of diacetate **53** using lipase AK as a catalyst using the enzymatic

route discussed in Scheme 17. In this work, we use two approaches for the desymmetrisation: (i) Batch process and (ii) Continuous flow process.

Lipase AK (catalyst) and vinyl acetate (acetylating agent) were chosen for the acetylation of diol **52** as they were found to afford the monoacetate (*R*)-**54** in high yields and enantioselectivity. Lipase AK was also established to be best for the hydrolysis of diacetate **53**.[97] Due to the obvious advantages of immobilisation of enzymes as mentioned in section 3, lipase AK will be immobilised on three different nanomaterials – Fe_3O_4 magnetic nanoparticles, [106] covalent triazine-piperazine linked polymer (CTPP-1)[107] and silica nanospheres (KCC-1)[108] to identify the most suitable support material. The optimum conditions for immobilisation of lipase AK on these nanomaterials will be tested by varying the method of immobilisation, temperature, pH of buffer used for immobilisation, concentration of cross-linking agent, etc.

Upon determining the optimum conditions for the immobilisation of lipase AK on the support materials, in batch process, the immobilised lipase AK-support material catalyst system will be used to catalyse the acetylation of diol **52**, followed by testing the recyclability of the catalyst system. The most suitable support material amongst the three will be identified based on the results of the acetylation reactions of diol **52** and the recyclability studies. Lipase AK immobilised on the identified suitable support material will then be used to catalyse the hydrolysis of diacetate **53**.

In the flow process, a simple bench-top PTFE tubular flow reactor will be used to perform the reactions for the synthesis of diol **52** and the desymmetrisation of diol **52** and diacetate **53**. Reaction parameters such as length of the reactor tube,

flow rate of the reactants and as a result, the residence time, and concentration of reactants will be modified to determine the optimum reactor configuration and conditions to achieve maximum possible product yield and enantioselectivity.

Chapter II : Synthesis of support materials for the immobilisation of lipase AK and optimisation of the conditions for immobilisation of lipase AK

1. Introduction

Immobilisation of lipase allows easy product purification, improves stability in organic solvents, enhances enzyme selectivity and specificity, and permits recyclability of the lipase.[9] However, depending on the nature of the support, there are certain disadvantages of immobilisation such as inactivation of the lipase due to binding in a closed configuration, possibility of low specific activity due to mass transfer limitations which in turn leads to lower reaction rates, etc. Therefore, it is crucial to identify a suitable support that not only effectively supports the lipase, but also enhances its specific activity.[27] A good support has high surface area, allows efficient enzyme-substrate interaction, is stable, sustainable, offers low mass transfer limitations, and can be easily separated from the reaction mixture after reaction completion.[109]

Due to their large surface areas, porous materials offer scope for high enzyme loading, improved thermal stability and efficient mass transfer due to enhanced diffusion of reactants and products.[110, 111] Where the enzyme is immobilised on the porous support depends on its diffusion rate. If the diffusion rate of the enzyme is faster than the immobilisation rate, the enzyme tends to diffuse homogeneously in and along the pores. If the diffusion rate of the enzyme is slower than the immobilisation rate, the enzyme can crowd on the surface of the pores of the support.[47] Depending on their pore sizes, porous support materials are classified into microporous materials, mesoporous materials and

macroporous materials. Microporous materials have pore diameters less than 2 nm and therefore cannot accommodate enzymes larger than that. Materials with pore sizes between 2 and 50 nm are called mesoporous materials. These have narrow pore size distributions and can accommodate relatively larger enzymes compared to microporous materials. They are often preferred as supports due to their highly ordered structure as a result of their pore sizes. Macroporous materials have pore diameters greater than 50 nm and have been widely used in enzyme immobilisation.[112] Mesoporous silica nanoparticles are easy to functionalise, possess high porosities and are largely biocompatible. Their large pore sizes decrease diffusion limitations and permit efficient mass transfer.[111] Enzymes immobilised on such materials are well dispersed in the reaction medium. As such, recycling is challenging since it requires high speed centrifugation.[47] On the other hand, magnetic nanoparticles, despite being well dispersed in the reaction solution, are easy to separate due to their superparamagnetic properties. Although there are different types of magnetic nanoparticles, Fe_3O_4 magnetic nanoparticles are used extensively because they are relatively less toxic and more biocompatible.[47]

Lipase can be immobilised on suitable supports either by physical adsorption or covalent binding. While physical adsorption of lipase on supports is through weak bonds such as hydrogen bonds and van der Waals forces, covalent binding involves the use of a cross-linker such as glutaraldehyde.[109] The use of a cross-linker, however, usually requires prior activation of the surface of the support. For example, lipase can be immobilised on a support material having free OH-groups on the surface through covalent binding using glutaraldehyde as a cross-

linker. For this purpose, a reagent such as (3-aminopropyl)triethoxysilane (APTES) can be used. APTES forms a Si-O- bond with the free OH- groups while the free amino terminal of APTES binds to the CHO- group on glutaraldehyde. The other free CHO- terminal on glutaraldehyde then binds to the amino group on lipase, leading to immobilisation *via* covalent binding.[113]

In this research, three support materials – Fe_3O_4 magnetic nanoparticles, KCC-1 silica nanospheres and covalent triazine-piperazine linked polymer (CTPP-1) will be investigated as supports for the immobilisation of lipase AK from *Pseudomonas fluorescens*.

1.1 Fe_3O_4 magnetic nanoparticles

The small size and high surface area of Fe_3O_4 magnetic nanoparticles make them viable support materials for immobilisation of catalysts since they allow high loading of catalyst thereby leading to good catalytic activity. By controlling the temperature, pH and concentration of reaction, magnetic nanoparticles of desired shape and size can be obtained. Some examples of magnetic nanoparticles used for the immobilisation of catalysts include $CoFe_2O_4$, Fe_3O_4, $MnFe_2O_4$ and $CuFe_2O_4$.[114] In comparison to other magnetic nanoparticles, Fe_3O_4 magnetic nanoparticles are easier and cheaper to prepare and are thus attractive materials for use as catalyst supports. Due to their small size and high loading capacity, heterogeneous catalysis using Fe_3O_4 magnetic nanoparticles is almost similar to that of homogeneous catalysis. This similarity is useful since a large area of the immobilised catalyst is available for binding to the substrate. Therefore, the yield of the reaction is expected to be similar as that obtained through homogeneous

catalysis. In addition, due to the magnetic nature of these nanoparticles, they can be easily separated using a simple magnet instead of separation strategies such as centrifugation or filtration.[8, 114]

1.2 Covalent triazine-piperazine linked polymer (CTPP-1)

A novel highly porous covalent triazine-piperazine linked polymer (CTPP-1) was synthesised by Das *et al*.[107] It possesses high surface area and a 3D porous dendrimer-like architecture. The dendrimer-like structure is due to the interlinking of triazine and piperazine components from the solvothermal treatment of cyanuric chloride and piperazine. The hierarchical porous architecture of CTPP-1 can effectively reduce transport limitations, high surface area, and high thermal and mechanical stability, making CTPP-1 an attractive catalyst support. Furthermore, this research will be the first attempt to study the role of this material as support for immobilisation of lipase.

1.3 KCC-1 silica nanospheres

KCC-1 are silica nanospheres having high surface area, easily accessible highly porous surface and a unique fibrous morphology.[108] Dendrimeric silica fibres and channel provide the material with high surface area. KCC-1 enables easy accessibility through its fibres instead of pores. Due to these reasons, KCC-1 has a high potential to be utilised as a catalyst support.

In this chapter, the synthesis of support materials for the immobilisation of lipase AK and optimisation of the conditions for immobilisation will be discussed.

2. Research Methodologies

The three materials under investigation as support for lipase immobilisation – Fe_3O_4 magnetic nanoparticles, CTPP-1 and KCC-1, will be synthesised. Since Fe_3O_4 magnetic nanoparticles and KCC-1 have reactive OH- groups on their surfaces, after synthesis, they will be pre-activated with APTES. Two methods of immobilisation of lipase AK on the surface of the support materials will be tested – physical adsorption and covalent binding using glutaraldehyde as a cross-linker. In the case of CTPP-1, the immobilisation of lipase AK will be performed only through the physical adsorption method, since there are no free groups on the surface of CTPP-1 suitable for glutaraldehyde binding. Glutaraldehyde was used as a linker given its high efficiency in the immobilization of enzymes, especially lipase.[9, 109, 113] The immobilisation will performed across a range of temperatures (25-40°C) and varying pH of 0.1 M sodium phosphate buffer (pH 6-pH 8). Immobilisation yield will be calculated using Bradford assay[115] with bovine serum albumin as a standard protein for reference. Activity of lipase AK immobilised on the three materials at the optimum temperature of immobilisation and using optimum pH of 0.1 M sodium phosphate buffer will be determined using *p*-NPP assay.[116]

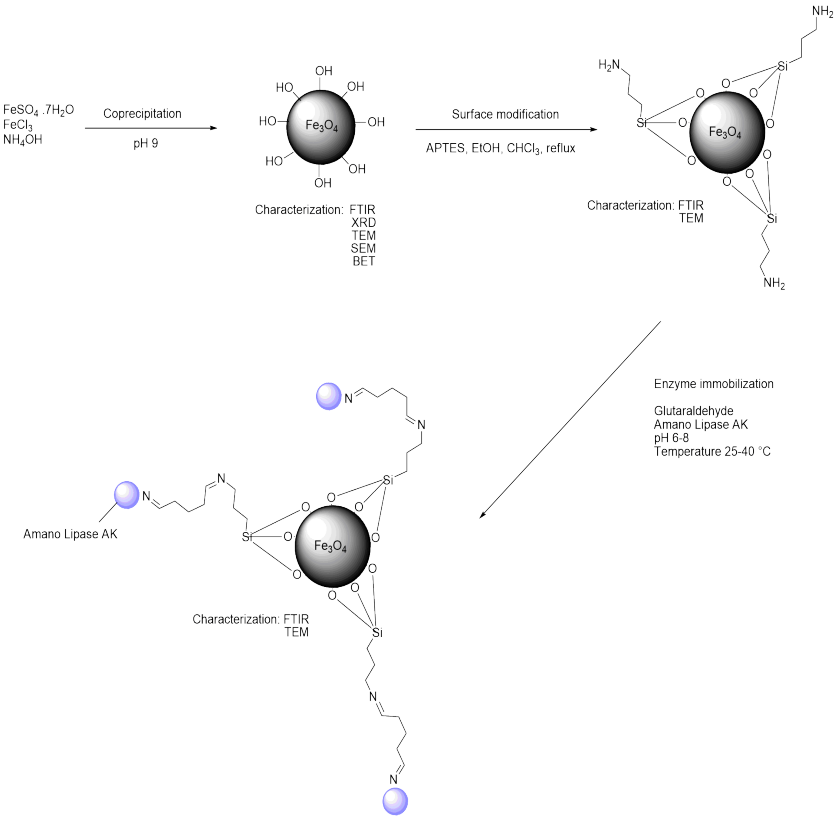

Scheme 18: Synthesis of Fe_3O_4 magnetic nanoparticles followed by pre-activation with APTES[117] and immobilisation of lipase AK through covalent binding

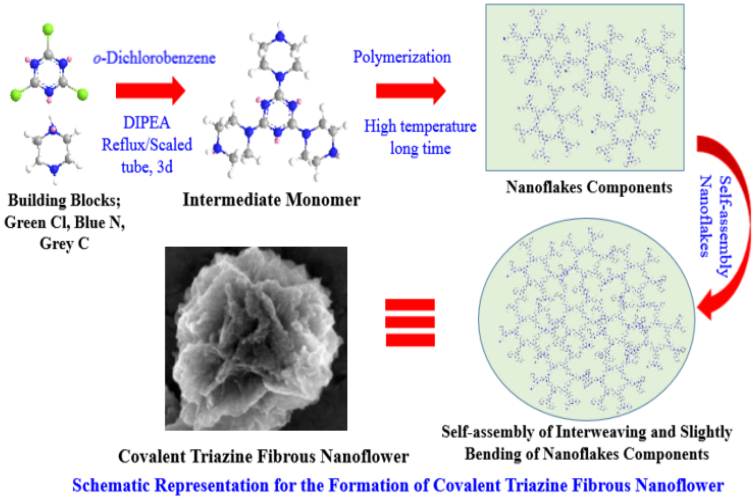

Scheme 19: Synthesis of CTPP-1[107] (Reprinted with permission from (Das, S.K., *et al.*, Highly stable porous covalent triazine–piperazine linked nanoflower as a feasible adsorbent for flue gas CO_2 capture. Chemical Engineering Science, 2016. 145: p. 21-30.).

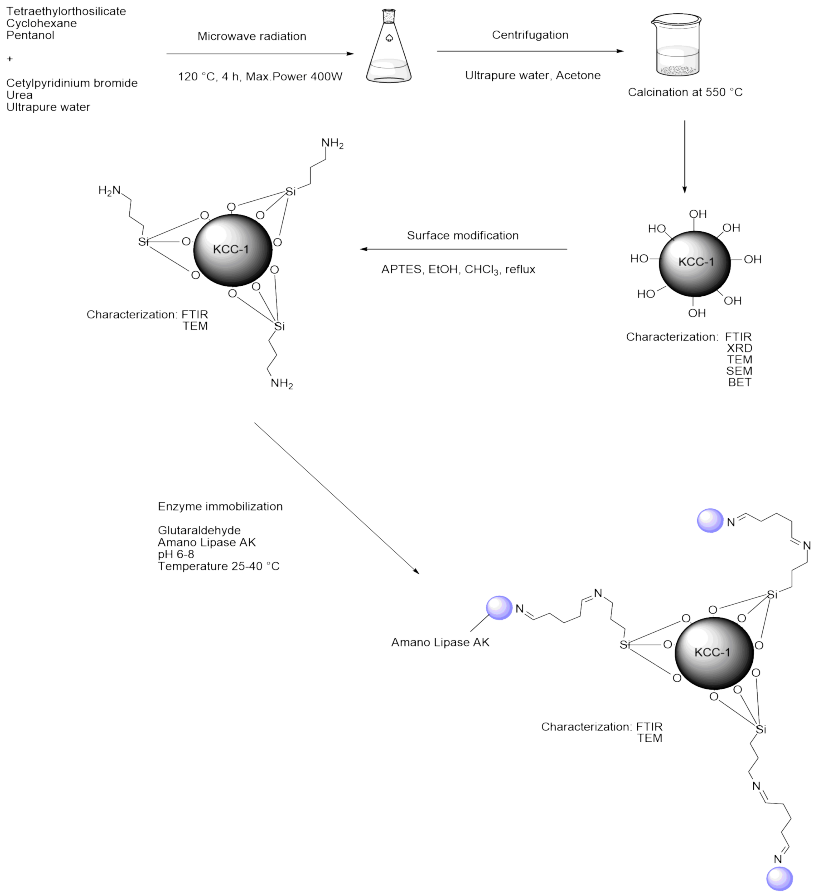

Scheme 20: Synthesis of KCC-1[108] followed by pre-activation with APTES and immobilisation of lipase AK through covalent binding

3. Synthesis of support materials

3.1 Synthesis and functionalisation of Fe_3O_4 magnetic nanoparticles

Synthesis of the Fe_3O_4 magnetic nanoparticles was performed using the co-precipitation method.[117] To confirm the size, structure and surface area of the nanoparticles, characterisation was completed *via* TEM, SEM and BET.

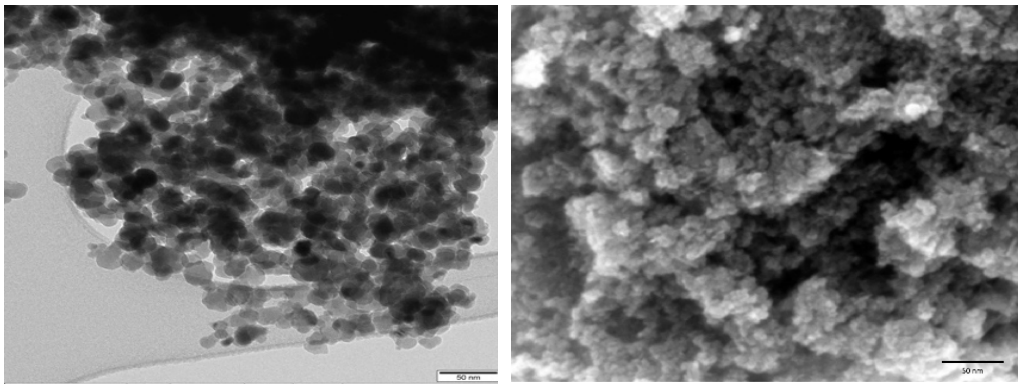

(a) **(b)**

Figure 5: (a) TEM image of Fe_3O_4 magnetic nanoparticles and (b) SEM image of Fe_3O_4 magnetic nanoparticles

TEM and SEM images (Figure 5) of the nanoparticles indicate agglomeration of the nanoparticles. The small size of nanoparticles could have caused increase in surface energy, which may possibly have led to physical aggregation of the nanoparticles in turn, leading to the cluster formation. This cluster formation reduced the amount of surface area available for lipase AK immobilisation. However, since the size of the clusters is less than 50 nm as can be observed in the SEM image, there is still a large area available for lipase AK immobilisation.

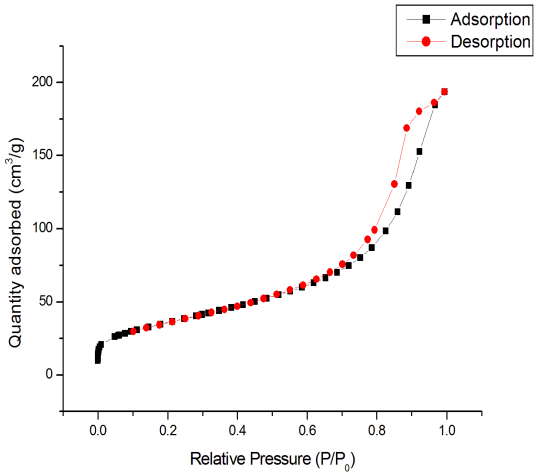

Figure 6: N_2 adsorption-desorption isotherms of Fe_3O_4 magnetic nanoparticles at STP

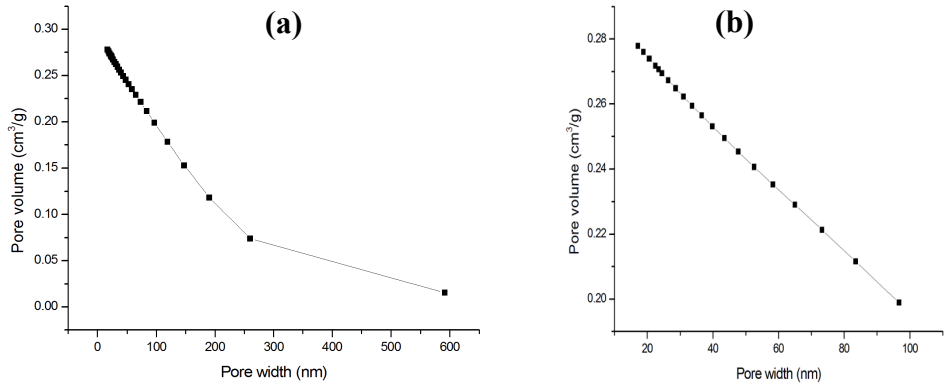

Figure 7: BJH pore volume distribution of Fe_3O_4 magnetic nanoparticles, calculated by the adsorption branch of isotherms (a) Pore size distribution from 0 nm to 700 nm (b) Magnified pore size distribution from 0 nm to 110 nm

The BET surface area of the Fe_3O_4 magnetic nanoparticles was determined to be 126.721 m^2/g. Figure 6 shows that the nanoparticles have the isotherm shape of type-IV with type H1 hysteresis loop which indicates the presence of mesopores due to possible agglomeration of small spheres of approximately uniform dimensions. The BJH isotherms presented in Figure 7 elucidate the pore size distribution in the mesoporous range. since the size of the particles is itself in the 10-20 nm range, with a few particles in the microporous range, which could be agglomerated particles. This is in concordance with the SEM data where Fe_3O_4 magnetic nanoparticles clusters of less than 50 nm were observed.

The surface of the Fe_3O_4 magnetic nanoparticles was modified using (3-aminopropyl)triethoxysilane (APTES). APTES binds to the free OH- groups on the surface of the Fe_3O_4 magnetic nanoparticles forming a Si-O- bond. The free amino terminal on APTES then binds to the CHO- group on glutaraldehyde, which is used in this research as a linker for lipase AK immobilisation on Fe_3O_4 magnetic nanoparticles. Lipase AK can also bind to lipase AK *via* physical

adsorption through hydrogen bonding, van der Waals forces, etc. XRD and FTIR studies confirmed the surface modification of Fe_3O_4 magnetic nanoparticles.

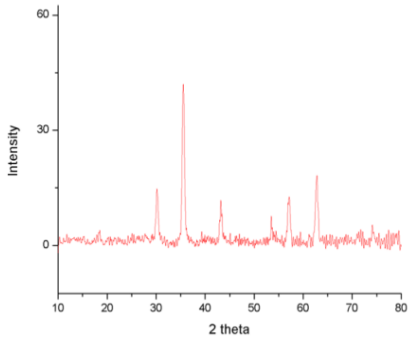

Figure 8: XRD image of the APTES pre-activated Fe_3O_4 magnetic nanoparticles

The XRD characteristic peaks (Figure 8) of the APTES coated Fe_3O_4 magnetic nanoparticles at 2-theta angles of 30°, 36°, 43°, 58° and 63° are concomitant to those reported in literature.[118, 119] Based on the XRD and FTIR studies, it was concluded that the surface modification of Fe_3O_4 magnetic nanoparticles with APTES was successful. These pre-activated Fe_3O_4 magnetic nanoparticles will hereafter be referred to as MNP.

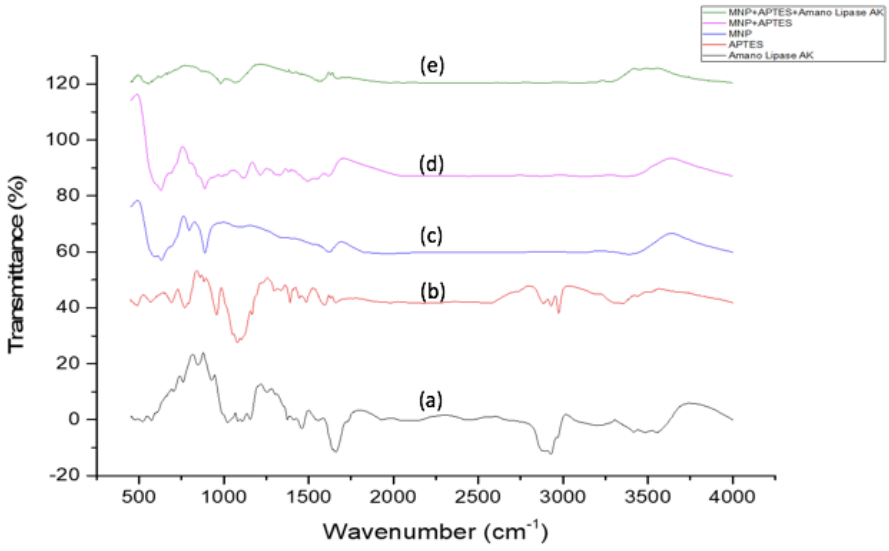

Figure 9: FTIR spectra (a) lipase AK (b) APTES (c) MNP (d) MNP functionalised with APTES and (e) lipase AK immobilised on APTES functionalised MNP

The peaks at around 580 cm^{-1} in (c), (d) and (e) in Figure 9 are due to Fe-O stretching of magnetic nanoparticles. The peaks at around 920 cm^{-1} in (b), (d) and (e) are due to the Si-O-Si stretching, which are observed only in the Fe_3O_4 magnetic nanoparticles coated with APTES. Similarly, peaks at around 1100 cm^{-1} are present only in (b), (d) and (e) due to Si-O-H bonds from APTES. The peak at around 1400 cm^{-1} in (b), (d) and (e) is due to C-N bond stretching vibration of APTES molecules. The peaks at around 1600 cm^{-1} and 3000 cm^{-1} are due to the N-H bending mode and N-H stretching vibration of the free NH_2 group respectively. The peaks at around 2900 cm^{-1} in (b), (d) and (e) are due to the C-H vibration of the propyl group of APTES. These peaks indicate the presence of APTES on the synthesised Fe_3O_4 magnetic nanoparticles.[118]

3.2 Synthesis of Covalent Triazine-Piperazine linked polymer (CTPP-1)

Synthesis of CTPF-1 was performed[1] using the procedure developed by Das *et al*.[107] The material obtained was characterised using TEM, SEM, BET and XRD.

[1] Synthesis of CTPP-1 was performed with the help of Dr. Swapan Kumar Das, former post-doctoral researcher, Inorganic Membranes Research Group, KAUST, Saudi Arabia.

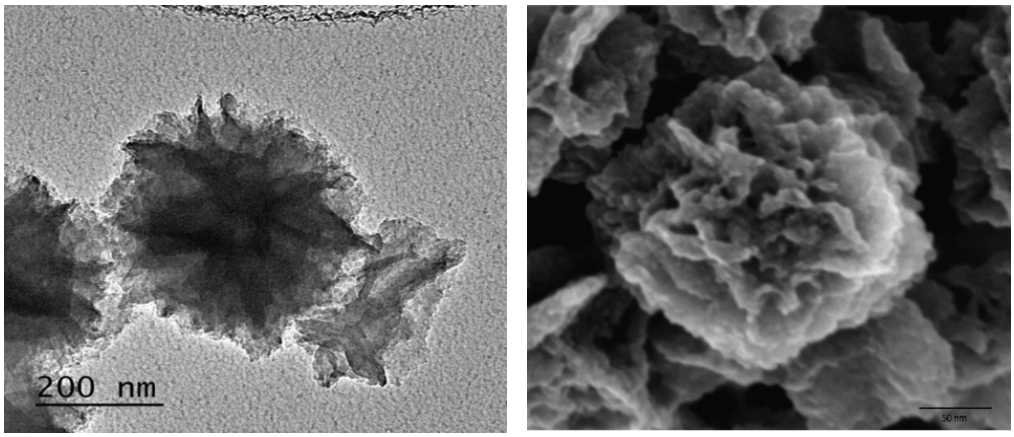

(a) **(b)**

Figure 10: (a) TEM image of CTPP-1 and (b) SEM image of CTPP-1[2]

The TEM image (Figure 10a) of CTPP-1 shows the average size of the nanoflowers to be around 350 nm in addition to a porous structure, which is desired since it would enable easy immobilisation of lipase AK and free movement of the substrate molecules for enzyme-substrate interaction and reaction. The unique flower-like morphology of the material can be observed from the SEM image (Figure 10b). This unique morphology gives the material high surface area which is expected to increase the amount of loading of lipase AK.

The observed XRD pattern of the CTPP-1 showed broad diffraction peaks at approximately 2-theta of 6.8°, 13.5°, 19.5° and 40.9°, which suggests that the framework of CTPP-1 materials has little order and is amorphous (Figure 11).[107, 120]

[2] TEM and SEM imaging was performed by Dr. Swapan Kumar Das

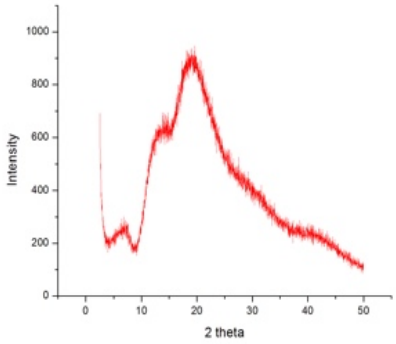

Figure 11: XRD image of CTPP-1[3]

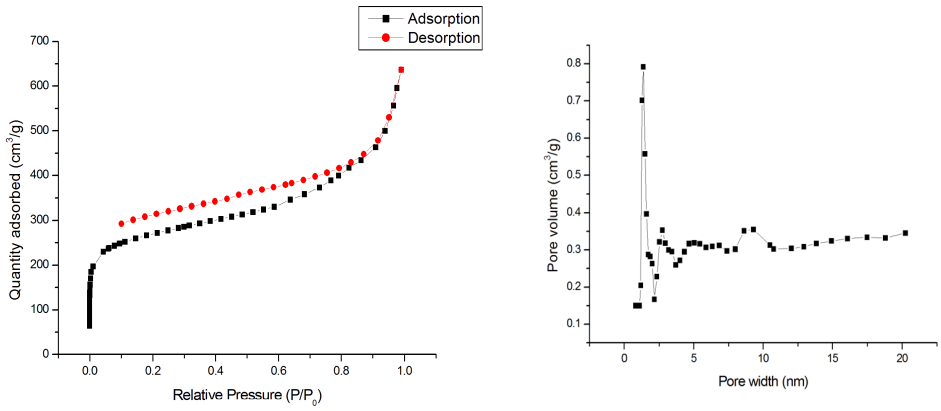

(a) **(b)**

Figure 12: (a) N_2 adsorption-desorption isotherm of CTPP-1 at STP and (b) BJH pore size distribution of CTPP-1 calculated by the adsorption branch of the isotherms[4]

Surface area of CTPP-1 was determined using BET. The isotherm displayed a typical type-I curve (Figure 12a). The polymeric framework architecture led to the formation of micropores while the interweaving and slight bending of nanoflake units in nanospheres, along with the interparticle separation, were responsible for the mesoporous nature of the CTPP-1 material. The BJH surface area of CTPP-1 was found to be 779 m^2/g. The pore size as noticed from the BJH

[3] XRD of CTPP-1 was performed by Dr. Swapan Kumar Das, former post-doctoral fellow, Inorganic Membranes Research Group, KAUST, Saudi Arabia
[4] BET analysis of CTPP-1 was performed by Dr. Swapan Kumar Das

isotherm (Figure 12b) shows that the majority of the pores are micropores with a pore size centred at approximately 1.25 nm, while the mesopores have a broad range of sizes. This high surface area is expected to increase the amount of lipase AK immobilisation.

Characteristic C-H bond stretching can be observed in Figure 13 between 2800 cm^{-1} and 3000 cm^{-1} in (b) and (c). Ring C-C stretching can be noticed at around 1000 cm^{-1} in (b) and (c). The peak at around 3500 cm^{-1} in (b) and (c) is attributed to N-H stretching absorption. Multiple peaks in the region between 1200 cm^{-1} and 1300 cm^{-1} in (b) and (c) are due to symmetric and asymmetric C-N bond stretching. The peaks observed around 1500 cm^{-1} in (b) and (c) are due to the asymmetric and symmetric CNH deformation vibrations. The strong peak at around 850 cm^{-1} assigned to the C-Cl bond stretching vibration is absent in (b) and (c) confirming the substitution of all three chlorine atoms. Comparing the results with literature,[121, 122] it was confirmed that the material synthesis was successful.

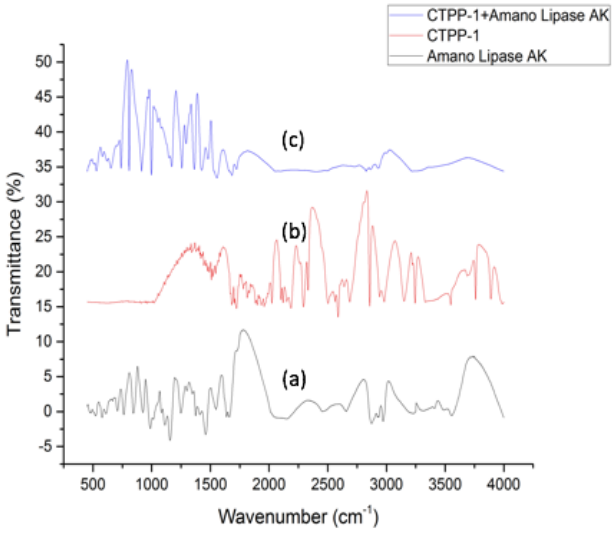

Figure 13: FTIR spectra (a) lipase AK (b) CTPP-1 and (c) lipase AK immobilised on CTPP-1

3.3 Synthesis and functionalisation of KCC-1

KCC-1 was synthesised using the procedure reported by Polshettiwar *et al*.[108] and characterisation was performed using TEM, SEM, XRD, BET and FTIR.

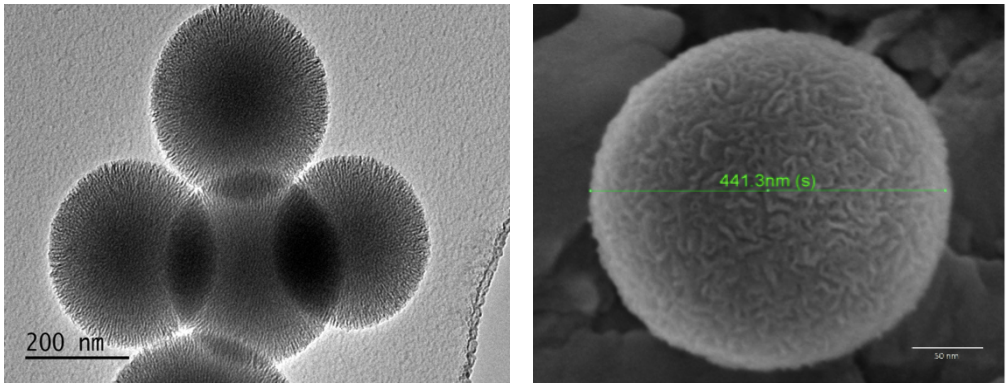

(a) **(b)**

Figure 14: (a) TEM image of KCC-1 and (b) SEM image of KCC-1

TEM image of KCC-1 (Figure 14a) shows uniform size particles with average diameter of around 400 nm, which was further confirmed in the SEM image with the average particle diameter determined to be 441.3 nm. The unique fibrous nature of KCC-1 can also be noticed in the SEM image (Figure 14b).

The XRD image of KCC-1 (Figure 15) showed only a single peak at a 2-theta of 20° which shows that the material is amorphous.[108] Surface area of the material was determined using BET (Figure 16).

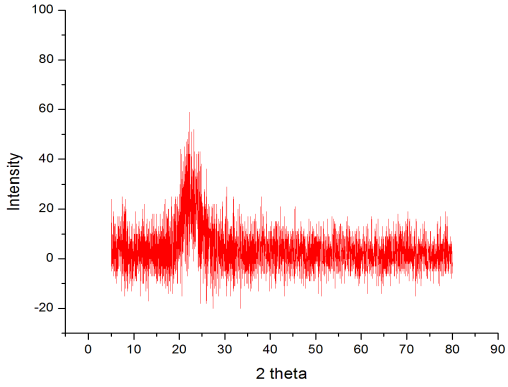

Figure 15: XRD image of KCC-1

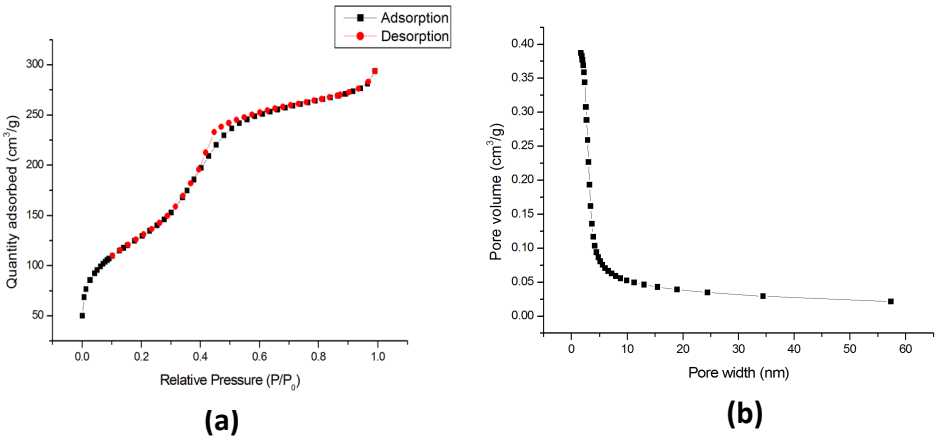

Figure 16: (a) N_2 adsorption-desorption isotherm of KCC-1 at STP and (b) BJH pore size distribution of KCC-1 calculated by the adsorption branch of the isotherms

Figure 16a shows that KCC-1 has the isotherm shape of type-IV that confirms that the material is mesoporous having well defined pores. This can also be noticed from the BJH isotherm in Figure 16b where the pore size distribution is mostly in the mesoporous range (2-50 nm) as desired. The BET surface area of KCC-1 was determined to be 469.066 m^2/g.

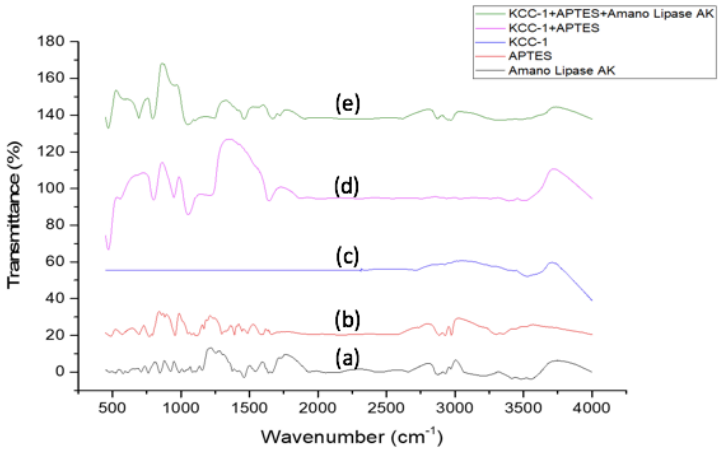

Figure 17: FTIR spectra (a) lipase AK (b) APTES (c) KCC-1 (d) APTES functionalised KCC-1 and (e) lipase AK immobilised on APTES functionalised KCC-1

FTIR spectra was confirmed with that available in the literature[108] and are as shown in Figure 17. The peaks at around 920 cm^{-1} in (b), (d) and (e) are due to the Si-O-Si stretching. Similarly, peaks at around 1100 cm^{-1} are due to Si-O-H bonds attributed to APTES. The peak at around 1400 cm^{-1} in (b), (d) and (e) is due to the C-N bond stretching vibration of APTES molecules. The peaks at around 1600 cm^{-1} and 3000 cm^{-1} are due to the N-H bending mode and N-H stretching vibration of the free NH_2 group respectively. The peaks at around 2900 cm^{-1} in (b), (d) and (e) are due to the C-H vibration of the propyl group of APTES. Based on the FTIR study, it was confirmed that the surfaces of the KCC-1 nanoparticles were modified with APTES.

4. Immobilisation of lipase AK on the support materials

Catalytic activity of immobilised lipase is primarily governed by the reaction environment. As discussed earlier, interaction with a hydrophobic surface will

shift the equilibrium of the lipase towards the open form.[19] In addition, protonation state of the lipase is particularly important in aqueous solvents. One of the methods to maintain the active protonation state of the lipase is by controlling the pH of the aqueous solvent. Sometimes, acidic or basic nature of the substrates might cause disturbances in the protonation state, in which case, a buffer can be used to maintain the optimal pH.[9] The presence of ionisable groups on the surface of the support materials can influence the type and extent of interactions between the amino acid groups on lipase and the electrostatic groups on the support materials. Modulating the pH of the buffer can help prevent structural changes to the enzyme upon immobilisation.[123] To ensure lipase AK is immobilised with high yield and activity, optimisation studies were performed using 0.1M sodium phosphate buffers of different pH at varying temperatures.

To determine the optimal conditions for the immobilisation of lipase AK on the support materials, two immobilisation strategies were adapted – physical adsorption and covalent binding. Physical adsorption of lipase AK on the support materials is through hydrogen bonding while covalent binding uses glutaraldehyde as a linker.[9]

FTIR studies confirmed the successful immobilisation of lipase AK on the functionalised Fe_3O_4 magnetic nanoparticles.

The characteristic amide peak of lipase AK at around 1500 to 1600 cm^{-1} in Figure 9 and Figure 17 can be observed in both (a) and (e), confirming the successful immobilisation of the enzyme on the surface of the MNPs and APTES functionalised KCC-1 respectively. The disappearance of the peaks at 1500 cm^{-1} and 2800 cm^{-1} in (e) indicate the covalent bond formation between the

characteristic functional group of lipase AK with glutaraldehyde. The immobilisation was in concordance with that reported in literature,[124] and it can thus be confirmed that lipase AK was successfully immobilised on MNPs and functionalised KCC-1.

Immobilisation of lipase AK was initially performed at room temperature for a duration of 24 hours using 0.1 M sodium phosphate buffer of pH 7. Subsequently, conditions such as pH of the 0.1 M sodium phosphate buffer used and temperature maintained during immobilisation were optimised. The immobilisation yield under each condition was determined using Bradford assay.[115] The following section discusses the results of the immobilisation in detail.

Table 2: Immobilisation yield of lipase AK immobilised on MNPs by physical adsorption and covalent binding at different temperatures and varying pH of 0.1M sodium phosphate buffer

Entry	pH of buffer	Immobilisation yield (%)							
		Physical adsorption				Covalent binding			
		Temperature (°C)				Temperature (°C)			
		25	30	35	40	25	30	35	40
1	6	97.6	97.9	98.4	98.5	97.9	98.1	98.1	98.2
2	6.5	97.7	98	98.4	98.5	97.9	98.1	98.3	98.5
3	7	97.8	98.1	98.4	98.6	98.2	98.3	98.4	98.9
4	7.5	98	98.1	98.5	98.6	98.2	98.6	98.7	99.3
5	8	98.1	98.3	98.6	98.6	98.2	98.6	98.7	99.4

The immobilisation yield of lipase AK on MNPs did not change significantly with changing the temperature at which the immobilisation was performed or with different pH of 0.1M sodium phosphate buffer used although a general trend

of mild increase in the immobilisation yield with increasing pH of the buffer and covalent binding was observed (Table 2, Entries 1-5). The immobilisation yield of lipase AK was greater than 97% under all conditions studied for the immobilisation. This means, of the total amount of lipase AK added to the immobilisation reaction, 97% of it was attached to the MNPs with less than 3% remaining unattached.

Aldehyde groups of glutaraldehyde added as a linker for covalent binding, react with the primary amine groups of the lysine residues of lipase leading to the reversible formation of Schiff bases which stabilise lipase by improving its rigidity and thus preventing conformational changes due to the use of organic solvents, heat or presence of denaturing agents.[27, 125, 126] Since glutaraldehyde plays an important role in the covalent binding of lipase AK to MNP and APTES functionalised KCC-1, optimisation of the concentration of glutaraldehyde added was attempted (Table 3).

Table 3: Immobilisation yield of lipase AK immobilised on MNPs by covalent binding using different concentrations of glutaraldehyde at 40 °C and pH 8 of 0.1 M sodium phosphate buffer

Entry	Concentration of glutaraldehyde (μl/mg of lipase AK)	Immobilisation Yield (%)
1	2	99.1
2	4	99.2
3	6	99.3
4	8	99.4
5	10	99.4
6	12	99.1

Though there was no significant increase in the immobilisation yield, a general trend of minute increase in the immobilisation yield with increase in pH and temperature was observed. Therefore, a temperature of 40 °C and pH 8 of 0.1 M sodium phosphate buffer were chosen for immobilisation. In addition, commercially available lipase AK (used in this work) is extracted from *Pseudomonas fluorescens* AK strain. This organism thrives at a temperature 40 °C and pH 8.[98] Since there was no effect on the concentration of glutaraldehyde on immobilisation, 10 (µl/mg of lipase AK) of glutaraldehyde was used for further experiments for measurement convenience.

Screening of optimum temperature for immobilisation and pH of 0.1M sodium phosphate buffer were performed for the immobilisation of lipase AK on CTPP-1 and functionalised KCC-1. Due to no significant difference between immobilisation yields when physical adsorption or covalent binding approaches were adopted for the immobilisation of lipase AK on MNP, immobilisation on APTES functionalised KCC-1 was performed only using covalent binding. KCC-1, being mesoporous silica materials require high speed centrifugation for separation from reaction mixture. Recycling the immobilised lipase would require repeated centrifugation which will cause shear stress and therefore leaching of the lipase. Since CTPP-1 do not have reactive groups on their surface for covalent binding, immobilisation was performed only through the physical adsorption method.

Immobilisation yield of lipase AK immobilised on CTPP-1 and APTES functionalised KCC-1 was always greater than 98% irrespective of the pH of the

0.1M sodium phosphate buffer used or the temperature at which immobilisation was performed (Table 4, Entries 1-5).

Table 4: Immobilisation of lipase AK on CTPP-1 and APTES functionalised KCC-1 at different temperatures and varying pH of 0.1M sodium phosphate buffer

Entry	pH of buffer	Immobilisation yield (%)							
		CTPP-1				APTES functionalised KCC-1			
		Physical adsorption				Covalent binding			
		Temperature (°C)				Temperature (°C)			
		25	30	35	40	25	30	35	40
1	6	98.9	99.1	99.2	99.3	98.9	99.1	99.2	99.3
2	6.5	99	99.2	99.5	99.5	99	99.2	99.3	99.5
3	7	99.1	99.5	99.7	99.8	99.2	99.4	99.5	99.6
4	7.5	99.3	99.6	99.8	99.8	99.3	99.6	99.8	99.8
5	8	99.4	99.8	99.9	99.9	99.5	99.7	99.8	99.9

High surface to volume ratios of the support materials, particularly in the case of CTPP-1 and KCC-1 where presence of porous architectures offer area within the pores for immobilisation of lipase AK permitted a large amount of lipase AK to be attached to the supports.

Hereafter lipase AK immobilised on MNP, CTPP-1 and APTES functionalised KCC-1 will be referred to as MNP-iAK, CTPP1-iAK and KCC1-iAK respectively.

Although theoretically all the lipase AK immobilised on the support materials can actively catalyse the reactions, practically, some of the lipase could be inaccessible to the substrate and can lower the activity due to several reasons. To

determine if the high immobilisation yield of lipase AK translated into high enzyme activity, the activity of lipase AK immobilised on MNP, CTPP-1 and functionalised KCC-1 was quantified using the *p*-NPP method.[116]

The activity of lipase AK immobilised on MNP, CTPP-1 and APTES functionalised KCC-1 was found to be 34.2 U/mg (Table 5, Entry 1), 10.4 U/mg (Table 5, Entry 2) and 30.0 U/mg (Table 5, Entry 3) respectively where the enzyme activity unit U is defined as 1 μmole of *p*-nitrophenol released per minute per ml of solution volume.

Table 5: Activity of lipase AK immobilised on MNP, CTPP-1 and APTES functionalised KCC-1 determined by *p*-NPP assay

Entry	Immobilisation support material	Activity of immobilised lipase AK (U/mg)
1	MNP	34.2
2	CTPP-1	10.4
3	APTES functionalised KCC-1	30.0

Table 6 illustrates reports of other immobilised lipase preparations and their activities.

Table 6: Activities of immobilised *Pseudomonas fluorescens* lipases (PFL)

Entry	Lipase	Support	Method of activity determination	Activity	Reference
1	PFL	SBA-15	Triacetin Assay	175 U/g	[127]

2	PFL	SBA-15	Olive oil hydrolysis	5424 U/g	[127]
3	PFL	Multiwalled carbon nanotubes	*p*-NPP assay	615 U/g	[128]
4	PFL	Amberlite	Olive oil hydrolysis	221.6 U/g	[129]
5	PFL	Octyl-silica	Olive oil hydrolysis	650 U/g	[129]
6	PFL	Polystyrene	Olive oil hydrolysis	79.6 U/g	[129]
7	PFL AK	Surface modified SBA-15-R-CHO	pH-stat method	112 μmol min^{-1} mg^{-1}	[130]
8	PFL AK	SBA-15	pH-stat method	375 μmol min^{-1} mg^{-1}	[130]
9	PFL AK	Polysiloxane-Polyvinyl alcohol composite modified with glutaraldehyde	Olive oil hydrolysis	360 U/mg	[131]
10	PFL AK	Polysiloxane-Polyvinyl alcohol composite modified with epichlorohydrin	Olive oil hydrolysis	740 U/mg	[131]
11	PFL	Epoxy-SiO_2-Polyvinyl alcohol reactor bed	Olive oil hydrolysis	2322 U/g	[132]

12	PFL	Fe_3O_4 magnetic nanoparticles	Resolution of 2-octanol	0.197 μmol min^{-1} mg^{-1}	[133]

Table 6 shows that the activity of immobilised *Pseudomonas fluorescens* lipase varies broadly. For instance, *Pseudomonas fluorescens* lipase AK immobilised on glutaraldehyde modified SBA-15 has a specific activity of 112 μmol min^{-1} mg^{-1} when the activity was measured using the pH-stat method (Table 6, Entry 7). Using the same method, the same lipase exhibited activity of 375 μmol min^{-1} mg^{-1} when immobilised on SBA-15 ((Table 6, Entry 8). It shows that both the mode of immobilisation as well as the support play a crucial role in determining the activity of immobilised lipases. When lipase AK was immobilised on Fe_3O_4 magnetic nanoparticles and its activity quantified based on the resolution of 2-octanol, it was found to be 0.197 μmol min^{-1} mg^{-1}(Table 6, Entry 12). This further strengthens the argument that support material and the immobilisation approach play an important role in the activity of lipase. The substrate used to determine the activity of lipases also plays an important role in the activity of lipases. For example, when *Pseudomonas fluorescens* lipase was immobilised on SBA-15 and its activity measured using triacetin assay, the activity was found to be 175 U/g whereas the activity of the same immobilised lipase when measured using olive oil hydrolysis was found to be 5424 U/g (Table 6, Entries 1 and 2). The same lipase when immobilised on multiwalled carbon nanotubes showed 615 U/g activity measured using *p*-NPP assay ((Table 6, Entry 3). Similarly, when *Pseudomonas fluorescens* lipase was immobilised on a reactor bed made of Epoxy-SiO2 and polyvinyl alcohol, the activity was determined to be 2322 U/g

using olive oil hydrolysis method ((Table 6, Entry 11). Lipase AK when immobilised on polysiloxane-polyvinyl alcohol membrane using epichlorohydrin as a linker had activity of 740 U/g ((Table 6, Entry 10) as determined by olive hydrolysis. All things remaining constant, when the linker used was glutaraldehyde, the activity reduced by more than 50% to 360 U/g ((Table 6, Entry 9). This reinforces the idea that the same enzyme can possess different activities based on the reaction environment and is highly dependent on the type of support material, method of immobilisation and the substrate it interacts with. As such, it is difficult to compare the performance of an enzyme under different conditions, unless it is compared to itself in its native form under the same conditions. This would give an idea of the loss or improvement in the activity of the enzyme due to immobilisation and would help quantify the efficiency of immobilisation.

The activity of lipase AK in its free form was determined using the *p*-NPP assay and was found to be 681.66 U/mg. Comparing to this, the activities of lipase AK immobilised on MNP, CTPP-1 and APTES functionalised KCC-1 are lower by 90% (Table 5). This drastic reduction in the activity of the immobilised lipase is hypothesised to be due to the orientation of the lipase such that the *p*-Nitrophenyl Phosphate is easily able to interact with the active site of the free lipase while the active sites on the immobilised lipases are out of reach or in their closed form thus preventing optimum enzyme-substrate interaction. Also, glutaraldehyde sometimes causes a decrease in the activity as a large portion of the surface of the support materials is rendered inaccessible to the lipase for immobilisation.[134] Glutaraldehyde also causes cross-linking of the lipases with each other leading

to a phenomenon called crowding where cross-linked layers of the enzyme cover the surface of the support material. This causes the lipases located inside the crowd to remain inaccessible to the substrate with the lipases on the outer layer also possibly remaining inactive as a result of their orientation and shift to the closed form.[135] However, since the diols and diacetate that are studied in this thesis are synthetic compounds, immobilised lipase AK can interact differently with the substrates and the extent of catalysis needs to be determined.

MNP-iAK, CTPP1-iAK and KCC1-iAK will be used to catalyse the desymmetrisation of *N*-benzyl-5-hydroxy-4-(hydroxymethyl)pentanamide **52** and *N*-benzyl-5-acetoxy-4-(acetoxymethyl)pentanamide **53**, which is discussed in detail in Chapter III.

5. Summary

1) Fe_3O_4 magnetic nanoparticles were successfully synthesised using the co-precipitation method.[117] BET surface area was determined to be 126.7421 m^2/g. SEM and TEM images showed agglomeration of the nanoparticles.
2) Covalent triazine-piperazine linked polymer (CTPP-1) nanoflowers were synthesised using the method reported by Das *et al*.[107] The average particle size was 350 nm and the BET surface area was found to be 779 m^2/g, with pore size of approximately 1.25 nm as inferred from BJH isotherm.
3) Silica nanospheres, KCC-1, were synthesised using the procedure reported by Polshettiwar *et al*.[108]. The uniform sized particles had an

average diameter of 400 nm and a BET surface area of 469.066 m^2/g with mesopores (2-50 nm) as inferred from the BJH isotherm.

4) Immobilisation yields of MNP-iAK, CTPP1-iAK and KCC1-iAK were always >97%. There were no significant effects of pH of 0.1 M sodium phosphate buffer used for immobilisation or the temperature on the immobilisation yields.
5) The activity of lipase AK immobilised on APTES pre-activated Fe_3O_4 magnetic nanoparticles, CTPP-1 and APTES pre-activated KCC-1 were found using *p*-NPP assay[116] to be 34.2 U/mg, 10.4 U/mg and 30.0 U/mg respectively, where, U or 1 enzyme unit is defined as 1 μmole of *p*-nitrophenol released per minute per ml of solution volume.

Chapter III Desymmetrisation of 1,3-diol 52 and 1,3-diacetate 53 using immobilised lipase AK

1. Introduction

Lipases have been used in a variety of reactions due to their stability in organic solvents and mild reaction conditions.[9] The immobilisation of lipases for use in organic solvents is especially advantageous since in addition to the inherent advantages of lipases, it also often increases the catalytic activity of the lipase, permits reuse of the lipase and enables easy purification of the product.[9] One such example is the use of Fe_3O_4 magnetic nanoparticles as supports for the immobilisation of *Pseudomonas fluorescens* lipase by Xun *et al*. to catalyse the resolution of 2-octanol **55**. The product (*R*)-octanol **56** was obtained in 99% *ee* (Scheme 21).[133]

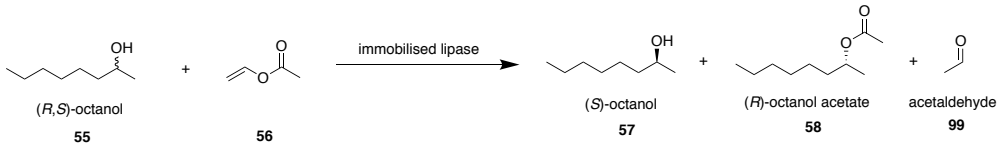

Scheme 21: Resolution of 2-octanol 55 catalysed by immobilised *Pseudomonas fluorescens* lipase[133]

Of our particular interest is the enantioselective acetylation of prochiral and *meso* diols using lipases. We have earlier reported the enantioselective syntheses of the two enantiomeric monoacetate products, (*R*)-**54** and (*S*)-**54**, through acetylation of diol **52** and diacetate **53** respectively.[97] Acetylation of diol **52** using lipase AK in its free form, gave the monoacetate (*R*)-**54** in 93% yield and 92% *ee* (Scheme 22).[97]

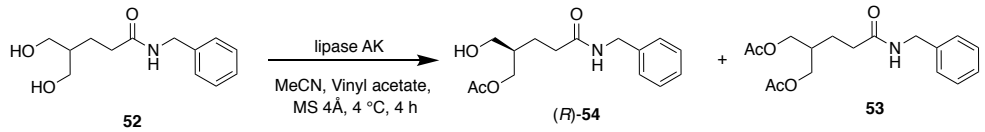

Scheme 22: Acetylation of diol 52 using lipase AK to obtain monoacetate (*R*)-54[97]

On the other hand, hydrolysis of diacetate **53** gave the opposite enantiomer, (*S*)-**54** monoacetate in up to 54% yield and 95% *ee* (Scheme 23).[97]

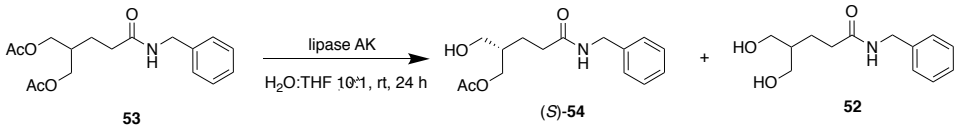

Scheme 23: Hydrolysis of diacetate 53 using lipase AK to obtain monoacetate (*S*)-54[97]

Based on the results obtained using free lipase AK (Scheme 22 and Scheme 23), we expect that immobilised lipase AK can be used successfully to obtain the two enantiomeric monoacetate products, (*R*)-**54** and (*S*)-**54** through the acetylation of diol **52** and the hydrolysis of diacetate **53** respectively, while providing advantages such as recyclability of the lipase and easy product purification.

2. Research Methodologies

Immobilised lipase AK (MNP-iAK, CTPP1-iAK and KCC1-iAK), synthesised using the procedures discussed in Chapter II will be used for the acetylation of diol **52** and hydrolysis of diacetate **53** in an attempt to obtain the enantiomeric monoacetate products, (*R*)-**54** and (*S*)-**54** at the optimal conditions identified for the desymmetrisation reactions, as earlier reported.[97] After optimising reaction parameters such as enzyme loading and time taken for the reaction to reach completion, recyclability tests will be performed based on which the most suitable lipase AK-support material catalyst system will be identified. To detect

any possibility of racemisation during the course of the acetylation reaction, a time-course study will be undertaken. Analogues to the diol **52** will be synthesised and their acetylation will be performed using the identified lipase AK-support material catalyst system. The identified lipase AK-support material catalyst system will be used in the hydrolysis of diacetate **53**.

3. Acetylation of diol 52 catalysed by immobilised lipase AK

3.1 Acetylation of diol 52 catalysed by MNP-iAK

Acetylation of diol **52** was previously performed under different conditions to establish the optimum solvent, temperature and enzyme loading that gave the monoacetate (*R*)-**54** in maximum yield and selectivity (Table 7).[97]

Table 7: Optimisation of acetylation of diol 52[a] using lipase AK[97]

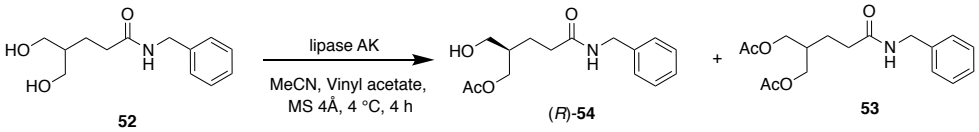

Entry	Solvent	Enzyme loading (mg/mmol **52**)	Vinyl acetate (equiv.)	Temperature (°C)	Time (min)	Monoacetate (*R*)-**54**[b] (%)	Diacetate **53**[b] (%)	*ee*[c] (%)
1	THF	150	10	25	60	80	17	87
2	MTBE	150	10	25	60	75	20	91
3	*i*Pr$_2$O	150	10	25	60	65	20	78
4	Toluene	150	10	25	120	88	0	85
5	$CHCl_3$	150	10	25	120	99	0	85
6	CH_2Cl_2	150	10	25	100	99	0	85
7	Acetone	150	10	25	60	91	0	82
8	MeCN	150	10	25	45	96	0	88
9	MeCN	250	10	25	30	95	0	87
10	MeCN	100	10	25	120	96	0	86
11	MeCN	150	20	25	40	96	0	87
12	MeCN	150	15	25	60	95	0	88

13	MeCN	150	5	25	90	94	0	88
14	MeCN	150	3	25	120	94	0	86
15	MeCN	150	10	4	300	93	0	93
16	MeCN	150	10	0	360	94	0	91

[a]: Diol **52** (0.2 mmol), lipase AK, vinyl acetate, molecular sieves (4 Å, 10 mg), solvent (3.125 ml). [b] Isolated yield

[c]: Measured by HPLC Chiralpak AD-H (Hexane:IPA, 95:5), 0.9 ml/min, 254 nm, t_1: 46.3 min, t_2: 49.8 min

Mixtures of monoacetate (*R*)-**54** and diacetate **53** were produced when ether type solvents THF, MTBE and *i*Pr2O were used. Acetone and MeCN which are polar aprotic solvents gave monoacetate (*R*)-**54** in high yield and enantioselectivity. On the other hand, non-polar solvents CH_2Cl_2 and $CHCl_3$ provided only monoacetate (*R*)-**54** in excellent yields but compared to the polar aprotic solvents, the enantioselectivity was lower. No significant changes were observed when the different lipase loading equivalents of vinyl acetate were used to carry out the desymmetrisation of diol **52** using MeCN as the solvent. When the temperature was decreased to 4 °C and 0 °C, the *ee* improved to 93% and 91% respectively. Since both the yield and *ee* of monoacetate (*R*)-**54** were excellent when MeCN were used as the solvent, with 150 mg/mmol **52** lipase loading and at 4 °C, these conditions were established to be optimum conditions for the desymmetrisation of diol **52**. As such, the same conditions were used for the desymmetrisation of diol **52** using immobilised lipase.

Diol **52** was reacted with vinyl acetate (10 equiv.) in MeCN (64 mM) in the presence of 4 Å molecular sieves at 4 °C. The molecular structure and stereochemistry of the product of this reaction were characterised by NMR and HPLC and found to be in agreement with the results reported in literature.[97]

3.1.1 Optimisation of enzyme loading

There are several factors that come into play upon immobilisation of an enzyme, most importantly transport and diffusion issues. These combined with conformational changes in the enzyme upon immobilisation will either lower or improve the activity of the immobilised enzyme. As such, it is important to determine optimal loading of the enzyme in order to minimise its wastage and to improve the economy of the reaction. Keeping this in mind, the acetylation of diol **52** was performed using MNP-iAK at 4 °C using different enzyme loading. In the first reaction, an enzyme loading of 150 (mg/mmol **52**) was used since it was previously determined to be optimum (Table 7, Entry 15) and monoacetate (*R*)-**54** was obtained in 92% *ee* and 89% yield (Table 8, Entry 1). Since the yield of the monoacetate obtained was lower than that obtained when free lipase AK was used as the catalyst, the enzyme loading was doubled to 300 (mg/mmol **52**). Under these conditions, the monoacetate was collected in 92% *ee* and 98% yield (Table 8, Entry 2). Therefore, further reactions of acetylation of diol **52** were performed under identical conditions using enzyme loading of 300 (mg/mmol **52**).

Table 8: Optimisation of enzyme loading – acetylation of diol 52[a]

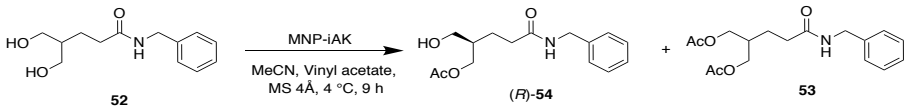

Entry	Enzyme loading (mg/mmol **52**)	Time taken for reaction completion (h)	Monoacetate (*R*)-**54**		Diacetate **53**	Unreacted diol **52**[b]
			Yield[b] (%)	*ee*[b] (%)	Yield[b] (%)	(%)
1	150	9	89	92	1	10
2	300	9	98	92	1	1

[a]: All the reactions were performed on a 0.2 mmol scale of diol **52** in the presence of MNP-iAK loading 300 (mg/mmol **52**), 4 Å molecular sieves using vinyl acetate (10 equiv.) in MeCN (64 mM)

[b]: Measured by HPLC with reference to known concentrations of diol **52**, monoacetates (*R*)-**54** and (*S*)-**54** and diacetate **53**: Chiralpak AS-H (Hexane:IPA, 85:15), 0.9 ml/min, 215 nm, t_1: 21.9 min, t_2: 25.4 min

3.1.2 Time-course study of acetylation of diol 52 by MNP-iAK

To determine if there was racemisation (conversion of one enantiomer to another) or intramolecular acyl migration with time, time-course study of the acetylation of diol **52** catalysed by MNP-iAK at a constant temperature of 4 °C and enzyme loading 300 (mg/mmol **52**) was performed.

Table 9: Time-course study of acetylation of diol 52 by MNP-iAK[a]

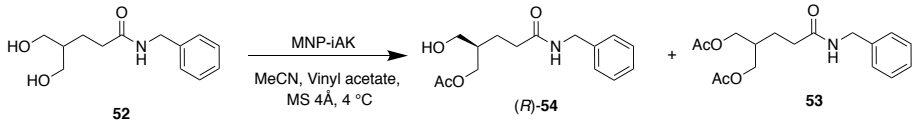

Entry	Time (h)	Monoacetate (*R*)-**54**		Diacetate **53**	Unreacted diol **52**[b] (%)
		Yield[b] (%)	*ee*[b] (%)	Yield[b] (%)	
1	1	38	89	0	62
2	2	48	89	0	52
3	3	58	87	0	42
4	4	64	89	0	36
5	5	76	89	0	24
6	6	85	92	1	14
7	7	89	93	1	10
8	8	95	93	1	4
9	9	98	92	1	1

[a]: All the reactions were performed on a 0.2 mmol scale of diol **52** in the presence of MNP-iAK loading 300 (mg/mmol **52**), 4 Å molecular sieves using vinyl acetate (10 equiv.) in MeCN (64 mM)

[b]: Measured by HPLC with reference to known concentrations of diol **52**, monoacetates (*R*)-**54** and (*S*)-**54** and diacetate **53**: Chiralpak AS-H (Hexane:IPA, 85:15), 0.9 ml/min, 215 nm, t_1: 21.9 min, t_2: 25.4 min

Time-course study of the acetylation of diol **52** catalysed by MNP-iAK at a loading of 300 (mg/mmol **52**) at 4 °C showed gradual increase of yield and *ee* of

monoacetate (*R*)-**54** with time (Table 9). The formation of diacetate **53** started after six hours of the reaction (Table 9, Entry 6) and remained constant even after nine hours of the reaction (Table 9, Entry 9). The enantioselectivity more or less remained constant throughout the reaction. Therefore, it was concluded that there was no racemisation taking place during the course of the reaction.

3.1.3 Recyclability of MNP-iAK determined from study of acetylation of diol 52

One of the major reasons for the immobilisation is to enable recyclability of lipases which offers several advantages, both environmental and economical. Recyclability of the MNP-iAK catalyst system was tested by repeating the acetylation reaction of diol **52** at 300 (mg/mmol **52**) enzyme loading, 4 °C and nine hours of reaction time.

Table 10: Acetylation of diol 52 catalysed by MNP-iAK – Recyclability test[a]

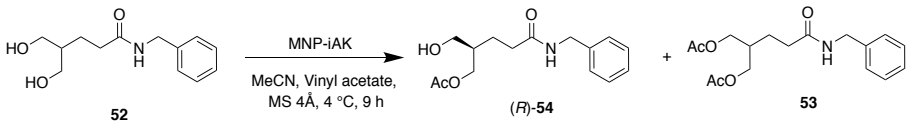

Entry	Number of recycles of MNP-iAK	Monoacetate (*R*)-**54**		Diacetate **53**	Unreacted Diol **52**[b] (%)
		Yield[b] (%)	*ee*[b] (%)	Yield[b] (%)	
1	1	96	87	1	3
2	2	96	87	1	3
3	3	95	87	0	5
4	4	94	88	0	6
5	5	93	87	0	7

[a]: All the reactions were performed on a 0.2 mmol scale of diol **52** in the presence of MNP-iAK loading 300 (mg/mmol **52**), 4 Å molecular sieves using vinyl acetate (10 equiv.) in MeCN (64 mM)
[b]: Measured by HPLC with reference to known concentrations of diol **52**, monoacetates (*R*)-**54** and (*S*)-**54** and diacetate **53**: Chiralpak AS-H (Hexane:IPA, 85:15), 0.9 ml/min, 215 nm, t_1: 21.9 min, t_2: 25.4 min

After the use of MNP-iAK for the enantioselective acetylation of diol **52**, the catalyst was recycled by washing with MeCN and THF (to remove any unreacted diol **52**) three times, vacuum dried, and used for subsequent acetylation reactions of diol **52**. After the first recycle, MNP-iAK catalysed the acetylation of diol **52** providing monoacetate (*R*)-**54** in 96% yield and 87% *ee* and the diacetate **53** in 1% yield (Table 10, Entry 1). In the second recycle, the yield and *ee* of monoacetate (*R*)-**54** remained the same at 96% yield and 87% *ee* (Table 10, Entry 2) While there was no formation of diacetate **53** after the third recycle, the yield of monoacetate (*R*)-**54** reduced to 95% without any decrease in the *ee* (Table 10, Entry 3). After four recycles, the yield of (*R*)-**54** reduced to 94% while the *ee* remained almost the same at 88% (Table 10, Entry 4). Thereafter, in the fifth recycle, an almost similar *ee* of 87% was observed while the yield of the monoacetate (*R*)-**54** reduced to 93% (Table 10, Entry 5). This data proves that MNP-iAK shows promising scope for recyclability and can be used for desymmetrisation of diols without significant loss in activity even up to five recycles.

3.2 Acetylation of diol 52 catalysed by CTPP1-iAK

3.2.1 Optimisation of enzyme loading

Acetylation of diol **52** was performed using CTPP1-iAK at different enzyme loading, 4 °C and 24 hours reaction time. Diol **52** was reacted with vinyl acetate (10 equiv.) in MeCN (64 mM) in the presence of 4 Å molecular sieves.

Table 11: Optimisation of enzyme loading – acetylation of diol 52[a]

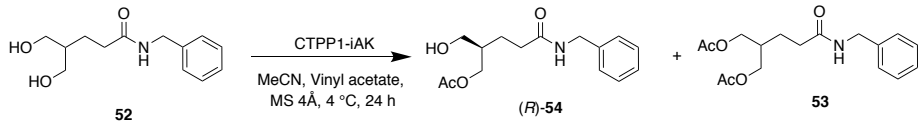

Entry	Enzyme loading (mg/mmol **52**)	Time taken for reaction completion (h)	Monoacetate (*R*)-**54**		Diacetate **53**	Unreacted diol **52**[b] (%)
			Yield[b] (%)	*ee*[b] (%)	Yield[b] (%)	
1	150	24	72	91	1	27
2	300	24	91	91	2	7

[a]: All the reactions were performed on a 0.2 mmol scale of diol **52** in the presence 4 Å molecular sieves using vinyl acetate (10 equiv.) in MeCN (64 mM)

[b]: Measured by HPLC with reference to known concentrations of diol **52**, monoacetates (*R*)-**54** and (*S*)-**54** and diacetate **53**: Chiralpak AS-H (Hexane:IPA, 85:15), 0.9 ml/min, 215 nm, t_1: 21.9 min, t_2: 25.4 min

The acetylation of diol **52** catalysed by CTPP1-iAK was initially performed at a enzyme loading of 150 (mg/mmol **52**). The reaction afforded the monoacetate (*R*)-**54** in a yield of 72% and 91% *ee*, with 1% yield of diacetate **53** after 24 hours of the reaction (Table 11, Entry 1) (Reaction completion was monitored using TLC) at 4 °C. When the reaction was repeated at the same temperature using double the enzyme loading, the yield of (*R*)-**54** increased to 91% while the *ee* remained the same at 91% with diacetate **53** obtained in 2% yield (Table 11, Entry 2). It was thus concluded that an enzyme loading of 300 (mg/mmol **52**), 4 °C and a reaction time of 24 hours were suitable conditions for the acetylation reaction catalysed by CTPP1-iAK.

3.2.2 Time-course study of acetylation of diol 52 by CTPP1-iAK

To determine if there was racemisation with time, time-course study of the acetylation of diol **52** catalysed by CTPP1-iAK at a constant temperature of 4 °C and enzyme loading 300 (mg/mmol **52**) was performed (Table 12).

Table 12: Time-course study of acetylation of diol 52 by CTPP1-iAK[a]

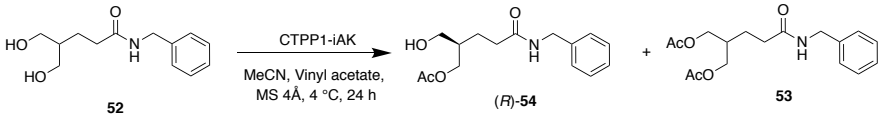

Entry	Time (h)	Monoacetate (*R*)-**54**		Diacetate **53**	Unreacted diol **52**[b]
		Yield[b] (%)	*ee*[b] (%)	Yield[b] (%)	(%)
1	1	23	77	0	77
2	2	31	84	0	69
3	3	36	91	0	64
4	4	47	89	0	53
5	5	60	85	0	40
6	6	74	87	0	26
7	7	81	88	1	18
8	8	82	90	1	17
9	9	84	90	1	15
10	24	91	91	2	7

[a]: All the reactions were performed on a 0.2 mmol scale of diol **52** in the presence of CTPP1-iAK loading 300 (mg/mmol **52**), 4 Å molecular sieves using vinyl acetate (10 equiv.) in MeCN (64 mM)

[b]: Measured by HPLC with reference to known concentrations of diol **52**, monoacetates (*R*)-**54** and (*S*)-**54** and diacetate **53**: Chiralpak AS-H (Hexane:IPA, 85:15), 0.9 ml/min, 215 nm, t_1: 21.9 min, t_2: 25.4 min

Initially the monoacetate (*R*)-**54** was obtained in 23% yield and 77% *ee* (Table 12, Entry 1), and increased to 31% yield and 84% *ee* after two hours of the reaction (Table 12, Entry 2). The yield of monoacetate (*R*)-**54** then gradually increased after three hours of the reaction from 36% to 91% of (*R*)-**54** obtained

after 24 hours of the reaction (Table 12, Entries 3-10) while the enantioselectivity remained the same at 90% *ee* (Table 12, Entries 3-10). It was thus concluded that there was no racemisation of monoacetate (*R*)-**54** during the course of the reaction.

3.2.3 Recyclability of CTPP1-iAK determined from study of acetylation of diol 52

Recyclability of the CTPP1-iAK catalyst system was determined by performing desymmetrisation of diol **52** using the recycled catalyst at an enzyme loading rate of 300 (mg/mmol **52**), 4 °C for 24 hours.

Table 13: Acetylation of diol 52 catalysed by CTPP1-iAK – Recyclability test[a]

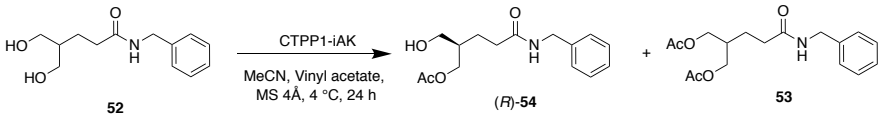

Entry	Number of recycles of CTPP1-iAK	Monoacetate (*R*)-**54**		Diacetate **53**	Unreacted Diol **52**[b] (%)
		Yield[b] (%)	*ee*[b] (%)	Yield[b] (%)	
1	1	80	89	1	19
2	2	75	89	0	25
3	3	74	88	0	26
4	4	37	88	0	63

[a]: All the reactions were performed on a 0.2 mmol scale of diol **52** in the presence of CTPP1-iAK loading 300 (mg/mmol **52**), 4 Å molecular sieves using vinyl acetate (10 equiv.) in MeCN (64 mM)

[b]: Measured by HPLC with reference to known concentrations of diol **52**, monoacetates (*R*)-**54** and (*S*)-**54** and diacetate **53**: Chiralpak AS-H (Hexane:IPA, 85:15), 0.9 ml/min, 215 nm, t_1: 21.9 min, t_2: 25.4 min

Acetylation of diol **52** catalysed by CTPP1-iAK produced monoacetate (*R*)-**54** in moderate yield and enantioselectivity (91% yield and 91% *ee*) (Table 11, Entry 2). After one reaction (Table 13, Entry 1), CTPP1-iAK was recycled to catalyse

the acetylation of diol **52**, and this time the product monoacetate (*R*)-**54** was obtained in 80% yield and 89% *ee*. After the second recycle, the product yield decreased further to 75% while enantioselectivity remained relatively similar at 88% (Table 13, Entry 2). After the third recycle, the product was obtained at a yield of 74% and 90% *ee* (Table 13, Entry 3). At the end of the fourth recycle, the yield of monoacetate (*R)*-**54** drastically reduced to 37% while the enantioselectivity remained at 88% *ee* (Table 13, Entry 4). While there was a decrease in the yield, the enantioselectivity was not affected much with every recycle. The optimal number of recycles in order to maintain a decent yield and enantioselectivity was three cycles. Unlike MNP-iAK, which can be separated using a magnet, the separation of CTPP1-iAK required the use of a nanofilter or centrifugation. Since nanofilters are more expensive and susceptible to loss of some of the catalyst, centrifugation was used to separate the CTPP1-iAK catalyst particles from the reaction mixture during work-up of the reaction. High speed centrifugation is required due to the low density of the CTPP1-iAK particles. However, the stress on the lipase AK, which was immobilised on CTPP1-iAK through physical adsorption, led to leaching of the lipase AK from the support material. This is in addition to conformational changes of lipase AK due to the way in which they are bound to the CTPP1-iAK nanoflowers, that led to loss of some activity.[42]

CTPP1-iAK, though successfully catalysed the desymmetrisation of diol **52**, could not retain its activity over four recycles. Between MNP-iAK and CTPP1-iAK, MNP-iAK clearly has an edge due to its recyclability as well as catalytic capability leading to high yield of the product.

3.3 Acetylation of diol 52 catalysed by KCC1-iAK

3.3.1 Optimisation of enzyme loading

KCC1-iAK was used in the acetylation of diol **52** at different enzyme loading. Diol **52** was reacted with vinyl acetate (10 equiv.) in MeCN (64 mM) in the presence of 4 Å molecular sieves at 4 °C and 24 hours reaction time (reaction completion monitored by TLC).

Table 14: Optimisation of enzyme loading – acetylation of diol 52[a]

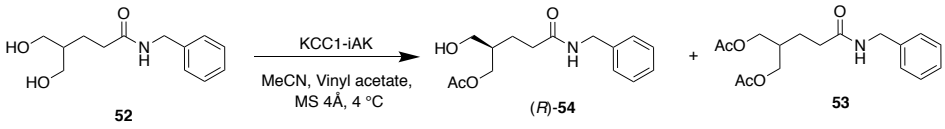

Entry	Enzyme loading (mg/mmol **52**)	Time taken for reaction completion (h)	Monoacetate (*R*)-**54**		Diacetate **53**	Unreacted diol **52**[b] (%)
			Yield[b] (%)	*ee*[b] (%)	Yield[b] (%)	
1	150	24	97	91	1	2
2	300	11	98	92	1	1

[a]: All the reactions were performed on a 0.2 mmol scale of diol **52** in the presence of 4 Å molecular sieves using vinyl acetate (10 equiv.) in MeCN (64 mM)

[b]: Measured by HPLC with reference to known concentrations of diol **52**, monoacetates (*R*)-**54** and (*S*)-**54** and diacetate **53**: Chiralpak AS-H (Hexane:IPA, 85:15), 0.9 ml/min, 215 nm, t_1: 21.9 min, t_2: 25.4 min

At an enzyme loading of 150 (mg/mmol **52**) of KCC1-iAK, the monoacetate (*R*)-**54** was obtained in excellent yield of 97% yield and 91% *ee* after 24 hours of the reaction (Table 14, Entry 1).The reaction was repeated at double the enzyme loading to determine if there was any reduction in the reaction time (Table 14, Entry 2).The reaction reached completion after 11 hours and the monoacetate (*R*)-**54** was obtained in 98% yield and 92% *ee* (Table 14, Entry 2). Thus, an enzyme loading of 150 (mg/mmol **52**) and reaction duration of 11 hours were found to be suitable for the acetylation of diol **52** catalysed by KCC1-iAK.

3.3.2 Time-course study of acetylation of diol 52 by KCC1-iAK

To determine if there was racemisation with time, time-course study of the acetylation of diol **52** catalysed by KCC1-iAK at a constant temperature of 4 °C and enzyme loading 300 (mg/mmol **52**) was performed (Table 15).

Table 15: Time-course study of acetylation of diol 52 by KCC1-iAK[a]

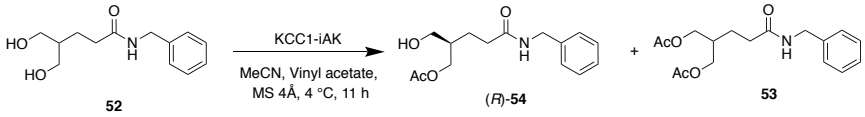

Entry	Time (h)	Monoacetate (*R*)-**54**		Diacetate **53**	Unreacted diol **52**[b]
		Yield[b] (%)	*ee*[b] (%)	Yield[b] (%)	(%)
1	1	30	81	0	70
2	2	48	83	0	52
3	3	60	86	0	40
4	4	71	88	0	29
5	5	73	88	0	27
6	6	78	87	0	22
7	7	80	90	1	19
8	8	84	90	1	15
9	9	91	90	1	8
10	11	98	92	1	1

[a]: All the reactions were performed on a 0.2 mmol scale of diol **52** in the presence of KCC1-iAK loading 300 (mg/mmol **52**), 4 Å molecular sieves using vinyl acetate (10 equiv.) in MeCN (64 mM)

[b]: Measured by HPLC with reference to known concentrations of diol **52**, monoacetates (*R*)-**54** and (*S*)-**54** and diacetate **53**: Chiralpak AS-H (Hexane:IPA, 85:15), 0.9 ml/min, 215 nm, t_1: 21.9 min, t_2: 25.4 min

The initial enantioselectivity of the product was 81% *ee* (Table 15, Entry 1). The enantioselectivity then gradually increased after three hours of the reaction to reach 92% *ee* (Table 15, Entries 2-10). Simultaneously, there was also a steady

increase in the yield of the monoacetate (*R*)-**54** obtained (Table 15, Entries 2-10), probably due to the reaction reaching a steady state. There was no decrease in the *ee* during the course of the reaction. It was thus concluded that there was no racemisation during the course of the reaction.

3.3.3 Recyclability of KCC1-iAK determined from study of acetylation of diol 52

Recyclability of the KCC1-iAK catalyst system was determined by performing desymmetrisation of diol **52** using the recycled catalyst at an enzyme loading rate of 300 (mg/mmol **52**) at 4 °C for 24 hours.

Table 16: Acetylation of diol 52 catalysed by KCC1-iAK – Recyclability test[a]

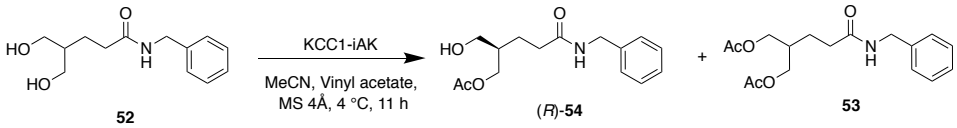

Entry	Number of recycles of KCC1-iAK	Monoacetate (*R*)-**54**		Diacetate **53**	Unreacted Diol **52**[b] (%)
		Yield[b] (%)	*ee*[b] (%)	Yield[b] (%)	
1	1	88	90	1	11
2	2	72	89	0	28
3	3	68	88	0	32
4	4	66	89	0	34

[a]: All the reactions were performed on a 0.2 mmol scale of diol **52** in the presence of KCC1-iAK loading 300 (mg/mmol **52**), 4 Å molecular sieves using vinyl acetate (10 equiv.) in MeCN (64 mM)

[b]: Measured by HPLC with reference to known concentrations of diol **52**, monoacetates (*R*)-**54** and (*S*)-**54** and diacetate **53**: Chiralpak AS-H (Hexane:IPA, 85:15), 0.9 ml/min, 215 nm, t_1: 21.9 min, t_2: 25.4 min

While the desymmetrisation of diol **52** produced monoacetate (*R*)-**54** in 98% yield and 92% *ee* (Table 15, Entry 10) and 1% yield of diacetate **53**, after using KCC1-iAK recycled once, the yield of monoacetate (*R*)-**54** reduced to 88% with 90% *ee* (Table 16, Entry 1). The yield further reduced to 72% and 88% *ee* after the second recycle (Table 16, Entry 2) with no formation of diacetate **53**. After four recycles, KCC1-iAK catalysed the desymmetrisation of diol **52** to provide the monoacetate (*R*)-**54** in 66% yield and 89% *ee* (Table 16, Entry 4). Similar to CTPP1-iAK, separation was an issue with KCC1-iAK as the material is of low density and requires high centrifugation speeds. Though there was a decrease in yield of (*R*)-**54** with every recycle, *ee* almost remained constant. It is due to a loss of lipase resulting from shear stress which caused leaching of lipase AK from the surface of functionalized KCC-1.[43, 111] Inactivation of lipase AK is ruled out since the enantioselectivity of the reaction remained almost constant.

The time taken and lipase loading for the acetylation of diol **52** and the recyclability of the immobilised lipase varies greatly among the three immobilised lipases MNP-iAK, CTPP1-iAK and KCC1-iAK and also compared to free lipase AK. This is mainly because of the way the immobilised lipase AK interacts with its microenvironment. Unlike free enzymes which are dependent on the bulk concentration, immobilised enzymes are dependent on the surface concentration. The activity of an immobilised enzyme depends on the nature of the immobilisation support, the type of substrate, the solvent used, the temperature at which the reaction is taking place, the method of immobilisation, the pH at which the reaction is being maintained, presence or absence of water and if it is recycled, the method of recycling. As such, the reaction kinetics are

much more complicated than those of free enzymes. Also, issues such as diffusion limitations arise that are usually not easy to solve unless detailed computational and kinetic studies are performed. For example, support materials that subject the immobilised lipase to low conformational strain and allow it to exist in the open form are preferred since they offer high thermal stability to the lipase and increase its activity.[123] In case of lipase in its free form, the amount of water added to the reaction affects the *ee* of the product which is not the case with immobilised lipases.[136] Also, enzymatic reactions performed at lower temperatures are much more stereospecific than those performed at higher temperatures since the former prevent unnecessary side reactions and undesired by-product formation from occurring.

Ionic liquids can be used to improve the activity of immobilised lipases. The use of ionic liquids is advantageous since they have negligible vapour pressure and not flammable thereby rendering them environmentally benign. Their properties can be tailored by choosing appropriate anions and cations that can help maintain desired physicochemical conditions. Although highly polar in nature and are natural solvents for hydrophilic substrates, their organic part also helps dissolve hydrophobic substrates.[48] Similarly, supercritical fluids have gained attention in enzymatic esterification because they improve mass transfer of the reactants and products as their properties such as viscosity and diffusivity are similar to those of gases. Supercritical carbon dioxide in particular, is attractive because its critical temperature (31.1 ºC) allows easy evaporation and regeneration from the reaction mixture once the pressure is reduced to atmospheric value.[48]

4. Identification of suitable support material for lipase AK immobilisation

To identify the suitable support material among MNPs, CTPP-1 and functionalised KCC-1, for lipase AK immobilisation, the results of acetylation reactions of diol **52** catalysed by the various immobilised lipase AK catalyst systems were compared with the results of the acetylation of diol **52** catalysed by free lipase AK.

Table 17: Screening for the most suitable support material lipase AK immobilisation[a]

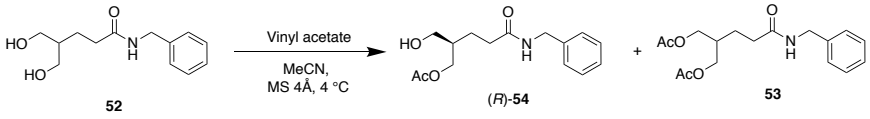

Entry	Catalyst	Enzyme loading (mg/mmol **52**)	Time (h)	Monoacetate (*R*)-**54**			
				Yield[b] (%)	*ee*[b] (%)	Yield[b] after four recycles (%)	*ee*[b] after four recycles (%)
1	MNP-iAK	300	9	98	92	94	88
2	CTPP1-iAK	300	24	91	91	37	88
3	KCC1-iAK	300	11	98	92	66	89

[a]: All the reactions were performed on a 0.2 mmol scale of diol **52** in the presence of 4 Å molecular sieves using vinyl acetate (10 equiv.) in MeCN (64 mM)

[b]: Measured by HPLC with reference to known concentrations of diol **52**, monoacetates (*R*)-**54** and (*S*)-**54** and diacetate **53**: Chiralpak AS-H (Hexane:IPA, 85:15), 0.9 ml/min, 215 nm, t_1: 21.9 min, t_2: 25.4 min

MNP-iAK at an enzyme loading of 300 (mg/mmol **52**) catalysed the desymmetrisation of diol **52** in nine hours to produce monoacetate (*R*)-**54** in 98% yield and 92% *ee* (Table 17, Entry 1). After four recycles, MNP-iAK still demonstrated excellent activity and produced (*R*)-**54** in 94% yield and 88% *ee* (Table 17, Entry 1). In comparison with MNP-iAK, the acetylation of diol **52** not only required 24 hours for completion when catalysed by CTPP1-iAK but

produced a relatively lower yield at 91% (Table 17, Entry 2). After four recycles, the catalytic activity of CTPP1-iAK decreased tremendously to afford monoacetate (*R*)-**54** in 37% yield and 88% *ee* (Table 17, Entry 2). KCC1-iAK demonstrated excellent catalytic activity comparable to MNP-iAK, producing (*R*)-**54** in 98% yield and 92% *ee* in 11 hours of reaction (Table 17, Entry 3). However, it could not retain its activity after four recycles, with the yield of the monoacetate product (*R*)-**54** decreasing to 66% and 89% *ee* after the fourth recycle (Table 17, Entry 3). MNP-iAK thus proved to be the best choice for lipase AK immobilisation, among the three support materials investigated, since it not only catalysed the desymmetrisation of diol **52** to give (*R*)-**54** in high yield and *ee*, but it also demonstrated good recyclability. Therefore, MNP-iAK was used as the catalyst to study the desymmetrisation of analogues of diol **52** as well as the hydrolysis of diacetate **53**.

5. Synthesis and acetylation of analogues of diol 52

Takabe *et al*. investigated the acetylation of different 1,3-diols that are analogues to diol **52**. They reported an interesting dependency of stereospecificity to the *C2*-substituent of the diols and how a small change in the amide group caused complete stereochemical inversion in the acetylated product.[137]

Therefore, based on the literature, analogues of diol **52** were synthesised and acetylated using MNP-iAK to determine change in the stereospecificity with the variation of the *C2*-substituent of the diols, particularly, the amide group.

5.1 Synthesis and acetylation of 5-hydroxy-4-(hydroxymethyl)-*N*-phenylpentanamide 61

5.1.1 Synthesis of 5-hydroxy-4-(hydroxymethyl)-*N*-phenylpentanamide 61

The synthesis of 5-hydroxy-4-(hydroxymethyl)-*N*-phenylpentanamide **61** was performed using a similar sequence strategy used to synthesise diol **52**. Reaction of acid **50** with aniline gave the amide product **60**, which was then reduced using $LiBH_4$ to give diol **61** as a yellow solid in 45 % yield, m.p. 86.5-87.3 °C.

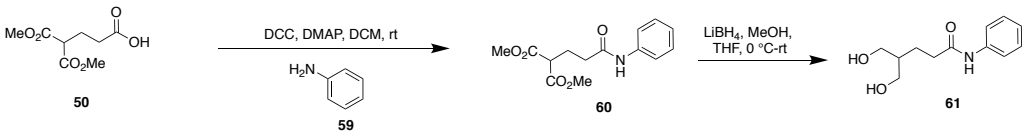

Scheme 24: Synthesis of diol 61

High resolution ESI-MS showed a molecular ion *m/z* value of 224.1298 corresponding to $[M+H]^+$ thus supporting the formula $C_{12}H_{17}NO_3$ (*m/z* calcd. for $C_{12}H_{17}NO_3$ $[M+H]^+$: 223.2676. The FTIR spectrum of the solid showed an absorption band at 1660 cm^{-1} corresponding to the amide C=O. The ^1H NMR spectrum showed aromatic proton signals at δ 6.91-6.96 (1H), δ 7.12-7.18 (2H) and δ 7.38 (2H) indicating the presence of phenyl ring. The ^{13}C NMR spectrum showed the characteristic carbon signals at δ 63.5 confirming the reduction of the diester groups and δ 179.8 corresponding to the amide group. Therefore, the diol was assigned the structure **61**.

5.1.2 Acetylation of diol 61

Acetylation of diol **61** was carried out using Ac_2O in DCM and the monoacetate product was purified using column chromatography (100% EA) to give a viscous oil in 63% yield. The FTIR spectrum of the oil revealed a peak at 1719 cm^{-1} that

corresponds to the absorption band of the C=O moiety. High resolution ESI-MS spectrum showed a molecular ion *m/z* value of 266.1389 corresponding to $[M+H]^+$ thus supporting the molecular formula $C_{14}H_{19}NO_4$ (*m/z* calcd. for $C_{14}H_{19}NO_4$ $[M+H]^+$: 265.3042). In comparison with ^1H NMR of its starting material diol **61**, the ^1H NMR of the oil revealed a proton signal corresponding to the acetyl moiety at δ 2.01 (1H). ^{13}C NMR showed the characteristic carbon signals of the acetyl moiety at δ 20.94 and δ 171.52 corresponding to the carbonyl carbon from methyl acetoxy moiety, confirming the acetylation of the hydroxyl group. Therefore, the monoacetate product was assigned the structure **62** (Figure 18).

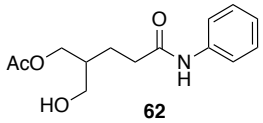

62

Figure 18: Monoacetate 62

Acetylation of diol **61** was performed using free lipase AK as well as MNP-iAK to determine the enantioselectivity and yield.

Table 18: Acetylation of diol 61[a]

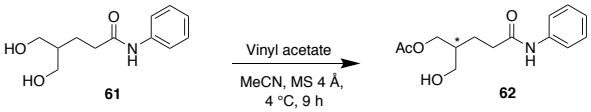

Entry	Catalyst	Monoacetate **62**	
		Yield[b] (%)	*ee*[b] (%)
1	Lipase AK	73	44
2	MNP-iAK	30	56

[a]: All the reactions were performed on a 0.2 mmol scale of diol **61** in the presence of 4 Å molecular sieves using vinyl acetate (10 equiv.) in MeCN (64 mM) with enzyme loading 300 (mg/mmol **61**)

[b]: Measured by HPLC Chiralpak AS-H (Hexane:IPA, 85:15), 0.7 ml/min, 215 nm, t_1: 18.67 min, t_2: 21.09 min

Acetylation of diol **61** by lipase AK in its native form, gave the monoacetate product **62** in 73% yield and 44% *ee* (Table 18, Entry 1). Under the same conditions, when MNP-iAK was used to catalyse the reaction, the monoacetate **62** was obtained in 30% yield and 56% *ee* (Table 18, Entry 2). This lowering of the enantioselectivity compared to that observed during acetylation of diol **52**, could be attributed to the change in the amide group of the *C2*-substitutent of 1,3-diol.

The monoacetate **62** showed optical rotation value of $[\alpha]_D^{19}$ = + 0.58 (*c* = 0.009, CH_2Cl_2) and therefore was assigned (+)-**62**.

5.2 Synthesis and acetylation of *N*-benzyl-4-hydroxy-3-(hydroxymethyl)butanamide 66

5.2.1 Synthesis of diol 66

Wittig reaction of 1,3-dihydroxyacetone **63** with a triphenylphosphine compound provided hydroxymethylbutanolide **64** which was double hydrogenated to obtain hydroxymethylbutanolide **65**. Reaction of **65** with benzylamine provided diol **66** in 72% yield.

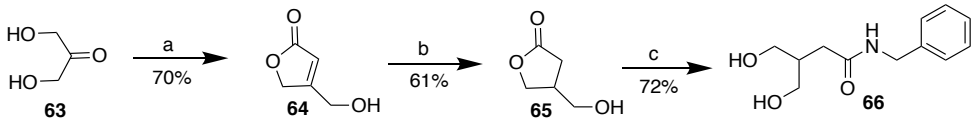

Scheme 25: Synthesis of diol 66

High resolution ESI-MS showed a molecular ion *m/z* value of 224.1300 corresponding to $[M+H]^+$ thus supporting the formula $C_{12}H_{17}NO_3$ (*m/z* calcd. for $C_{12}H_{17}NO_3$ $[M+H]^+$: 223.2676. The ^1H NMR spectrum showed aromatic proton

signals at δ 7.13-7.21 (5H) indicating the presence of phenyl ring and characteristic peaks at δ 1.99-2.07 (m, 1H) and δ 3.46-3.48 (m, 4H). The ^{13}C NMR spectrum showed the carbon signal of -*C*H_2OH at δ 64.77 ppm and at δ 176.61 corresponding to the amide carbonyl carbon -*C*ONHBn . Therefore, the diol was assigned the structure **66**.

5.2.2 Acetylation of diol 66

Acetylation of diol **66** using Ac_2O in DCM provided monoacetate product which was purified using column chromatography (EA:Hexane 1:1) to give a viscous oil in 74% yield. High resolution ESI-MS spectrum showed a molecular ion *m/z* value of 266.1395 corresponding to $[M+H]^+$ thus supporting the molecular formula $C_{14}H_{19}NO_4$ (*m/z* calcd. for $C_{14}H_{19}NO_4$ $[M+H]^+$: 265.3042). In comparison with ^1H NMR of its starting material diol **66**, the ^1H NMR of the oil revealed a proton signal corresponding to the acetyl moiety at δ 1.94-1.99 (m, 3H). ^{13}C NMR showed the characteristic carbon signals of the acetyl moiety at δ 20.02 and δ 170.24 corresponding to the carbonyl carbon from methyl acetoxy moiety, confirming the acetylation of the hydroxyl group. Therefore, the monoacetate product was assigned the structure **67** (Figure 19).

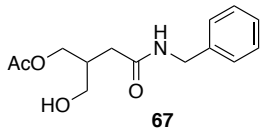

67

Figure 19: Monoacetate 67

Acetylation of diol **66** was performed using free lipase AK as well as MNP-iAK to determine the enantioselectivity and yield of monoacetate **67**.

Table 19: Acetylation of diol 66[a]

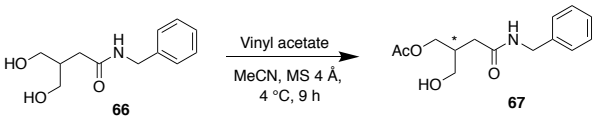

Entry	Catalyst	Monoacetate **67**	
		Yield[b] (%)	*ee*[b] (%)
1	Lipase AK	61	78
2	MNP-iAK	29	50

[a]: All the reactions were performed on a 0.2 mmol scale of diol **66** in the presence of 4 Å molecular sieves using vinyl acetate (10 equiv.) in MeCN (64 mM) with enzyme loading 300 (mg/mmol **66**)
[b]: Measured by HPLC Chiralpak AS-H (Hexane:IPA, 85:15), 0.7 ml/min, 215 nm, t_1: 47.5 min, t_2: 50.6 min

Lipase AK was used to catalyse the acetylation of diol **66** at 4 °C in MeCN, using vinyl acetate as acetylating agent in the presence of 4 Å molecular sieves. After nine hours of reaction, monoacetate **67** was obtained in 61% yield and 78% *ee* (Table 19, Entry 1). When the reaction was repeated at the same conditions using MNP-iAK as the catalyst, there was a decrease in both the yield and enantioselectivity, with the monoacetate product **67** collected in 29% yield and 50% *ee*.

Optical rotation value of the monoacetate **67** was observed to be $[\alpha]_D^{19}$ = -0.65 (*c* = 0.015, CH_2Cl_2) and therefore it was assigned monoacetate (-)-**67**.

5.3 Synthesis and acetylation of 5-hydroxy-4-(hydroxymethyl)-*N*-(4-methoxybenzyl)pentanamide 70

Diols **61** and **66** had *C2*-substituents of the same length with different amide groups and position of the carbonyl moiety. This difference was pronounced in their optical rotation values with the monoacetates **62** and **67** displaying opposite

stereochemistry. Diol **70** will be synthesised to determine the effect of a bulkier amide group on the stereochemistry of the acetylation reaction.

5.3.1 Synthesis of diol 70

Steglich esterification of acid **50** with 4-Methoxybenzylamine **68** produced amide **69** which was then reduced using $LiBH_4$ to provide diol **70** in 71% yield (Scheme 26).

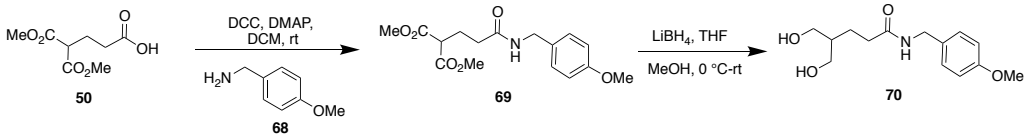

Scheme 26: Synthesis of diol 70

High resolution ESI-MS spectrum showed a molecular ion *m/z* value of 266.1389 corresponding to $[M+H]^+$ thus supporting the molecular formula $C_{14}H_{19}NO_4$ (*m/z* calcd. for $C_{14}H_{19}NO_4$ $[M+H]^+$: 265.3042). FTIR spectrum showed absorption band at 1631 cm^{-1} corresponding to the amide C=O. ^1H NMR did not show any ester signals while the signals from the aromatic group remained as such. A doublet at δ 3.50-3.51 (d, *J*=5.4 Hz, 4H) was observed which accounted for the -*C*H_2OH groups. ^{13}C NMR indicated a carbon signal at δ 64.76 corresponding to the -*C*H_2OH. The compound was therefore assigned the structure **70** (Scheme 26).

5.3.2 Acetylation of diol 70

Acetylation of diol **70** with Ac_2O in DCM provided a viscous oil which was purified by column chromatography (EA:Hexane, 1:1) to obtain the monoacetate

product in 67% yield. FTIR spectra indicated a sharp peak at 1731 cm^{-1} that corresponds to the acetoxy group. ^{1}H NMR showed proton signal at δ 1.95-1.97 (s, 3H) indicating successful acetylation of the hydroxyl group. The $^{1}3C$ NMR spectrum indicated a carbon signal at δ 172.69 corresponding to the carbonyl carbon from the methyl acetoxy moiety. Thus, the compound was assigned structure **71**.

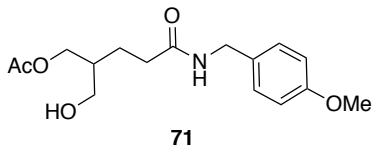

71

Figure 20: Monoacetate 71

Acetylation of diol **70** was performed using lipase AK in its native form and MNP-iAK to determine the yield and enantioselectivity of the monoacetate product.

Table 20: Acetylation of diol 70[a]

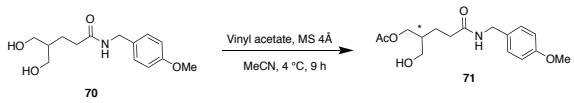

Entry	Catalyst	Monoacetate **71**	
		Yield[b] (%)	*ee*[b] (%)
1	Lipase AK	98	63
2	MNP-iAK	98	80

[a]: All the reactions were performed on a 0.2 mmol scale of diol **70** in the presence of 4 Å molecular sieves using vinyl acetate (10 equiv.) in MeCN (64 mM) with enzyme loading 300 (mg/mmol **70**)
[b]: Measured by HPLC Chiralpak OD-H (Hexane:IPA, 85:15), 0.7 ml/min, 215 nm, t_1: 21.9 min, t_2: 25.4 min

Acetylation of diol **70** provided monoacetate **71** in 98% yield and 63% *ee* when lipase AK was used in its native form as a catalyst. The monoacetate product **71**

was obtained in 98% yield and 80% *ee* when MNP-iAK was used as a catalyst. Compared to the monoacetate products of other analogues of diol **52** - diol **61** and diol **66** that were investigated before, the monoacetate **71** is obtained in a much higher yield and enantioselectivity.

Optical rotation value of the monoacetate was found to be $[\alpha]_D^{19}$ = + 14.69 (*c* = 0.009, CH_2Cl_2). Therefore, the monoacetate was assigned (+)-**71**.

5.4 Synthesis and acetylation of 5-hydroxy-4-(hydroxymethyl)-*N*-phenethylpentanamide 74

To investigate the effect of a long chain amide group of *C2*-substituent on the stereoselectivity of the monoacetate product of the diol, diol **74** will be synthesised.

5.4.1 Synthesis of diol 74

Steglich esterification of acid **50** with phenethylamine gave the amide product **73** which was reduced using $LiBH_4$ to provide diol **74** in 70% yield.

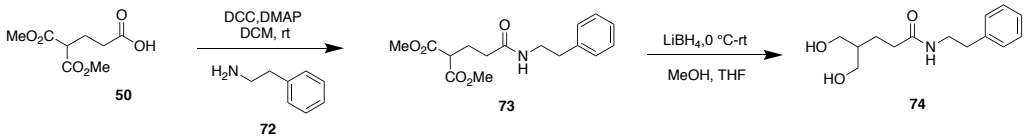

Scheme 27: Synthesis of diol 74

High resolution ESI-MS spectrum showed a molecular ion *m/z* value of 252.1593 corresponding to $[M+H]^+$ thus supporting the molecular formula $C_{14}H_{21}NO_3$ (*m/z* calcd. for $C_{14}H_{21}NO_3$ $[M+H]^+$: 251.3206). FTIR spectrum showed absorption band at 1629 cm^{-1} corresponding to the amide C=O. ^1H NMR did not show any ester signals while the signals from the aromatic group remained as such. A

doublet at δ 3.47-3.49 (d, *J*=6 Hz, 4H) was observed which accounted for the -*C*H_2OH groups. ^{13}C NMR indicated a carbon signal at δ 64.77 corresponding to the -*C*H_2OH. The compound was therefore assigned the structure **74** (Scheme 27).

5.4.2 Acetylation of diol 74

Acetylation of diol **74** with Ac_2O in DCM provided a pale yellow oil which was purified by column chromatography (EA:Hexane, 1:1) to obtain the monoacetate product in 63% yield. FTIR spectra indicated a sharp peak at 1729 cm^{-1} that corresponds to the acetoxy group. ^{1}H NMR showed proton signal at δ 2.09 (s, 3H) indicating successful acetylation of the hydroxyl group. The ^{13}C NMR spectrum indicated a carbon signal at δ 171.52 corresponding to the carbonyl carbon from the methyl acetoxy moiety. Thus, the compound was assigned structure **75**.

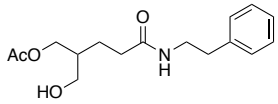

75

Figure 21: Monoacetate 75

Acetylation of diol **74** was performed using lipase AK in its native form and MNP-iAK to determine the yield and enantioselectivity of the monoacetate product.

Table 21: Acetylation of diol 74[a]

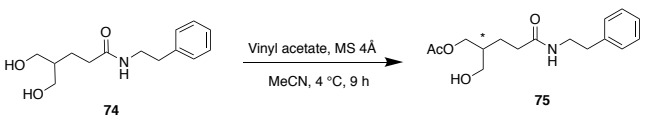

74 **75**

Entry	Catalyst	Monoacetate **75**

		Yield[b] (%)	*ee*[b] (%)
1	Lipase AK	89	69
2	MNP-iAK	36	44

[a]: All the reactions were performed on a 0.2 mmol scale of diol **74** in the presence of 4 Å molecular sieves using vinyl acetate (10 equiv.) in MeCN (64 mM) with enzyme loading 300 (mg/mmol **74**)
[b]: Measured by HPLC Chiralpak AD-H (Hexane:IPA, 80:20), 0.7 ml/min, 215 nm, t_1: 9.6 min, t_2: 10.2 min

Acetylation of diol **74** provided monoacetate **75** in 89% yield and 69% *ee* (Table 21, Entry 1) when lipase AK was used in its native form as a catalyst. The monoacetate product **75** was obtained in 36% yield and 44% *ee* when MNP-iAK was used as a catalyst (Table 21, Entry 2).

Optical rotation value of the monoacetate was found to be $[\alpha]_D^{20} = +6.673$ (c = 0.010, CH_2Cl_2). Therefore, the monoacetate was assigned (+)-**75**.

5.5 Synthesis and acetylation of *N*-(3,4-dimethoxyphenethyl)-5-hydroxy-4-(hydroxymethyl)pentanamide 78

Following the synthesis and acetylation of diol **74**, the synthesis of diol **77** was attempted since it has a longer and bulkier amide group of the *C2*-substituent.

5.5.1 Synthesis of diol 78

Acid **50** was reacted with 3,4-Dihydroxyphenethylamine **76** through Steglich esterification to provide the amide **77** which was then reduced to give the diol **78** (Scheme 28).

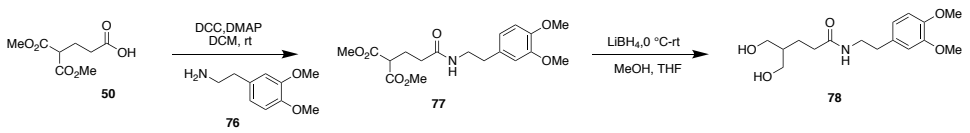

Scheme 28: Synthesis of diol 78

High resolution ESI-MS spectrum showed a molecular ion *m/z* value of 312.1819 corresponding to $[M+H]^+$ thus supporting the molecular formula $C_{16}H_{25}NO_5$ (*m/z* calcd. for $C_{16}H_{25}NO_5$ $[M+H]^+$: 311.3724). FTIR spectrum showed absorption band at 1629 cm^{-1} corresponding to the amide C=O. ^1H NMR in methanol-*d4* did not show any ester signals while the signals from the aromatic group remained as such at δ 6.72-6.75 (d, *J*=10.2 Hz, 1H), δ 6.82-6.86 (d, *J*=13.5 Hz, 2H. ^{13}C NMR indicated a carbon signal at δ 64.77 corresponding to the -CH_2OH. The compound was therefore assigned the structure **78** (Scheme 28).

5.5.2 Acetylation of diol 78

Acetylation of diol **78** with Ac_2O in DCM provided a colourless oil which was purified by column chromatography (EA:Hexane, 1:1) to obtain the monoacetate product in 61% yield. FTIR spectra indicated a sharp peak at 1729 cm^{-1} that corresponds to the acetoxy group. ^1H NMR showed proton signal at δ 2.09 (s, 3H) indicating successful acetylation of the hydroxyl group. The ^{13}C NMR spectrum indicated a carbon signal at δ 172.10 corresponding to the carbonyl carbon from the methyl acetoxy moiety. Thus, the compound was assigned structure **79** (Figure 22).

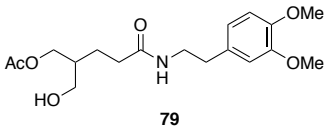

79

Figure 22: Monoacetate 79

Acetylation of diol **78** was performed using lipase AK in its native form and MNP-iAK to determine the yield and enantioselectivity of the monoacetate product.

Table 22: Acetylation of diol 78[a]

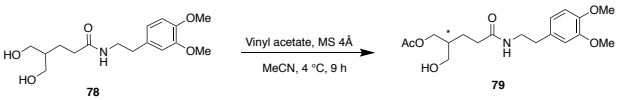

78 79

Entry	Catalyst	Monoacetate **79**	
		Yield[b] (%)	*ee*[b] (%)
1	Lipase AK	98	74
2	MNP-iAK	29	75

[a]: All the reactions were performed on a 0.2 mmol scale of diol **78** in the presence of 4 Å molecular sieves using vinyl acetate (10 equiv.) in MeCN (64 mM) with enzyme loading 300 (mg/mmol **78**)
[b]: Measured by HPLC Chiralpak AD-H (Hexane:IPA, 80:20), 0.7 ml/min, 215 nm, t_1: 18.7 min, t_2: 20.5 min

Acetylation of diol **78** provided monoacetate **79** in 98% yield and 74% *ee* when lipase AK was used in its native form as a catalyst (Table 22, Entry 1). The monoacetate product **79** was obtained in 29% yield and 75% *ee* when MNP-iAK was used as a catalyst (Table 22, Entry 2).

Optical rotation value of the monoacetate was found to be $[\alpha]_D^{20} = +4.464$ (*c* = 0.009, CH_2Cl_2). The monoacetate was therefore assigned (+)-**79**.

As such, it is concluded that there was no specific variation of stereochemistry of the monoacetate observed with changing the *C2*-substituent, especially the amide group.

6. Hydrolysis of diacetate 53

While acetylation of diol **52** provides monoacetate (*R*)-**54**, its enantiomer (*S*)-**54** can be obtained by the hydrolysis of diacetate **53**. When catalysed by lipase AK in its native form, the hydrolysis of diacetate **53** produced monoacetate (*S*)-**54** in 92% *ee* and 54% yield.[97] Since immobilisation improves the stability and activity of lipase in organic solvents, particularly at the aqueous-organic interface, MNP-iAK will be used to catalyse the hydrolysis of diacetate **53** with an aim to improve the yield of the monoacetate (*S*)-**54** compared with the yield obtained when lipase AK was used in its free form.

6.1 Optimisation of enzyme loading

Since diacetate **53** is a different substrate and its interaction with MNP-iAK differs from that of desymmetrisation of diol **52**, hydrolysis of diacetate **53** was performed at different enzyme loading of MNP-iAK in the presence of buffer with THF as the co-solvent at room temperature.

Table 23: Optimization of enzyme loading – hydrolysis of diacetate 53[a]

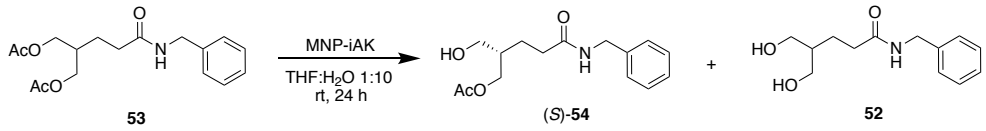

Entry	pH of buffer	Enzyme loading (mg/mmol **53**)	Monoacetate (*S*)-**54**		Diol **52**	Unreacted diacetate **53** (%)
			Yield[b] (%)	*ee*[b] (%)	Yield[b] (%)	
1	7	300	37	80	10	53
2	7	450	57	91	11	32

[a]: All the reactions were performed on a 0.2 mmol scale of diacetate **53** at room temperature in the presence of THF: H_2O 1:10

[b]: Measured by HPLC with reference to known concentrations of diol **52**, monoacetates (*R*)-**54** and (*S*)-**54** and diacetate **53**: Chiralpak AS-H (Hexane:IPA, 85:15), 0.9 ml/min, 215 nm, t_1: 21.9 min, t_2: 25.4 min

Hydrolysis of diacetate **53** using buffer of pH 7 and enzyme loading of 300 (mg/mmol **53**) provided monoacetate (*S*)-**54** in 37% yield and 80% *ee* and diol **52** in 10% yield (Table 23, Entry 1). When the reaction was repeated under the same conditions using enzyme loading of 450 (mg/mmol **53**), the yield and enantioselectivity of the monoacetate (*S*)-**54** obtained increased to 57% yield and 91% *ee* respectively while the yield of diol **52** was 11% (Table 23, Entry 2). Further hydrolysis of diacetate **53** using MNP-iAK will be performed using enzyme loading of 300 (mg/mmol **53**).

6.2 Optimisation of pH of buffer

Since there is a scope for improvement of the yield of monoacetate (*S*)-**54**, the hydrolysis reaction was performed using buffers of different pH to investigate any possible effect of pH on the yield of the monoacetate product. Also, the protonation state of the lipase determines its extent of activity in aqueous reactions. The buffer will allow maintenance of the active state of the enzyme and will mitigate loss or reduction of catalytic activity.[9]

Table 24: Optimisation of pH of buffer – hydrolysis of diacetate 53[a]

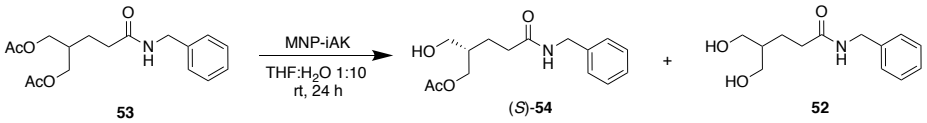

53

Entry	pH of buffer	Monoacetate (*S*)-**54**		Diol **52**	Unreacted diacetate **53** (%)
		Yield[b] (%)	*ee*[b] (%)	Yield[b] (%)	
1	6	54	90	10	36
2	6.5	54	90	9	37
3	7	57	91	11	32

4	7.5	53	90	13	34
5	8	35	57	20	45

[a]: All the reactions were performed on a 0.2 mmol scale of diacetate **53** at room temperature in the presence of THF: H_2O 1:10 and enzyme loading 450 (mg/mmol **53**)

[b]: Measured by HPLC with reference to known concentrations of diol **52**, monoacetates (*R*)-**54** and (*S*)-**54** and diacetate **53**: Chiralpak AS-H (Hexane:IPA, 85:15), 0.9 ml/min, 215 nm, t_1: 21.9 min, t_2: 25.4 min

Hydrolysis of diacetate **53** using a buffer of pH 6 provided the monoacetate (*S*)-**54** in 54% yield and 90% *ee* and diol **52** in 10% yield (Table 24, Entry 1). Use of buffer of pH 6.5 for the hydrolysis reaction under the same conditions gave the monoacetate (*S*)-**54** in 54% yield and 90% *ee* and diol **52** in 9% yield (Table 24, Entry 2). The monoacetate (*S*)-**54** was obtained in 53% yield and 90% *ee* when a buffer of pH 7.5 was used during hydrolysis of diacetate **53**, and the diol was collected in 13% yield (Table 24, Entry 4). However, on use of a buffer of pH 8, a decreased yield and enantioselectivity of the product (*S*)-**54** was observed with the monoacetate (*S*)-**54** collected in 35% yield and 57% *ee* and a yield of 20% of diol **52** (Table 24, Entry 5). there was no evidence of pH of the buffer having an effect on the yield of the monoacetate product (*S*)-**54**.

6.3 Screening of co-solvent

Protein hydration shell theory gives insights into the behaviour of enzymes in organic solvent. It signifies the importance of water content of the solvent as water can affect the thermodynamic stability of enzymes.[138] Although lipases exhibit high catalytic activity in organic solvents, water plays a crucial role as its distribution in the reaction is a delicate and complicated balance between the immobilised enzyme, the support used and the type of solvent. Water also acts as the co-substrate in hydrolysis of esters that are catalysed by lipases.[48] For the reaction to take place successfully, logarithm of the partition coefficient, logP of

the reaction mixture should be similar to the logP of the solvent used for the reaction. Also the thermodynamic water activity, a_w which is defined as the ratio of vapour pressure of sample to the vapour pressure of water under identical conditions plays an important role in determining the success of a reaction. An a_w of 0.55 is reported to be optimum to preserve the catalytic activity of the lipase as it helps form a monomolecular layer of water on its surface. Any further increase in water promotes the reverse reaction of ester hydrolysis or hampers the mass transfer.[48] Therefore, it is important to choose the right co-solvent that helps maintain appropriate quantities of water and help preserve its thermodynamic water activity a_w. After concluding that relatively higher yield and *ee* of the monoacetate (*S*)-**54** were observed when pH 7 buffer and enzyme loading of 450 (mg/mmol **53**) were used, the same conditions were used for screening co-solvents. The solvents tested include non-polar solvents such as dichloromethane, hexane, toluene; polar aprotic solvents such as acetonitrile, acetone and polar protic solvents like methanol.

Table 25: Screening of co-solvent – hydrolysis of diacetate 53[a]

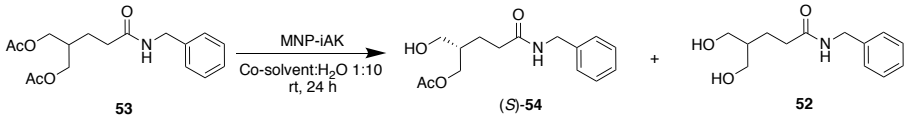

53 (*S*)-54 52

Entry	Co-solvent	Monoacetate (*S*)-**54**		Diol **52**	Unreacted diacetate **53** (%)
		Yield[b] (%)	*ee*[b] (%)	Yield[b] (%)	
1	THF	57	91	11	32
2	Toluene	34	50	1	65
3	Hexane	27	52	2	71
4	MeOH	23	53	1	76

5	Et_2O	30	56	2	68
6	DMSO	36	59	1	63
7	MTBE	57	43	1	76
8	DCM	14	54	2	84
9	MeCN	25	65	1	10
10	*i*Pr_2O	35	58	1	64
11	Acetone	22	57	2	76

[a]: All the reactions were performed on a 0.2 mmol scale of diacetate **53** at room temperature in the presence of MNP-iAK with enzyme loading 450 (mg/mmol **53**)

[b]: Measured by HPLC with reference to known concentrations of diol **52**, monoacetates (*R*)-**54** and (*S*)-**54** and diacetate **53**: Chiralpak AS-H (Hexane:IPA, 85:15), 0.9 ml/min, 215 nm, t_1: 21.9 min, t_2: 25.4 min

Although both the ether type solvents THF and MTBE provided the monoacetate (*S*)-**54** in 57% yield, the enantioselectivity of the monoacetate product was higher at 91% *ee* when THF was used as the co-solvent in the reaction, while MTBE provided the monoacetate (*S*)-**54** in 43% *ee* (Table 25, Entries 1 and 7). Hence, it is observed from Table 25, that there is no relation between polarity of the solvent and the performance of the reaction. However, the difference in the rate of reaction and interfacial activation in different solvents could possibly be due to how the lipase interacts with the solvent. In some cases, the solvent could act as a competitive inhibitor thus reducing the rate of the reaction. Complete dissolution of the solvent in water can also cause inactivation of the lipases.[9] Computational studies, particularly focussing on the thermodynamic nature of interaction of the lipase with the solvents can throw more light on the difference in the way the solvents interact with the lipase. Kinetic studies will also give an idea of turnover number, which is defined as the maximum number of molecules of a substrate that can convert an enzyme into a product per catalytic site per unit of time. For lipases, it can be calculated from Michaelis-Menten kinetics where

the assumption is that each mole of the catalyst contains one mole of active sites.[139]

7. Summary

1) MNP-iAK was used to catalyse the acetylation of diol **52** and the monoacetate product (*R*)-**54** was obtained in yield up to 98% and 92% *ee*. The MNP-iAK catalyst maintained its activity even up to five recycles, providing the monoacetate (*R*)-**54** in 93% yield and 87% *ee* after the fifth recycle.
2) CTPP1-iAK was used to catalyse the acetylation of diol **52** and the monoacetate (*R*)-**54** was obtained in yield up to 91% and 91% *ee*. However, with increase in the number of recycles, there was a decrease in the activity of CTPP1-iAK with 37% yield and 88% *ee* of monoacetate (*R*)-**54** collected after the fourth recycle.
3) Acetylation of diol **52** catalysed by KCC1-iAK provided the monoacetate (*R*)-**54** in up to 98% yield and 92% *ee*. After four recycles, the activity of KCC1-iAK reduced, since the yield of the monoacetate product obtained decreased to 66% yield while the enantioselectivity decreased mildly to 89% *ee*.
4) MNP-iAK as identified as a suitable catalyst system among the three tested catalysts since it not only offered excellent recyclability, but also provided monoacetate (*R*)-**54** in high yield in a relatively shorter reaction time.
5) Analogues of diol **52** were synthesised and acetylated using MNP-iAK. However, no correlation between the different *C2*-substituents on the stereochemistry of the monoacetate product was observed.

6) Hydrolysis of diacetate **53** afforded the monoacetate (*S*)-**54** in up to 57% yield and 90% *ee*. There was no observed effect of pH of buffer used on the reaction.

Chapter IV : Flow chemistry: Desymmetrisation of diol 52 and diacetate 53 and semi-continuous flow synthesis of diol 52

1. Introduction

In 2007, the American Chemical Society (ACS) Green Chemistry Institute (GCI) Pharmaceutical Roundtable listed continuous processing as one of the main areas for sustainable manufacturing.[140] Currently, however, flow chemistry is predominantly employed by the petrochemical and bulk chemistry industries. Pharmaceutical and fine chemical industries, which have traditionally utilised batch processes, have off late started paying attention to flow technologies due to the unique advantages they offer over batch processes.

The benefits of flow processes include but are not limited to excellent mixing of reagents, high surface-to-volume ratios leading to efficient heat and mass transfer, easy scale-up of reactions, enhanced safety as reactions with dangerous reagents or intermediates can be easily controlled within the reactor, reduced use of solvents, ease of applying extreme reaction conditions, energy efficiency and cost-effectiveness.[60, 63] While flow chemistry is highly advantageous, blockage of the flow due to precipitation of solid particles in the reactors is one of the major problems associated with flow processes.[141] This can be overcome by using solvents which can dissolve the precipitates or employing other recently reported methods such as ultrasonic radiation.

In one of the pioneering works in flow chemistry, Allum *et al*., in 1976, reported the successful hydrogenation of hexane, cyclohexene, and isoprene under continuous flow conditions using complexes of rhodium and iridium chemically

bonded to silica through tertiary phosphine ligand-silanes as catalysts.[142] Moraglio and Trotta, in 1989, reported the development of gas-liquid phase-transfer catalysis (GL-PTC), which is a continuous-flow procedure where, a molten phase-transfer catalyst supported on a solid is used through which gaseous reagents flow, without the use of any solvent.[143] More recently, in a noteworthy work, the end-to-end synthesis of an API, aliskiren hemifumarate was reported by researchers from the Novartis-MIT Center for Continuous Manufacturing. The final step in the process delivers tablets containing 112 mg of free aliskiren. The flow process requires 48h and 13 unit operations, with the continuous reactor having the capacity to produce up to 0.8 tons/year of aliskiren compared to the batch process which requires 300h and 21 unit operations.[144] These reports clearly demonstrate the use of flow chemistry as a sustainable method to obtain high value, high purity chemical products in short reaction times.

As discussed in Chapter III, the yield of monoacetate (*S*)-**54** obtained from the hydrolysis of diacetate **53** was up to 57%. Flow reactors have been reported by several researchers to improve the reaction performance, with products being obtained in high yields within short reaction times. Therefore, in this research, the enzymatic hydrolysis of diacetate **53** will be performed in a flow process, with an aim to improve the yield of the monoacetate (*S*)-**54** formed. Semi-continuous synthesis of diol **52** and its acetylation will also be attempted using a flow process.

2. Research Methodologies

A simple bench-top laboratory scale flow reactor will be assembled using a syringe pump, PTFE tubing and PEEK T-junctions and fittings.

Hydrolysis of diacetate **53** will be performed using the reactor, with lipase AK in its native form as the catalyst. Upon identifying optimum conditions for the hydrolysis of the diacetate **53**, the same conditions will be used to perform the hydrolysis reaction using MNP-iAK as a catalyst.

The reactor will be used to perform the acetylation of diol **52** initially using lipase AK in its native form. Once the optimum conditions for the acetylation reaction are identified, the same conditions will be used to perform the acetylation of diol **52** using MNP-iAK.

Synthesis of diol **52** is a four-step process comprising of Michael addition, carboxylation, amidation and reduction reactions. The synthesis will be attempted in a continuous flow process using the assembled reactor. Every step of the sequence of synthesis of diol **52** will be optimised to adapt to the flow process. Once the optimum conditions are identified, a semi-continuous synthesis of diol **52** will be attempted.

3. Assembly of flow reactor

A small-scale bench-top flow reactor was assembled using a dual channel syringe pump, PTFE tubing and PEEK T-junction and fittings. The syringe pump used was either SPLab02 by Baoding Shenchen Precision Pump Co. Ltd. or KDScientific KDS 200 dual syringe pump. PTFE tubing of varying length was used and had an internal diameter of 0.040” and an outer diameter of 1/16”.

Reactor volume was calculated by adding the total volume of the mixing junction and volume of the PTFE tube used for the reaction.

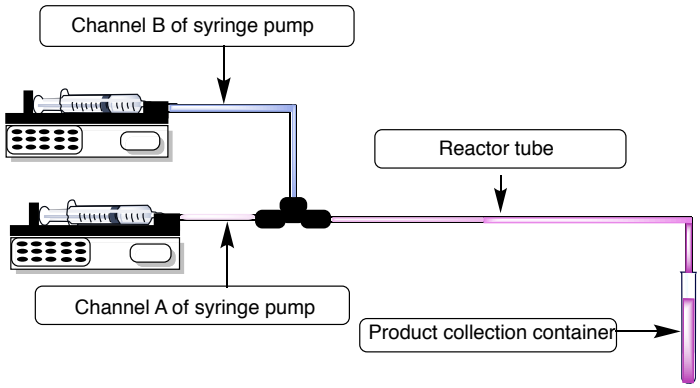

Figure 23: Representation of the assembled flow reactor set-up

4. Desymmetrisation of diacetate 53

4.1 Desymmetrisation of diacetate 53 using lipase AK in its native form

4.1.1 Optimisation of residence time

The time taken for the hydrolysis of diacetate **53** to reach completion and provide monoacetate (*S*)-**54** was 24 hours in a batch process. However, the time taken for a reaction to reach completion is usually faster in a flow process compared to the batch process. This is because of efficient mixing in the mixing modules such as T-junctions, as well as the small cross section of the reactor tubing which also promotes further mixing of the reactants. Therefore, it is important to optimise the residence time (time spent by the reactants in the reactor) for the hydrolysis of diacetate **53**. Hydrolysis of diacetate **53** was performed at different residence times, which were set by varying the flow rate of the reactants. A syringe containing the diacetate **53** in THF:pH 7 buffer (1:10 v/v ratio) was placed in channel A and connected to the T-junction. Lipase AK (300 (mg/mmol **53**)) in THF: pH 7 buffer (1:10 v/v) was withdrawn into a syringe, which was placed in

channel B and connected to the same T-junction. The third arm of the T-junction was connected to the PTFE reactor tube. The exit of the reactor tube was connected to a collection vessel with DCM so that as soon as the reaction mixture containing the product exits the reactor, it flows into the DCM solution where the unreacted diacetate (if any) and the monoacetate product are collected in the organic stream, while lipase AK remains in the aqueous buffer stream.

Table 26: Optimisation of residence time – hydrolysis of diacetate 53 in a flow process[a]

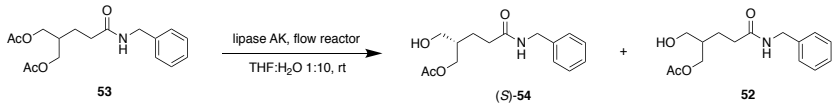

Entry	Residence time (h)	Monoacetate (*S*)-**54**		Diol **52**	Unreacted diacetate **53**[b] (%)
		Yield[b] (%)	*ee*[b] (%)	Yield[b] (%)	
1	1	18	68	0	82
2	2	19	76	0	81
3	3	22	76	0	78
4	4	35	91	0	65
5	12	65	95	2	33
6	24	79	96	7	14

[a]: All the reactions were performed on a 0.2 mmol scale of diacetate **53** at room temperature in the presence of lipase AK with enzyme loading 300 (mg/mmol **53**)

[b]: Measured by HPLC with reference to known concentrations of diol **52**, monoacetate **54** and diacetate **53**: Chiralpak AS-H (Hexane:IPA, 85:15), 0.9 ml/min, 215 nm, t_1: 21.9 min, t_2: 25.4 min

Hydrolysis of diacetate **53** in the flow reactor provided the monoacetate (*S*)-**54** in 18% yield and 68% *ee* after one hour of residence time (Table 26, Entry 1). When the reaction was repeated for a residence time of two hours, monoacetate (*S*)-**54** was obtained in 19% yield and 76% *ee* (Table 26, Entry 2). The yield and enantioselectivity of the monoacetate (*S*)-**54** collected after hydrolysis of

diacetate **53** for a residence time of three hours, was almost the same as that obtained after two hours of the reaction at 22% yield and 76% (Table 26, Entry 3). However, when the hydrolysis of diacetate **53** was performed in the reactor for a residence time of four hours, the yield of the monoacetate (*S*)-**54** increased to 35% and 91% *ee* (Table 26, Entry 4). This increase in the yield and *ee* of the monoacetate (*S*)-**54** is possibly due to the reaction reaching the steady state sometime between 3 and 4 hours of residence time. When the reactions were repeated with increasing residence times of the reactants, the yield and enantioselectivity of monoacetate (*S*)-**54** had a gradual increase (Table 26, Entries 4 to 6) with the monoacetate (*S*)-**54** obtained in 79% yield and 96% *ee* and a yield of 7% of diol **52** after a residence time of 24 hours (Table 26, Entry 6).

4.1.2 Optimisation of mixing speed

Since the rate of mixing significantly alters the course of the reaction and the amount of product formed in a flow reactor, the hydrolysis of diacetate **53** was performed at different mixing speeds. This was done by using reactor tubing of different length. This ensures that the residence time of the reactants in the reactor remains the same. However, since the length of the tube is varied, the flow rate of the reactants must be adjusted so as to maintain the same residence time, which will alter the rate of mixing of the reactants mainly in the T-junction, in addition to mixing in the reactor tubing.

Table 27: Optimisation of mixing speed – hydrolysis of diacetate 53 in a flow process[a]

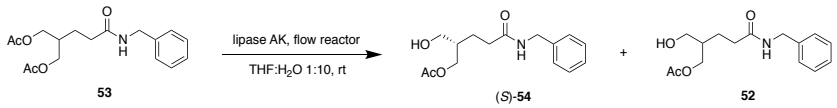

Entry	Residence time (h)	Length of reactor tubing (ft.)	Monoacetate (*S*)-**54**		Diol **52**	Unreacted diacetate **53**[b] (%)
			Yield[b] (%)	*ee*[b] (%)	Yield[b] (%)	
1	12	5	65	95	2	33
2	12	50	78	88	2	20
3	24	5	79	96	7	14
4	24	50	75	85	7	18

[a]: All the reactions were performed on a 0.2 mmol scale of diacetate **53** at room temperature in the presence of lipase AK with enzyme loading 300 (mg/mmol **53**)

[b]: Measured by HPLC with reference to known concentrations of diol **52**, monoacetate **54** and diacetate **53**: Chiralpak AS-H (Hexane:IPA, 85:15), 0.9 ml/min, 215 nm, t_1: 21.9 min, t_2: 25.4 min

Hydrolysis of diacetate **53** using a reactor tube of length five ft. and for a residence time of 12 hours provided the monoacetate (*S*)-**54** in 65% yield and 95% *ee* and diol **52** in 2% yield (Table 27, Entry 1) . To increase the mixing speed, a longer reactor tube of 50 ft. length was used, and the reaction repeated for the same residence time. The yield of the monoacetate (*S*)-**54** obtained was 78% and 88% *ee* with a 2% yield of diol **52** (Table 27, Entry 2). Hydrolysis of diacetate **53** using a five ft. long reactor tube and after a residence time of 24 hours afforded the monoacetate product (*S*)-**54** in 79% yield and 96% *ee* and the diol **52** in 7% yield (Table 27, Entry 3). When the reaction was repeated with a longer tube of 50 ft. while ensuring the maintenance of the same residence time, the monoacetate (*S*)-**54** was produced in 75% *ee* and 85% *ee* with 7% yield of diol **52** (Table 27, Entry 4). Therefore, it was concluded that a 5 ft. long reactor tube and hence lower mixing speeds provided the monoacetate (*S*)-**54** in relatively higher yield and excellent enantioselectivity.

4.1.3 Effect of temperature

To determine the effect of temperature on the hydrolysis of diacetate **53**, the reaction was performed at two different temperatures to compare the yield and enantioselectivity of the monoacetate (*S*)-**54** obtained, towards an attempt to improving the yield of the monoacetate. The temperature was maintained by immersing the reactor tubing in a hot water bath connected to a temperature controller.

Hydrolysis of diacetate **53** at room temperature using lipase AK in its native form, a reactor of 5 ft. length and reactant residence time of 24 hours, the monoacetate (*S*)-**54** was obtained in 79% yield and 96% *ee* with 7% of diol **52** formation (Table 28, Entry 1). On repeating the hydrolysis reaction at 40 °C, the yield of monoacetate (*S*)-**54** showed an improvement (85% yield) while the enantioselectivity dropped to 83% *ee* with 5% yield of diol **52** (Table 28, Entry 2)**.** Therefore, further hydrolysis of diacetate **53** were performed using the same set-up at room temperature.

Table 28: Effect of reaction temperature – hydrolysis of diacetate 53 in a flow process[a]

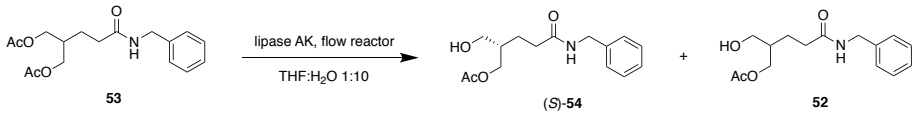

53

Entry	Residence time (h)	Reaction temperature (°C)	Monoacetate (*S*)-**54**		Diol **52**	Unreacted diacetate **53**[b] (%)
			Yield[b] (%)	*ee*[b] (%)	Yield[b] (%)	
1	24	rt	79	96	7	14
2	24	40	85	83	5	10

[a]: All the reactions were performed on a 0.2 mmol scale of diacetate **53** in the presence of lipase AK with enzyme loading 300 (mg/mmol **53**)
[b]: Measured by HPLC with reference to known concentrations of diol **52**, monoacetate **54** and diacetate **53**:
Chiralpak AS-H (Hexane:IPA, 85:15), 0.9 ml/min, 215 nm, t_1: 21.9 min, t_2: 25.4 min

4.1.4 Optimisation of enzyme loading

The yield of the monoacetate (*S*)-**54** formed by hydrolysis of diacetate **53** at room temperature with an enzyme (lipase AK) loading of 300 (mg/mmol **53**) was 79% while the enantioselectivity was 96% *ee* (Table 29, Entry 1). With an aim to increase the yield of the monoacetate product (*S*)-**54**, the hydrolysis reaction was repeated using an enzyme loading of 450 (mg/mmol **53**), with all other reaction conditions remaining the same. However, there was no significant improvement in the yield of the monoacetate (*S*)-**54** formed (81% yield) while the enantioselectivity remained about the same at 95% *ee* (Table 29, Entry 2).

Table 29: Optimisation of enzyme loading – hydrolysis of diacetate 53 in a flow process[a]

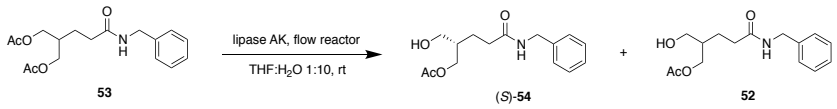

Entry	Residence time (h)	Enzyme loading (mg/mmol **53**)	Monoacetate (*S*)-**54**		Diol **52**	Unreacted diacetate **53**[b] (%)
			Yield[b] (%)	*ee*[b] (%)	Yield[b] (%)	
1	24	300	79	96	7	14
2	24	450	81	95	7	12

[a]: All the reactions were performed on a 0.2 mmol scale of diacetate **53** at room temperature in the presence of lipase AK
[b]: Measured by HPLC with reference to known concentrations of diol **52**, monoacetate **54** and diacetate **53**:
Chiralpak AS-H (Hexane:IPA, 85:15), 0.9 ml/min, 215 nm, t_1: 21.9 min, t_2: 25.4 min

Residence time of 24 hours, enzyme loading 300 (mg/mmol **53**), 25 °C, and a reactor of length 5 ft. were found to be optimum conditions for the hydrolysis of diacetate **53** using a flow reactor.

4.2 Desymmetrisation of diacetate 53 using MNP-iAK

Since lipase AK is soluble in the buffer used for the reaction, recycling the enzyme is not possible. Therefore, hydrolysis of diacetate **53** was performed using MNP-iAK constrained in stainless steel columns with an aim to recycle the catalyst. Also, unlike lipase AK, MNP-iAK settle down in the syringe before pumping due to their insolubility, thereby not catalysing the hydrolysis of diacetate **53** efficiently. Therefore, the restriction of the MNP-iAK in the stainless-steel columns is beneficial since it not only allows the reactants to flow through allowing MNP-iAK and diacetate **53** interaction, but it also allows facile purification of the monoacetate product (*S*)-**54** and recyclability of the MNP-iAK.

For this purpose, three types of columns of length (Dimensions of the stainless steel columns: 5 cm and 0.4 mm ID) were prepared:

1) Column 1 – MNP-iAK (containing immobilised lipase AK corresponding to enzyme loading 300 (mg/mmol diacetate **53**) was taken and housed between two cotton plugs in the column (Figure 24).
2) The height of the first cotton plug and height of the plug plus the added MNP-iAK was calculated in order to determine the flow rate required to maintain the desired residence time.

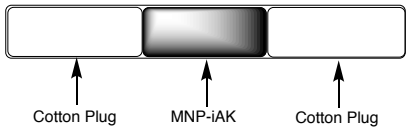

Figure 24: Column 1

3) Column 2 - MNP-iAK (containing immobilised lipase AK corresponding to enzyme loading 300 (mg/mmol diacetate **53**)) was added to the column directly without any additional restraints like cotton plugs. Residence time was calculated based on the volume of the column.

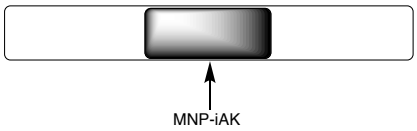

Figure 25: Column 2

4) Column 3 – The column was completely filled with MNP-iAK without calculating the enzyme loading. Residence time was calculated based on the volume of the column.

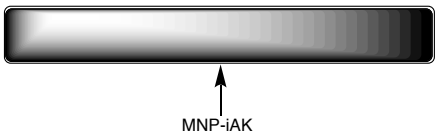

Figure 26: Column 3

Hydrolysis of diacetate **53** was carried out by injecting diacetate **53** in THF:pH 7 buffer (1:10 v/v) into the column using a syringe pump. There was no necessity for a quenching step at the exit stream because MNP-iAK are restricted in the column.

Table 30: Hydrolysis of diacetate 53 using MNP-iAK constrained in a column[a]

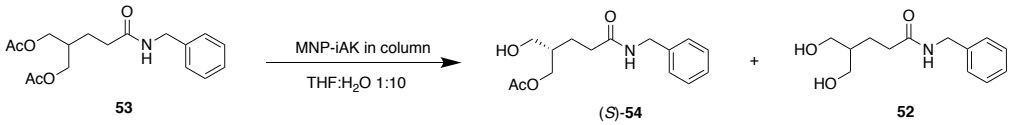

Entry	Column	Residence time (h)	Monoacetate (*S*)-**54**		Diol **52**	Unreacted diacetate **53**[b] (%)
			Yield[b] (%)	*ee*[b] (%)	Yield[b] (%)	
1	Column 1	24	11	67	0	89
2	Column 2	24	15	73	0	85
3	Column 3	24	35	81	0	65

[a]: All the reactions were performed on a 0.2 mmol scale of diacetate **53** at room temperature in the presence of MNP-iAK in column

[b]: Measured by HPLC with reference to known concentrations of diol **52**, monoacetate **54** and diacetate **53**: Chiralpak AS-H (Hexane:IPA, 85:15), 0.9 ml/min, 215 nm, t_1: 21.9 min, t_2: 25.4 min

Hydrolysis of diacetate **53** using MNP-iAK in column 1 configuration provided the monoacetate (*S*)-**54** in 11% yield and 67% *ee* (Table 30, Entry 1). The monoacetate (*S*)-**54** was produced in 15% yield and 73% *ee* when MNP-iAK housed in column 2 was used to catalyse the reaction (Table 30, Entry 2). When MNP-iAK, completely filled in column 3 was used in the hydrolysis of diacetate **53**, the monoacetate (*S*)-**54** was obtained in 35 % yield and 81% *ee* (Table 30 Entry 3). Out of the three configurations, the yield and enantioselectivity of monoacetate (*S*)-**54** was highest when MNP-iAK in column 3 was used to catalyse the hydrolysis of diacetate **53**. This is because of the much higher enzyme loading in the column, which means the ratio of immobilised lipase AK available to the diacetate **53** is higher. Nevertheless, the yield and enantioselectivity of the monoacetate (*S*)-**54** produced was not as high as

expected. This is because of diffusion limitations and lower void volume in the tightly packed column which renders some of the MNP-iAK unreachable to the diacetate **53** molecules flowing through the column.

To improve the yield through enhancing the interaction between MNP-iAK and diacetate **53**, ultrasonication was used during the course of the reaction. Column 3, containing MNP-iAK was placed in an ultrasonic bath into which diacetate **53** in THF:pH 7 buffer (1:10 v/v) was pumped in using a syringe pump.

Table 31: Hydrolysis of diacetate 53 using MNP-iAK in column 3 under ultrasonication[a]

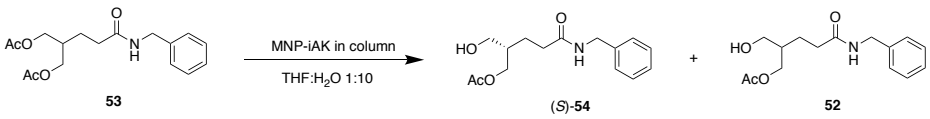

Entry	Ultrasound frequency (kHz)	Pulse Duration (min)	Residence time (h)	Monoacetate (*S*)-**54**		Diol **52**	Unreacted diacetate **53**[b] (%)
				Yield[b] (%)	*ee*[b] (%)	Yield[b] (%)	
1	35	30	12	29	85	0	71
2	60	30	12	43	84	2	55
3	60	-	24	12	71	0	88

[a]: All the reactions were performed on a 0.2 mmol scale of diacetate **53** at room temperature in the presence of MNP-iAK in column 3

[b]: Measured by HPLC with reference to known concentrations of diol **52**, monoacetate **54** and diacetate **53**: Chiralpak AS-H (Hexane:IPA, 85:15), 0.9 ml/min, 215 nm, t_1: 21.9 min, t_2: 25.4 min

Hydrolysis of diacetate **53** performed using MNP-iAK packed in column 3 as catalyst and subject to ultrasonic frequency of 35 kHz in pulses of 30 minutes each for 12 hours, provided monoacetate (*S*)-**54** in 29% yield and 85% *ee* (Table 31, Entry 1). All conditions remaining the same, when the hydrolysis of diacetate **53** was performed at an ultrasonic frequency of 60 kHz, the yield of the

monoacetate (*S*)-**54** slightly improved to 43% yield while the enantioselectivity remained about the same at 84% *ee* (Table 31, Entry 2). The monoacetate (*S*)-**54** was produced in 12% yield and 71% *ee* when the hydrolysis of diacetate **53** was carried out at an ultrasonic frequency of 60kHz continuously without any pulses for a residence time of 24 hours (Table 31, Entry 3). The low yield of monoacetate (*S*)-**54** when hydrolysis of diacetate **53** was performed with continuous ultrasonication, is due to the high localised temperatures generated which could have deactivated the enzyme or lowered its activity.

5. Desymmetrisation of diol 52

Acetylation of diol **52** was performed using lipase AK as a catalyst. Since the acetylation takes place in MeCN, in which lipase AK is insoluble, the lipase AK was constrained in a column, housed between two cotton plugs. Residence time was calculated by determining the height of first the cotton plug filled in the column, before and after the addition of lipase AK. Using the information, the volume occupied by lipase AK in the column was calculated which was used to maintain the desired residence time by setting the appropriate flow rate of the diol **52** inlet stream. Diol **52** is poorly soluble in MeCN, so it was ground to a fine powder and dispersed in the solvent along with 4 Å molecular sieves.

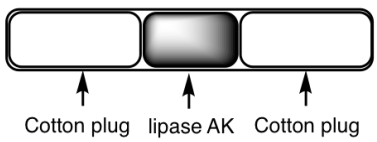

Figure 27: Column with lipase AK used for acetylation of diol 52

Table 32: Acetylation of diol 52 using lipase AK housed in a column[a]

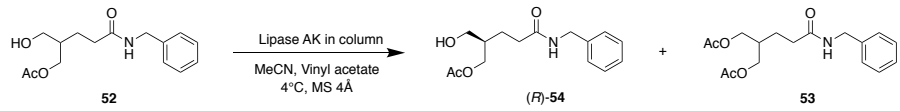

Entry	Residence time (h)	Monoacetate (*R*)-**54**		Diacetate **53**	Unreacted diol **52**[b] (%)
		Yield[b] (%)	*ee*[b] (%)	Yield[b] (%)	
1	2	74	93	1	25
2	9	76	93	1	23
3	12	82	93	3	15

[a]: All the reactions were performed on a 0.2 mmol scale of diol **52** in the presence of lipase AK in column (enzyme loading 300 (mg/mmol **52**)), 4 Å molecular sieves using vinyl acetate (10 equiv.) in MeCN (64 mM)

[b]: Measured by HPLC with reference to known concentrations of diol **52**, monoacetates (*R*)-**54** and (*S*)-**54** and diacetate **53**: Chiralpak AS-H (Hexane:IPA, 85:15), 0.9 ml/min, 215 nm, t_1: 21.9 min, t_2: 25.4 min

Acetylation of diol **52** provided monoacetate (*R*)-**54** in 74% yield and 93% *ee* and diacetate **53** in 1% yield after two hours of reaction (Table 32, Entry 1). When the reaction was repeated for a residence time of nine hours, the monoacetate product (*R*)-**54** was obtained in 76% yield and 93% *ee* and diacetate **53** in 1% yield (Table 32, Entry 2). Monoacetate (*R*)-**54** was produced in 82% yield and 93% *ee* with 3% diacetate **53** formation, after the acetylation of diol **52** was performed for a residence time of 12 hours (Table 32, Entry 3).

Investigation of acetylation of diol **52** in flow using MNP-iAK as a catalyst was not performed because lipase AK is as such insoluble in MeCN and is constrained in the column. It can be easily recycled by washing with MeCN and THF (to remove any residual unreacted diol **52**) and dried before using for the subsequent acetylation reaction. As such, the recyclability of lipase AK housed in the column was studied by using it to carry out the acetylation of diol **52** for a residence time of 12 hours.

Table 33: Acetylation of diol 52 – Recyclability of lipase AK in column[a]

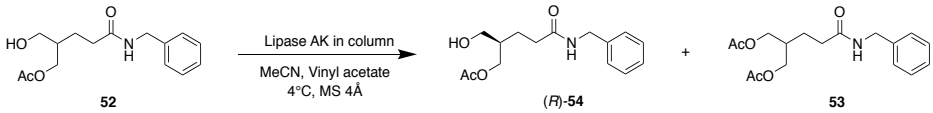

Entry	Number of recycle(s)	Monoacetate (*R*)-**54**		Diacetate **53**	Unreacted diol **52**[b] (%)
		Yield[b] (%)	*ee*[b] (%)	Yield[b] (%)	
1	1	81	93	1	18
2	2	80	93	1	19
3	3	76	92	1	23
4	4	74	92	0	26
5	5	70	91	0	30

[a]: All the reactions were performed on a 0.2 mmol scale of diol **52** in the presence of lipase AK in column (enzyme loading 300 (mg/mmol **52**)), 4 Å molecular sieves using vinyl acetate (10 equiv.) in MeCN (64 mM)

[b]: Measured by HPLC with reference to known concentrations of diol **52**, monoacetates (*R*)-**54** and (*S*)-**54** and diacetate **53**: Chiralpak AS-H (Hexane:IPA, 85:15), 0.9 ml/min, 215 nm, t_1: 21.9 min, t_2: 25.4 min

Yield of monoacetate (*R*)-**54** obtained after using once recycled lipase AK for acetylation of diol **52** was 81% while the enantioselectivity was 93% *ee*. The same reaction also produced diacetate **53** in 1% yield (Table 33, Entry 1). The enantioselectivity of monoacetate (*R*)-**54** was greater than 91% *ee* for the subsequent acetylations of diol **52** catalysed by the corresponding recycles of lipase AK (Table 33, Entries 2 to 5). However, the yield of monoacetate (*R*)-**54** dropped gradually when the acetylation of diol **52** was performed with the recycled lipase AK (Table 33, Entries 2 to 5), eventually dropping to 70% after the fifth recycle of lipase AK in column (Table 33, Entry 5). It may be concluded that though the activity of lipase AK in the column decreased slowly with every

recycle, the enantioselectivity remained high as evident from the high *ee* of monoacetate (*R*)-**54** even after the fifth recycle of lipase AK in the column.

6. Synthesis of diol 52 in flow

The synthesis of diol **52** comprises of four steps (Scheme 17)[97]

1) Michael addition reaction of dimethyl malonate **48** to *tert*-butyl acrylate **47** to produce triester **49**
2) Selective hydrolysis of *tert*-butyl ester group of triester **49** using TFA to obtain acid **50**
3) Coupling of acid **50** with benzylamine to provide amide **51**
4) Reduction of ester groups of amide **51** using $LiBH_4$ in MeOH-THF to produce diol **52**

   The four steps will be optimised and the optimised conditions will be used to synthesise diol **52** using a semi-continuous flow process.

6.1 Synthesis of triester 49

Michael addition reaction of dimethyl malonate **48** to *tert*-butyl acrylate **47** was performed in flow in the presence of DBU. A syringe containing dimethyl malonate **48** and DBU in THF was connected to one arm of the T-junction. The other arm of the T-junction was connected to another syringe containing *tert*-butyl acrylate **47**. The reactants were pumped through the T-junction and reactor tube (which was connected to the third arm of the T-junction) using a syringe pump. Product was collected at the end of the reactor tube.

Table 34: Synthesis of triester 49[a]

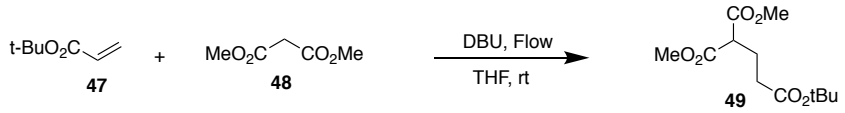

Entry	Residence time (h)	Triester **49**[b] (%)
1	2	52
2	6	64
3	12	73
4	24	86

[a]: All reactions were performed using 8 mmol of dimethyl malonate **48,** *tert*-butyl acrylate **47** (1 equiv.), DBU (1.5 equiv.) and THF (1.1 mM) using a 5 ft. long reactor tube

[b]: Isolated yield

Since the time taken for the Michael addition reaction of dimethyl malonate **48** to *tert*-butyl acrylate **47** in the flow reactor is unknown, initial reaction was set up with a residence time of two hours. The product stream was collected at regular time intervals of 10 minutes and worked up to prevent the reaction from continuing in the collection vessel.

For an initial residence time of two hours, the Michael addition reaction provided the triester **49** in 52% yield (Table 34, Entry 1). When the reaction was set up for a residence time of six hours, the product **49** was produced in 64% yield (Table 34, Entry 2). To further improve the yield of the triester **49**, the reaction was carried out in the flow reactor for a residence time of 12 hours which gave the triester **49** in 73% yield (Table 34, Entry 3). Upon repeating the reaction for a residence time of 24 hours, triester **49** was obtained in 86% yield (Table 34, Entry 4).

The same Michael addition reaction was earlier performed in a batch process in the presence of NaH instead of DBU. The reaction required maintenance of temperature at 0 °C initially during the addition step because of the exothermic nature. The triester **49** was produced in 91% yield after 21 hours of reaction.[97] However, the reaction in flow, using DBU, produced the triester **49** in 86% yield after 24 hours of the reaction (Table 34). Though the yield of the triester product **49** obtained through the flow process is slightly lower compared to that of the batch process, the advantage of the flow process for this reaction is the ease of setting up since it takes place at room temperature and does not release any gas, thus maintaining homogeneity of the reaction stream for efficient flow through the reactor.

6.2 Synthesis of acid 50

Hydrolysis of *tert*-butyl ester group of the triester **49** was performed using trifluoroacetic acid (TFA). A syringe containing the triester **49** in DCM was connected to one arm of the T-junction. Another syringe containing TFA in DCM was connected to the perpendicular arm of the T-junction. The third arm was connected to the reactor tube. A collection vessel was placed at the end of the reactor tube for collection of the reaction stream.

Table 35: Synthesis of acid 50[a]

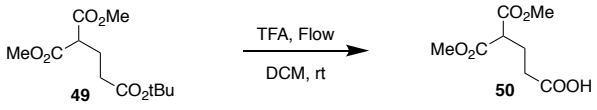

Entry	Residence time	Length of reactor tube	Acid **50**[b]

	(h)	(ft.)	(%)
1	3	5	60
2	12	5	79
3	24	5	80
4	12	50	83
5	24	50	87

[a]: All reactions were performed using 2 mmol of triester **49** in DCM (0.2M) and TFA (5 equiv.)
[b]: Isolated yield

Three hours of the chemoselective hydrolysis of the *tert*-butyl ester group of the triester **49** using a reactor tube of 5 ft. length provided the acid **50** in 60% yield (Table 45, Entry 1). Using the same conditions, when the reaction was repeated for a residence time of 12 hours, the acid **50** was produced in 79% yield (Table 45, Entry 2). On further increasing the residence time to 24 hours and repeating the reaction, 80% of the acid **50** was formed (Table 45, Entry 3). To determine if there would be any improvement in the yield if faster mixing speeds are used, the length of the reactor tube was increased to 50 ft. Since the residence time needs to be maintained, the flow rates of the reactant streams were increased. The acid **50** was obtained in 83% yield in 12 hours when the reaction was performed using a 50 ft. long reaction tube (Table 45, Entry 4). Reaction in the 50 ft. reactor tube was carried out for a residence time of 24 hours to afford the acid **50** in 87% yield (Table 45, Entry 5). In a batch process, the same reaction provided acid **50** in 95% yield after 12 hours of the reaction.[97]

6.3 Synthesis of amide 51

Coupling of acid **50** with benzylamine was performed through Steglich esterification in the presence of EDC and DMAP. A syringe containing the acid **50**, EDC and DMAP in DCM was connected to the T-junction of the reactor. Perpendicular arm of the T-junction was connected to a syringe containing benzylamine in DCM. The third arm of the T-junction was connected to the reactor tube. However, for this reaction, there is an issue with clogging of the reactor tube due to formation of the corresponding urea. Therefore, appropriate volume of DCM should be used to ensure smooth flow of reagents in the reactor.

Table 36: Synthesis of amide 51[a]

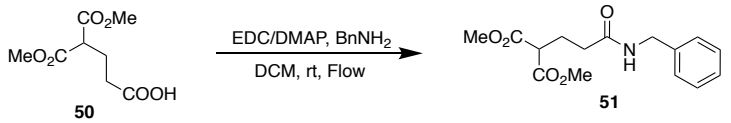

Entry	Residence time (h)	Molar equiv. of DCM (M)	Length of reactor tube (ft.)	Amide **51**[b] (%)
1	18	0.02	5	74
2	24	0.02	5	80
3	12	0.04	5	80
4	12	0.1	5	81

[a]: All reactions were performed using 0.4 mmol of acid **50**, EDC (1.2 equiv.), DMAP (0.1 equiv.), DCM and $BnNH_2$ (1.2 equiv.)
[b]: Isolated yield

Coupling reaction of acid **50** with benzylamine in DCM (0.02 M equiv.) with a residence time of 18 hours provided amide **51** in 74% yield (Table 36, Entry 1). When the reaction was carried out under the same conditions for a residence time

of 24 hours, amide **51** was obtained in 80% yield (Table 36, Entry 2). The coupling reaction was performed for a residence time of 12 hours in 0.04 M equiv. DCM. The product, amide **51** was afforded in 80% yield (Table 36, Entry 3). Under the same conditions, when the reaction was repeated in 0.1M equiv. DCM, the amide **51** was obtained in 81% yield (Table 36, Entry 4). Further attempts to increase the molar equiv. of DCM and perform the reaction failed as clogging was observed in the reactor tube when DCM was used in 0.15 M. The coupling of acid **50** with benzylamine was performed in batch using the $(COCl)_2$/DMF coupling provided the amide **51** in 91% yield after 2.5 hours.[97] However, the method requires maintaining a temperature of 0 °C during addition of $(COCl)_2$ and later, during the addition of benzylamine. In comparison, the reaction in flow can be performed at room temperature.

6.4 Synthesis of diol 52

Reduction of amide **51** using $LiBH_4$ in dry THF to provide diol **52** was carried out using the flow reactor. The reactor tube along with the T-junction was purged with nitrogen. Glass syringes used for the reaction were dried at high temperature to remove moisture and purged with nitrogen. A syringe containing amide **51** in dry THF and MeOH was connected to one arm of the T-junction through a PTFE tube. The perpendicular arm of the T-junction was connected to another syringe containing $LiBH_4$ in THF, *via* a PTFE tube. The third arm was connected to a reactor tube.

Table 37: Synthesis of diol 52[a]

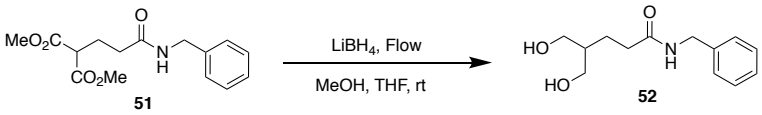

Entry	Residence time (h)	Length of reactor tube (ft.)	Diol **52**[b] (%)
1	2	5	68
2	3	5	70
3	2	50	73
4	3	50	76

[a]: All reactions were performed using 2 mmol of amide **51**, $LiBH_4$ (4 equiv.) and THF (0.1 M)

[b]: Isolated yield

Reduction of the ester groups of amide **51** using $LiBH_4$ provided the diol **52** in 68% yield after a two hour residence time in a reactor tube of length 5 ft. (Table 37, Entry 1). On repeating the reaction with a residence time of three hours in the same reactor tube, the diol **52** was afforded in 70% yield. The length of the reactor tube was increased to 50 ft. and the reduction reaction was performed for a residence time of two hours. The diol **52** was obtained in 73% yield. Using the same conditions, when the reaction was set up for a residence time of three hours, the diol was obtained in 76% yield. In batch process, the reduction of amide **51** using $LiBH_4$ provided diol in 85% yield after two hours of reaction.[97] In the flow process, despite our best efforts, there was some moisture leaking into the syringe, and $LiBH_4$ being hygroscopic, reacts with the moisture. In addition, the H_2 gas generated during the reduction of the diester groups of the amide **51**, also

flows into the reaction system, thereby altering the rate of the reaction since the system is no longer homogeneous.

Since the optimal conditions for each step of the synthesis process of diol **52 in** in flow have been identified (Scheme 29), a semi-continuous flow synthesis of diol **52** was attempted.

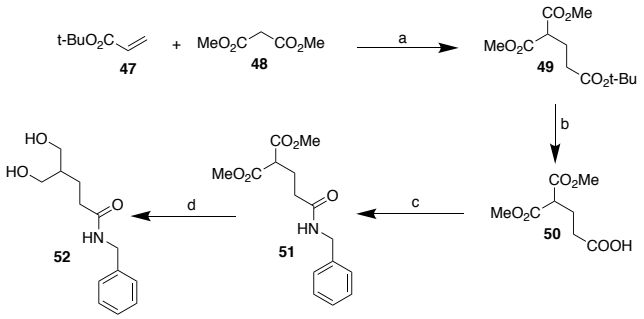

Reagents and conditions: (a) DBU, THF, rt, 24 h; (b) TFA, DCM, rt, 24 h; (c) EDC, DMAP, DCM, $BnNH_2$, rt, 12 h; (d) $LiBH_4$, THF, MeOH, rt, 3 h

Scheme 29: Optimum conditions for each step of diol 52 synthesis in flow

While a continuous flow system is ideal, there are two steps in the process of synthesis of diol **52** where a change of solvent is required – from THF to DCM after the synthesis of triester **49** and from DCM to THF after the synthesis of amide **51**. Instead, the reactions were performed at the optimum conditions, and the crude products were used for the subsequent reaction steps without any purification process in between. This required manual intervention for evaporation of the solvent and re-adding the solvent for the next step of the synthesis process. Upon performing this sequence of steps, the yield of diol **52** obtained was only 6%. This is attributed to the presence of impurities, which lower the yield of the product formed as well as reduce the effectiveness of the reagents which can react with the impurities.

7. Summary

1) A simple bench-top flow reactor was assembled using dual channel syringe pump, PTFE tubing and PEEK T-junction and fittings.
2) Hydrolysis of diacetate **53** in the flow reactor using lipase AK in its free form as catalyst provided monoacetate (*S*)-**54** in up to 79% yield and 93% *ee*. The yield of the monoacetate obtained in flow is much higher than that obtained using a batch process (57%). Hydrolysis of diacetate **53** in flow using MNP-iAK provided the monoacetate (*S*)-**54** in up to 41% yield and 84% *ee*.
3) Acetylation of diol **52** using lipase AK in a column, provided monoacetate (*R*)-**54** in up to 82% yield and 93% *ee*. Recyclability of the lipase AK in column was tested and was shown to be active even after five recycles.
4) Optimal conditions in flow for each reaction step in the synthesis of diol **52** were identified. Michael addition of dimethyl malonate **48** and *tert*-butyl acrylate provided triester **49** in 86% yield. Hydrolysis of the *tert*-butyl ester group of the triester **49** provided acid **50** in 87% yield. Coupling of acid **50** with benzylamine provided the amide **51** in 81% yield. Reduction of the amide **51** with $LiBH_4$ gave diol **52** in 76% yield.
5) A semi-continuous flow synthesis of diol **52** was attempted using the optimum conditions identified for each step in the synthesis process. However, the overall yield of the diol **52** obtained was only 6%.

Chapter V : Future work

While we have optimised the conditions for every step in the synthesis of diol **52**, we believe there is a scope for a continuous flow synthesis of the diol **52** starting from the Michael addition of dimethyl malonate **48** and *tert*-butyl acrylate **47** to the reduction of amide **51** to afford diol **52**. We propose to establish such a system by incorporating some of the following suggestions:

1) Optimising every step of the reaction sequence using the same solvent. This will remove the necessity for manual intervention in working up intermediate reactions just to change the solvent. Alternatively, a solvent changing system such as Vapourtec V-10 solvent evaporator can be used and a subsequent stream of new solvent may be added.[145]
2) The first step in the synthesis of diol **52**, the Michael addition reaction, take place in the presence of DBU. The DBU can be supported on an inert polymer such as styrene and restricted in a column. Dimethyl malonate **48** and *tert*-butyl acrylate **47** can be injected into the column for the reaction to take place. The product stream is expected to be much cleaner without the necessity for any additional purification steps since the DBU is restricted in the column. Alternatively, DBU can be made to flow through the reactor along with the other reagents, and a scavenging column containing an acid can be used to quench the DBU, thereby leaving a clean product stream.

   For example, catalytic hydrogenation of acetophenone using Cu salts was catalysed by polystyrene supported DBU to provide 1-phenylethanol (Scheme 30).[146]

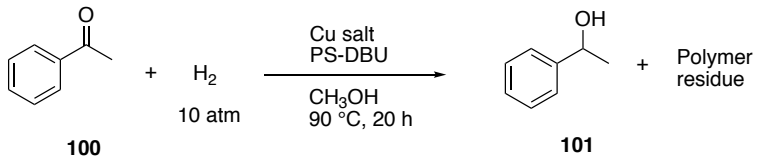

Scheme 30:Catalytic hydrogenation of acetophenone using DBU supported on polystyrene as catalyst

3) The second step of synthesis of diol **52**, the hydrolysis of the *tert*-butyl ester bonds of the triester **49**, the TFA can be supported by a polymer and immobilised in a column such that the product stream is devoid of excess acid. Another option is to let TFA flow in the reactor along with the other reagents and later pass the reaction stream through a column containing a base on silica. This would also provide a clean product stream without the necessity for elaborate work up procedures.
4) In the final step of diol **52** synthesis, the reduction of diester groups of the amide **51** requires the presence of $LiBH_4$. While the reaction is fast and effective, in flow, it is quite tricky to maintain accurate flow rates due to gas generation which changes the nature of the flow from homogeneous to heterogeneous. Air tight gas syringes and stainless steel reactor tubing, which is inert to external conditions and devoid of moisture can be used.
5) Where improper or slow mixing is found to either lower the yield of the product formed or slow down the reaction, a static mixer module can be incorporated within the flow system. Also, if there is a necessity for liquid extraction of a compound of interest, a multi-stage extraction unit, such as one built by Zaiput Technologies, can be used in the flow system.[59] Recently, such a system was used in the synthesis of Lomustine **104** which is an anti-cancer drug. The extraction unit was used to remove

triethylamine present in the first reaction which could have interfered in the second step of the reaction (Scheme 31).[147]

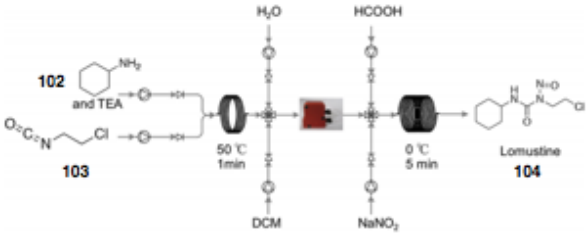

Scheme 31: Synthesis of Lomustine 104[147]

Chapter VI : Experimental Procedures

General: Chemicals were purchased from Sigma-Aldrich and were used as received without further purification. Lipase from *Pseudomonas fluorescens* (Lipase AK) was obtained in powder form from Sigma-Aldrich. ^{1}H and ^{13}C NMR spectra were obtained at 300 MHz and 75.47 MHz respectively using a Bruker Avance DPX 300 spectrometer with TMS as an internal reference. HPLC was performed on Agilent 1100 using Diacel chiralcel OD-H, Chiralpak AD-H, AS-H chiral columns. High resolution mass spectra were recorded using Qstar XL MS/MS system. FTIR spectra were recorded with a Bruker MPA NearIR FTIR system. Optical rotation values were measured using a JASCO P-1020 polarimeter. Analytical thin layer chromatography was performed using pre-coated silica gel plates (Merck 60 F_{254}, 0.2 mm thickness) and visualized using UV radiation (254 nm). Flash chromatography was performed using Merck silica gel 60 (230-400 mesh). Transmission electron microscopy images were obtained using a Carl Zeiss Libra 120 Plus microscope. Scanning electron microscopy images were obtained using a FEI Quanta 600 FEG microscope.

1. Experimental Procedures of Chapter II

Synthesis and functionalisation of Fe_3O_4 magnetic nanoparticles (MNPs)

The synthesis of Fe_3O_4 magnetic nanoparticles was performed *via* the co-precipitation method.[117] A 400 ml solution of $FeSO_4.7H_2O$ (0.03 M) and $FeCl_3$ (0.057 M) was prepared by dissolving the salts in DI water. To this solution, NH_4OH solution was added drop-wise until pH reached 9. The resulting black

suspension was separated using a magnet and washed several times with DI water and ethanol. Surface modification to introduce terminals for covalent binding on the surface was carried out using (3-aminopropyl)triethoxysilane (APTES). The magnetic nanoparticles synthesized were re-suspended in ethanol (300 ml) and left to stir at 1000 rpm. To this solution, APTES (15 ml) was injected slowly and heated under reflux for 24 h. The resulting suspension was again separated by magnetization, washed with $CHCl_3$ three times, and dried under vacuum to obtain MNPs.

Synthesis of Covalent triazine-piperazine linked polymer (CTPP-1)

Synthesis of CTPP-1 was performed based on the procedure designed by Das *et al*.[107] Piperazine (142 mg, 1.65 mmol) was dissolved in 10 ml 1,2-dichlorobenzene through sonication and was allowed to stir at 0 °C under argon protection. *N,N*-diisopropylethylamine (DIPEA) was added to the mixture at 0 °C under vigorous stirring. Cyanuric chloride (184 mg, one mmol) was dispersed in five ml 1,2-dichlorobenzene through sonication and was added drop-wise into the mixture under complete argon protection and was allowed to stir for six hours at 0 °C. The temperature was slowly increased to 25 °C and the mixture was allowed to stir for four hours. The solution was then transferred to Teflon coated autoclave which was placed in a synthesis oven with slow increase of temperature to 180 °C and the reaction was allowed to proceed at this temperature for three days. After completion, the autoclave was slowly cooled and CTPF-1 was collected as an off-white powder after filtration and washing several times with 1,2-dichlorobenzene, THF, 1,4-dioxane, $CHCl_3$ and EtOH.

Synthesis of KCC-1 and its pre-activation using APTES

Synthesis of KCC-1 was performed following the procedure reported by Polshettiwar *et al*.[108] Cyclohexane (30 ml) and pentanol (1.5 ml) were mixed and allowed to stir to which Tetraethylorthosilicate (TEOS) (2.5 g, 12 mmol) was then added to form a homogeneous solution. In a separate round bottom flask (RBF), cetylpyridinium bromide (CPB) (1 g, 2.6 mmol) was dissolved in 30 ml water and allowed to stir. After 15 minutes, urea (0.6 g, 10 mmol) was added to the aqueous solution of CPB. The solution was allowed to stir at room temperature for 30 minutes until complete dissolution of urea. The aqueous solution of CPB and urea was then added dropwise to the silica solution and the resulting mixture was allowed to stir for 30 minutes at room temperature. The resulting solution was placed in a Teflon sealed microwave (MW) reactor. The reaction mixture was irradiated with MW (400 W maximum power) at 120 °C for four hours. After completion of the reaction, the mixture was allowed to cool to room temperature and the silica formed was isolated by centrifugation, washed with distilled water and acetone, and air dried for 24 hours. The synthesised material was then calcined at 550 °C for six hours in air. Surface modification to introduce free NH_2- groups on the surface of KCC-1 nanospheres was carried out using APTES. KCC-1 particles synthesised were re-suspended in 300 ml EtOH and left to stir at 1000 rpm. To this solution, APTES (15 ml) was injected slowly and heated under reflux for 24 h. The resulting suspension was again separated by centrifugation and washed with $CHCl_3$ three times and dried under vacuum to obtain APTES coated KCC-1.

General procedure for immobilisation of lipase AK on support materials

To 100 mg of support material, 3.3 ml of 0.1 M sodium phosphate was added. To this suspension, 100 mg of lipase AK in its native form is added and the resulting suspension is allowed to shake at 800 rpm for 24 hours. In case of covalent binding of lipase AK, prior to adding the lipase, 1 ml of glutaraldehyde is added to the support material-buffer suspension, followed by addition of lipase AK. The suspension is then allowed to shake at the desired temperature at 800 rpm for 24 hours. After the immobilisation, the immobilised lipase AK with support is separated and dried after washing five times with buffer. The supernatant is used to quantify the immobilisation yield.

2. Experimental Procedures of Chapter III

General procedure for desymmetrisation of diols

To 0.2 mmol of diol dissolved in 64 mM of MeCN under vacuum and 4 °C, molecular sieves were added. The mixture was allowed to stir followed by addition of vinyl acetate (10 eq.) after 15 minutes. The reactions were allowed to proceed at 4 °C until completion.

Hydrolysis of diacetate under optimal conditions

To a solution of diacetate **53** (0.2 mmol) in buffer (pH 7) and THF (10:1, v/v) was added lipase AK/MNP-iAK at room temperature. The reaction was stirred for 24 h and extracted with brine, dried with $MgSO_4$, filtered and evaporated under reduced pressure to provide a crude mixture of diol **52** and monoacetate (*S*)-**54**.

Dimethyl 2-(3-oxo-3-(phenylamino)propyl)malonate 60

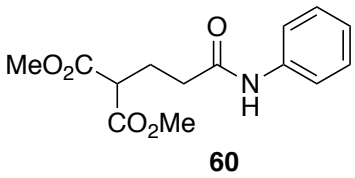

60

To a solution of acid (3.0 g, 14.75 mmol) in CH_2Cl_2 (74 ml, 0.2 M) was added *N*,*N*'-Dicyclohexylcarbodiimide (DCC) (3.6 g, 17.7 mmol). 4-Dimethylaminopyridine (DMAP) (0.18 g, 1.47 mmol) was then added to the resulting slurry which was allowed to stir until complete dissolution of DCC and DMAP. Aniline (1.6 ml, 17.7 mmol) was then added dropwise and the reaction was monitored by TLC and allowed to proceed until completion. The mixture was then filtered and CH_2Cl_2 was removed under reduced pressure. The resulting yellow oil was purified using column chromatography (EtOAc/Hexane 1:1) to obtain the amide as a yellow solid (1.37 g, yield 54%), m.p. 99-101 °C. FTIR (KBr): $\tilde{\nu}_{max}$= 1744, 1729, 1688, 1536, 769, 698 cm-1. ^{1}H NMR ($CDCl_3$, 300 MHz): δ = 2.29-2.36 (t, *J*=21 Hz, 2H), 2.44-2.49 (m, 2H), 3.55-3.60 (t, *J*=14.1 Hz, 1H), 3.72-3.75(s, 6H), 7.08-7.13 (t, *J* = 14.7 Hz, 1H), 7.29-7.34 (t, *J* = 15.9 Hz, 2H), 7.49 (d, *J* = 2H) ppm. ^{13}C NMR ($CDCl_3$, 75 MHz): δ = 24.4, 25.6, 34.4, 50.4, 52.7, 119.8, 124.3, 129.0, 137.8, 169.6 ppm. HRMS (ESI-positive mode): *m/z* calcd. for $C_{14}H_{17}NO_5$ 279.2878, found 280.1181 $[M + H]^+$.

5-hydroxy-4-(hydroxymethyl)-*N*-phenylpentanamide 61

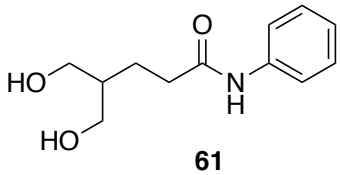

61

MeOH (0.8 mL, 20.21 mmol) was added to a solution of amide (1.2 g, 4.29 mmol) in anhydrous THF (43 mL). To this solution, $LiBH_4$ 2 M in THF (17.17 mmol) was added dropwise at 0 °C under an inert atmosphere. The reaction was warmed to room temperature and allowed to stir for 1 h, monitored

by TLC and quenched with saturated NH_4Cl solution after completion. The mixture was then separated, and the aqueous phase was extracted with ^{i}PrOH: $CHCl_3$ (1:4 v/v). The combined organic phases were washed with brine, dried with $MgSO_4$ and concentrated under reduced pressure. The crude yellow oil obtained was triturated with EtOAc to give diol as a yellow solid (63% yield), m.p. 86-88 °C. FTIR (KBr): $\tilde{\nu}_{max}$=1660, 1598, 1528, 757 cm^{-1}. ^{1}H NMR (CD_3OD, 300 MHz): δ = 1.45-1.72 (m, 3H), 2.29-2.34 (t, *J* = 15 Hz, 2H), 3.42-3.48 (d, *J* = 16.2 Hz, 4H), 4.49-4.56 (2H), 6.91-6.96 (1H), 7.12-7.18 (2H), 7.38 (2H) ppm. ^{13}C NMR (CD_3OD, 75 MHz): δ = 26.7, 37.1, 45.5, 64.8, 122.8, 126.6, 131.3, 141.3, 176.1 ppm. HRMS (ESI-positive mode): *m/z* calcd. for $C_{12}H_{17}NO_3$ 223.2676, found 224.1300 $[M + H]^+$.

(+)-2-(hydroxymethyl)-5-oxo-5-(phenylamino)pentyl acetate 62

$[\alpha]_D^{19}$ = + 0.58 (*c* = 0.009, CH_2Cl_2). FTIR (KBr): $\tilde{\nu}_{max}$= 1719, 1665, 1599, 1545, 758 cm^{-1}. ^{1}H NMR ($CDCl_3$, 300 MHz): δ = 1.62-1.84 (m, 4H), 1.99-2.01 (s, 3H), 2.38-2.51 (m, 1H), 3.55-3.57 (d, *J* = 6 Hz, 1H), 3.66 (s, 1H), 4.03-4.04 (d, *J* = 3 Hz, 2H), 7.22-7.28 (t, *J* = 9 Hz, 3H), 7.43-7.46 (d, *J* = 9 Hz, 2H) ppm. ^{13}C NMR ($CDCl_3$, 75 MHz): δ = 20.94, 23.18, 33.54, 40.63, 61.67, 64.49, 126.56, 128.66, 128.75, 138.78, 171.52, 173.05 ppm. HRMS (ESI-positive mode): *m/z* calcd. for $C_{14}H_{19}NO_4$ 265.3042, found 266.1389 $[M + H]^+$. HPLC: Chiralpak AS-H (hexane:PrOH, 85:15), 0.7 mL/min, 254 nm, t_1: 16.47 min, t_2: 18.36 min.

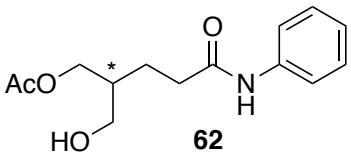

62

4-(hydroxymethyl)furan-2(5H)-one 64

To a solution of 1,3-dihydroxyacetone (2.16 g, 24 mmol) in CH_2Cl_2 (0.3 M), $Ph_3P{=}CHCO_2Me$ (6.6 g, 20 mmol) was added. The reaction was allowed to stir at room temperature for 24 h. The mixture was then filtered and washed with DI water several times to provide the hydroxymethyl butenolide as white solid (70% yield). ^{1}H NMR ($CDCl_3$, 300 MHz): δ = 3.69 (t, 1H), 4.53-4.54 (d, *J*= 1.8 Hz, 2H), 4.79-4.80 (s, 2H), 5.97-5.99 (t, *J*= 3.6 Hz, 1H) ppm. Literature values for: ^{1}H NMR: ($CDCl_3$, 400 MHz): δ = 2.55 (t, J = 5 Hz, 1H, OH), 4.60 (d, J = 5Hz, 2H, CH_2OH), 4.88 (s, 2H, CO_2CH_2), 6.04 (t with fine structure, 1H, =C*H*-) ppm.

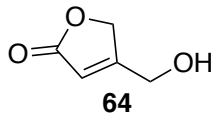

64

4-(hydroxymethyl)dihydrofuran-2(3H)-one 65

To a mixture of hydroxymethyl butenolide **11** (1 g, 8.74 mmol) in MeOH (0.4 M) was added $HCOONH_4$ (2.7 g, 43.74 mmol). Palladium on carbon (43 mg, 5 mg/mmol of **11**) was then added to this mixture followed by Et_3N (244 µL, 1.75 mmol). The reaction was allowed to react overnight under continuous H_2 supply with the reactor pressure set to 50 psig. The reaction was filtered after completion through a Celite bed and the solvent was evaporated under vacuum to obtain the hydroxymethyl butanolide **12** (61% yield) as a white solid. ^{1}H NMR ($CDCl_3$, 300 MHz): δ = 2.38-2.46 (m, 1H), 2.58-2.67 (m, 1H), 2.76-2.83 (m, 1H), 3.66-3.78 (m, 3H), 4.21-4.26 (m, 1H), 4.39-4.45 (m, 1H) ppm. Literature values for **12**:[148] ^{1}H NMR ($CDCl_3$, 400 MHz): δ = 2.3-2.9 (m, 3H), 3.65 (d, *J*= 6 Hz, 2H), 3.90 (s, 1H), 4.1-4.6 (m, 2H) ppm.

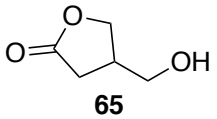

65

***N*-benzyl-4-hydroxy-3-(hydroxymethyl)butanamide 66**

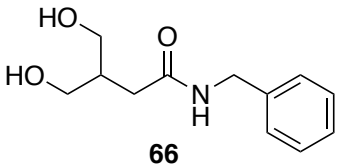

66

To a solution of hydroxymethyl butanolide **12** (0.6 g, 5.23 mmol) in toluene (0.3 M) was added $BnNH_2$ (1.1 mL, 10.46 mmol). The reaction was stirred at room temperature for 24 h. The mixture was filtered and triturated with EtOAc to provide diol **13** (72% yield) as white solid, m.p. 108-110 °C. FTIR (KBr): $\tilde{\nu}_{max}$= 1639, 1605, 1585, 1547, 733, 694 cm^{-1}. ^1H NMR (CD_3OD, 300 MHz): δ = 1.99-2.07 (m, 1 H), 2.19-2.21 (d, *J* = 6.9 Hz, 2 H), 3.20-3.21 (m, 5 H), 3.46-3.48 (m, 4 H), 4.26 (d, *J* = 2 H), 7.13-7.21 (m, 5 H) ppm. ^{13}C NMR (CD_3OD, 75 MHz): δ = 37.7, 43.6, 45.7, 64.7, 129.7, 130.1, 131.1, 141.5, 176.6 ppm. HRMS (ESI-positive mode): *m/z* calcd. for $C_{12}H_{17}NO_3$ 223.2676, found 224.1300 $[M + H]^+$.

(-)-4-(benzylamino)-2-(hydroxymethyl)-4-oxobutyl acetate 67

$[\alpha]_D^{19}$ = - 0.65 (*c* = 0.015, CH_2Cl_2). FTIR (KBr): $\tilde{\nu}_{max}$= 1638, 1608, 1585, 1548, 736, 694 cm^{-1}. ^1H NMR ($CDCl_3$, 300 MHz): δ = 1.94-1.99 (m, 3 H), 2.18-2.34 (m, 3 H), 3.49-3.60 (d, *J* = 32.1 Hz, 2 H), 3.98-4.09 (d, *J* = 33.9 Hz, 2 H), 4.34-4.36 (d, *J* = 6 Hz, 2 H), 7.18-7.26 (m, 5 H) ppm. ^{13}C NMR ($CDCl_3$, 75 MHz): δ = 20.0, 33.9, 34.6, 43.0, 63.1, 126.8, 127.0, 128.0, 137.2, 169.6, 170.2 ppm. HRMS (ESI-positive mode): *m/z* calcd. for $C_{14}H_{19}NO_4$ 265.3042, found 266.1395 $[M + H]^+$. HPLC: Chiralpak AS-H (hexane:PrOH, 80:20), 0.2 mL/min, 215 nm, t_1: 47.51 min, t_2: 50.61 min.

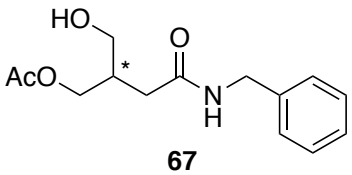

67

Dimethyl 2-(3-((4-methoxybenzyl)amino)-3-oxopropyl)malonate 69

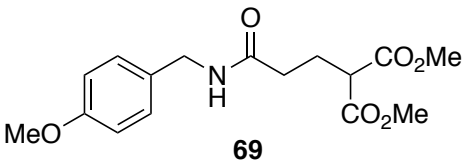

69

To a solution of acid **4** (3.0 g, 14.75 mmol) in CH_2Cl_2 (74 ml, 0.2 M) was added *N,N'*- Dicyclohexylcarbodiimide (DCC) (3.6 g, 17.7 mmol). 4-Dimethylaminopyridine (DMAP) (0.18 g, 1.475 mmol) was then added to the resulting slurry which was allowed to stir until complete dissolution of DCC and DMAP. 4-Methoxybenzylamine (1.6 ml, 17.7 mmol) was then added dropwise and the reaction was monitored by TLC and allowed to proceed until completion. The mixture was then filtered and CH_2Cl_2 was removed under reduced pressure. The resulting yellow oil was purified using column chromatography (EtOAc/hexane 1:1) to obtain the amide **14** as a white solid (1.3 g, yield 54%) m.p. 62-64 °C. FTIR (KBr): $\tilde{\nu}_{max}$= 1747, 1640, 1612, 1585, 1545, 1516, 818, 786, 728, 701 cm^{-1}.^{1}H NMR ($CDCl_3$, 300 MHz): δ = 2.06-2.18 (m, 4 H), 3.35-3.40 (t, *J* = 14.1 Hz, 1 H), 3.59 (s, 6 H), 3.65 (s, 3 H), 4.17-4.18 (d, *J* = 5.4 Hz, 2 H), 6.69-6.73 (d, *J* = 11.4 Hz, 3 H), 7.04-7.07 (d, *J* = 8.7 Hz, 2 H) ppm. ^{13}C NMR ($CDCl_3$, 75 MHz): δ = 24.4, 33.1, 42.7, 50.5, 52.4, 55.1, 113.8, 128.9, 130.5, 158.7, 169.5, 171.5 ppm. HRMS (ESI-positive mode): *m/z* calcd. for $C_{16}H_{21}NO_6$ 323.3402, found 324.1449 $[M + H]^+$.

5-hydroxy-4-(hydroxymethyl)-N-(4-methoxybenzyl)pentanamide 70

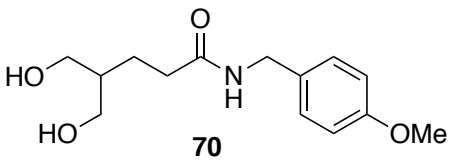

70

MeOH (0.8 mL, 20.21 mmol) was added to a solution of amide (1.2 g, 4.299 mmol) in anhydrous THF (43 mL). To this solution, $LiBH_4$ 2 M in THF (17.18 mmol) was added dropwise at 0 °C under an inert atmosphere. The reaction was warmed to room temperature and allowed to

stir for 1 h, monitored by TLC and quenched with saturated NH_4Cl solution after completion. The mixture was then separated, and the aqueous phase was extracted with *i*PrOH: $CHCl_3$ (1:4 v/v). The combined organic phase was washed with brine, dried with $MgSO_4$ and concentrated under reduced pressure. The crude yellow oil was triturated with EtOAc to give diol **15** as a white solid m.p. 55.1-56.2 °C. FTIR (KBr): $\tilde{\nu}_{max}$= 1631, 1582, 1511, 803 cm^{-1}. ^1H NMR (CD_3OD, 300 MHz): δ = 1.53-1.64 (m, 3H), 2.2-2.27 (t, *J* = 21 Hz, 2H), 3.50-3.51 (d, *J* = 5.4 Hz, 4H), 3.70 (s, 3H), 4.22-4.35 (2H), 6.79-6.83 (d, *J* = 11.7 Hz, 2H), 7.12-7.15 (d, *J* = 8.7 Hz, 2H) ppm. ^{13}C NMR (CD_3OD, 75 MHz): δ = 26.8, 36.2, 45.1, 45.5, 57.1, 64.7, 116.4, 131.4 ppm. HRMS (ESI-negative mode): *m/z* calcd. for $C_{14}H_{21}NO_4$ 267.3200, found 266.1391 $[M - H]^-$.

(+)-2-(hydroxymethyl)-5-((4-methoxybenzyl)amino)-5-oxopentyl acetate 71

$[\alpha]_D^{19}$ = + 14.69 (*c* = 0.009, CH_2Cl_2).

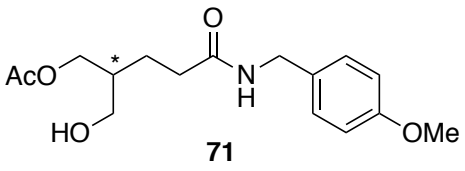

71

FTIR (KBr): $\tilde{\nu}_{max}$= 1731, 1642, 1610, 1542, 1513, 814 cm^{-1}. HRMS (ESI-positive mode): *m/z* calcd. for $C_{16}H_{23}NO_5$ 309.3566, found 310.1651 $[M + H]^+$. ^1H NMR ($CDCl_3$, 300 MHz): δ = 1.54-1.74 (3H), 1.95-1.97 (3H), 2.18-2.25 (2H), 3.46-3.48 (2H), 3.71-3.72 (3H), 3.97-4.01 (2H), 4.25-4.27 (2H), 6.75-6.80 (2H), 7.09-7.13 (2H) ppm. ^{13}C NMR ($CDCl_3$, 75 MHz): δ = 20.9, 23.1, 33.5, 40.3, 43.2, 55.3, 61.7, 64.5, 114.1, 129.2, 130.2, 159.1, 171.5, 172.7 ppm. HPLC: Chiralpak OD-H (hexane:PrOH, 85:15), 0.7 mL/min, 215 nm, t_1:21.9 min, t_2:25.4 min.

Dimethyl 2-(3-oxo-3-(phenethylamino)propyl)malonate 73

To a solution of acid (3.0 g, 14.75 mmol) in CH_2Cl_2 (74 ml, 0.2 M) was added *N,N'*-Dicyclohexylcarbodiimide (DCC)(3.6 g, 17.7 mmol). 4-Dimethylaminopyridine (DMAP) (0.18 g, 1.475 mmol) was then added to the resulting slurry which was allowed to stir until complete dissolution of DCC and DMAP. 2-Phenethylamine (1.616 ml, 17.7 mmol) was then added dropwise and the reaction was monitored by TLC and allowed to proceed until completion. The mixture was then filtered and CH_2Cl_2 was removed under reduced pressure. The resulting yellow oil was purified using column chromatography (EtOAc/hexane 1:1) to obtain the amide as a colourless oil (1.3 g, yield 54%) FTIR (KBr): $\tilde{\nu}_{max}$= 1732, 1644, 1543, 748, 699 cm^{-1}. ^1H NMR($CDCl_3$, 300 MHz): δ = 2.21-2.22 (m, 4H), 2.80-2.85 (t, *J* = 14.1 Hz, 2H), 3.45-3.56 (m, 3H), 3.74 (s, 6H), 7.19-7.32 (m, 5H) ppm. ^{13}C NMR ($CDCl_3$, 75 MHz): δ = 24.5, 33.5, 35.6, 40.6, 50.5, 52.6, 126.5, 128.6, 128.7, 138.8, 169.5, 171.4 ppm. HRMS (ESI-positive mode): *m/z* calcd. for $C_{16}H_{21}NO_5$ 307.3408, found 308.1491 $[M + H]^+$.

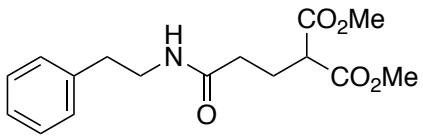

73

5-hydroxy-4-(hydroxymethyl)-N-phenethylpentanamide 74

MeOH (0.8 mL, 20.21 mmol) was added to a solution of amide (1.2 g, 4.3 mmol) in anhydrous THF (43 mL). To this solution, $LiBH_4$ 2 M in THF (17.17 mmol) was added dropwise at 0 °C under an inert atmosphere. The reaction was warmed to room temperature and allowed to stir for 1 h, monitored by TLC and quenched with saturated NH_4Cl solution after

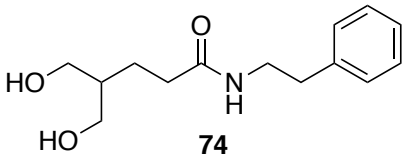

74

completion. The mixture was then separated and the aqueous phase was extracted with *i*PrOH: $CHCl_3$ (1:4 v/v). The combined organic phase was washed with brine, dried with $MgSO_4$ and concentrated under reduced pressure. The crude yellow oil was triturated with EtOAc to give diol **17** as a white solid (63% yield) m.p. 106.5-107.1 °C. FTIR (KBr): $\tilde{\nu}_{max}$= 1629, 1602, 1545, 769, 746, 696 cm^{-1}. ^1H NMR(CD_3OD, 300 MHz): δ = 1.49-1.58 (m, 3H), 2.16-2.22 (t, *J* = 12 Hz, 2H), 2.69-2.74 (t, *J* = 9 Hz, 2H), 3.30-3.35 (t, *J* = 9 Hz, 2H), 3.47-3.49 (d, *J* = 6 Hz, 4H), 7.09-7.23 (m, 5H) ^{13}C NMR(CD_3OD, 75 MHz): δ = 26.7, 36.1, 38.0, 43.5, 45.4, 64.7, 128.8, 131.0, 131.3, 142.0, 177.7 ppm. HRMS (ESI-positive mode): *m/z* calcd. for $C_{14}H_{21}NO_3$ 251.3206, found 252.1593 $[M + H]^+$.

(+)-2-(hydroxymethyl)-5-oxo-5-(phenethylamino)pentyl acetate 75

$[\alpha]_D^{20}$ = + 6.673 (*c* = 0.010, CH_2Cl_2). FTIR (KBr): $\tilde{\nu}_{max}$=1729, 1650, 1547, 748, 700 cm^{-1}. ^1H NMR ($CDCl_3$, 300 MHz): δ = 1.53-1.73

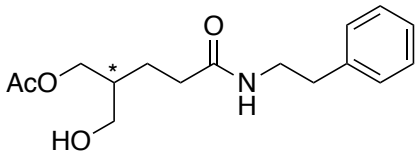

75

(m, 3H), 1.97-1.98 (s, 3H), 2.09-2.14 (t, *J* = 9 Hz, 2H), 2.72-2.77 (t, *J* = 6 Hz, 2H), 3.42-3.46 (m, 4H), 4.02-4.04 (d, *J* = 4 Hz, 2H), 7.11-7.27 (m, 5H) ppm. ^{13}C NMR ($CDCl_3$, 75 MHz): δ = 20.9, 23.2, 33.5, 35.5, 40.1, 40.6, 61.6, 64.5, 126.5, 128.6, 128.7, 138.8, 171.5, 173.0 ppm. HRMS (ESI-positive mode): *m/z* calcd. for $C_{16}H_{23}NO_5$ 309.3566, found 310.1651 $[M + H]^+$. HPLC: Chiralpak AD-H (hexane:PrOH, 85:15), 0.7 mL/min, 215 nm, t_1: 9.6min, t_2:10.2 min.

Dimethyl 2-(3-((3,4-dimethoxyphenethyl)amino)-3-oxopropyl)malonate 77

To a solution of acid (3.0 g, 14.75 mmol) in CH_2Cl_2 (74 ml, 0.2 M) was added *N,N'*- Dicyclohexylcarbodiimide (DCC) (3.6 g, 17.7 mmol). 4-Dimethylaminopyridine (DMAP) (0.18 g, 1.4 mmol) was then added to the resulting slurry which was allowed to stir until complete dissolution of DCC and DMAP. 3,4-Dimethoxyphenethylamine (1.6 ml, 17.7 mmol) was then added dropwise and the reaction was monitored by TLC and allowed to proceed until completion. The mixture was then filtered and CH_2Cl_2 was removed under reduced pressure. The resulting yellow oil was purified using column chromatography (EtOAc/hexane 1:1) to obtain the amide as a colourless oil (1.3 g, yield 54%). FTIR (KBr): $\tilde{\nu}_{max}$= 1724, 1648, 1513, 821, 761 cm^{-1}. ^1H NMR ($CDCl_3$ 300 MHz): δ = 2.22-2.24 (m, 4 H), 2.76-2.80 (t, *J* = 13.8 Hz, 2 H), 3.48-3.55 (m, 3 H), 3.75 (s, 6 H), 3.89-3.90 (s, 6 H), 6.76 (t, *J* = 2.1 Hz, 2 H), 6.82-6.87 (d, *J* = 14.7 Hz, 1 H) ppm. ^{13}C NMR ($CDCl_3$, 75 MHz): δ = 24.5, 33.5, 35.2, 40.7, 50.4, 50.5, 52.6, 52.6, 55.8, 55.9, 111.3, 111.8, 120.6, 131.2, 147.7, 149.0, 169.5, 171.5 ppm. HRMS (ESI-positive mode): *m/z* calcd. for $C_{18}H_{25}NO_7$ 367.3926, found 368.1712 $[M + H]^+$.

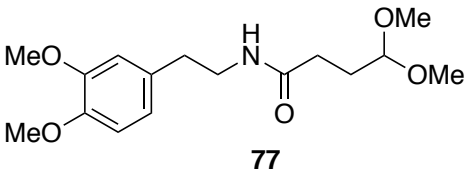

77

_N_-(3,4-dimethoxyphenethyl)-5-hydroxy-4-(hydroxymethyl)pentanamide 78

MeOH (0.8 mL, 20.21 mmol) was added to a solution of amide (1.2 g, 4.3 mmol) in anhydrous THF (43 mL). To this solution, $LiBH_4$ 2 M in THF (17.17 mmol) was added dropwise at 0 °C under an inert atmosphere. The reaction was warmed to room temperature and allowed to stir for 1 h, monitored by TLC and quenched with saturated NH_4Cl solution

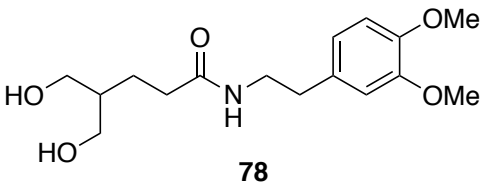

78

after completion. The mixture was then separated, and the aqueous phase was extracted with ^{i}PrOH: $CHCl_3$ (1:4 v/v). The combined organic phase was washed with brine, dried with $MgSO_4$ and concentrated under reduced pressure. The crude yellow oil was triturated with EtOAc to give diol **19** as a white solid (67% yield) m.p. 97-99 °C. FTIR (KBr): $\tilde{\nu}_{max}$= 1691, 1629, 1602, 1591, 1538, 1516, 849, 812, 765, 705 cm^{-1}. ^{1}H NMR (CD_3OD, 300 MHz): δ = 1.54-1.63 (m, 3 H), 2.19-2.24 (t, *J* = 15.3 Hz, 2 H), 2.69-2.74 (t, *J* = 14.4 Hz, 2 H), 3.29-3.30 (m, 1 H), 3.34-3.39 (t, *J* = 14.7 Hz, 2 H), 3.52-3.54 (t, *J* = 5.1 Hz, 2 H), 3.78-3.81 (s, 6 H), 6.72-6.75 (d, *J* = 10.2 Hz, 1 H), 6.82-6.86 (d, *J* = 13.5 Hz, 2 H) ppm. ^{13}C NMR (CD_3OD, 75 MHz): δ = 26.8, 36.2, 37.6, 43.5, 45.4, 57.9, 58.0, 64.7, 114.6, 115.2, 123.6, 134.9, 150.5, 151.9, 177.6 ppm. HRMS (ESI-positive mode): *m/z* calcd. for $C_{16}H_{25}NO_5$ 311.3724, found 312.1819 $[M + H]^+$.

(+)-5-((3,4-dimethoxyphenethyl)amino)-2-(hydroxymethyl)-5-oxopentyl acetate 79

$[\alpha]_D^{20}$ = + 4.464 (*c* = 0.009, CH_2Cl_2).

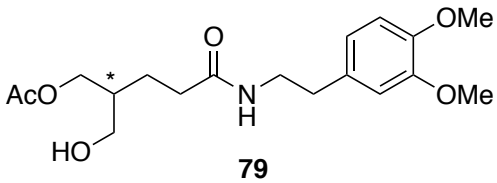

79

FTIR (KBr): $\tilde{\nu}_{max}$= 1729, 1642, 1587, 1545, 1515, 805, 762 cm^{-1}. HRMS (ESI-positive mode): *m/z* calcd. for $C_{18}H_{27}NO_6$ 353.4090, found 354.1926 $[M + H]^+$. ^{1}H NMR ($CDCl_3$, 300 MHz): δ = 1.54 – 1.73 (m, 3H), 1.99 (s, 5H), 2.66-2.71 (t, *J* = 6 Hz, 2H), 3.40-3.48 (m, 6H), 4.01-4.03 (d, *J* = 6 Hz, 2H), 6.72-6.75 (t, *J* = 3 Hz, 2 H), 6.64 -6.67 (m, 3H) ppm. ^{13}C NMR ($CDCl_3$, 75 MHz): δ = 19.9, 22.2, 32.5, 34.1, 39.1, 39.7, 54.8, 54.9, 60.6, 63.4, 110.3, 110.9, 119.6, 130.2,

146.7, 148.0, 170.5, 172.1 ppm. HPLC: Chiralpak AD-H (hexane:*i*PrOH, 85:15), 0.7 mL/min, 215 nm, t_1: 18.7 min, t_2: 20.5 min.

3. Experimental Procedures of Chapter IV

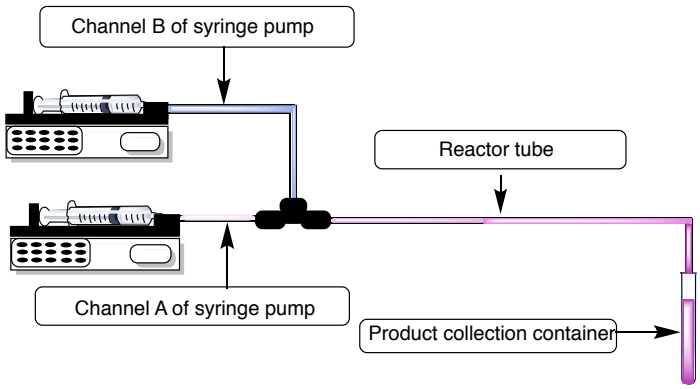

A simple flow reactor system was assembled using syringe pumps and PTFE tubing. A syringe containing one of the reactants dissolved in the reaction solvent was placed in one of the syringe pumps forming channel A. Channel B comprised of another syringe pump containing other reactant(s) and/or catalyst in a syringe. Both channels were connected to a PEEK T-junction. The third arm of the T-junction was connected to PTFE tubings of varying lengths (depending on the reaction). The other end of the PTFE tubing was connected to a container for product collection.

In case of reactions which required heating or cooling, the reactor tubing was placed accordingly in a temperature controlled hot water/oil bath or ice bath.

In case of reactions performed under ultrasonication, the reaction tubing or the reaction column were placed in the ultrasonicator.

In case of use of columns in reactions involving immobilised lipase AK, the columns were placed either in the ultrasonicator or water bath according to the reaction conditions.

Supplementary Information

^{1}H and ^{13}C NMR spectra

Dimethyl 2-(3-oxo-3-(phenylamino)propyl)malonate 60

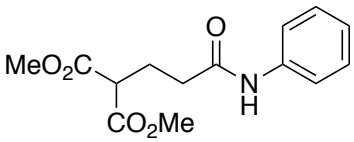

60

^{1}H NMR

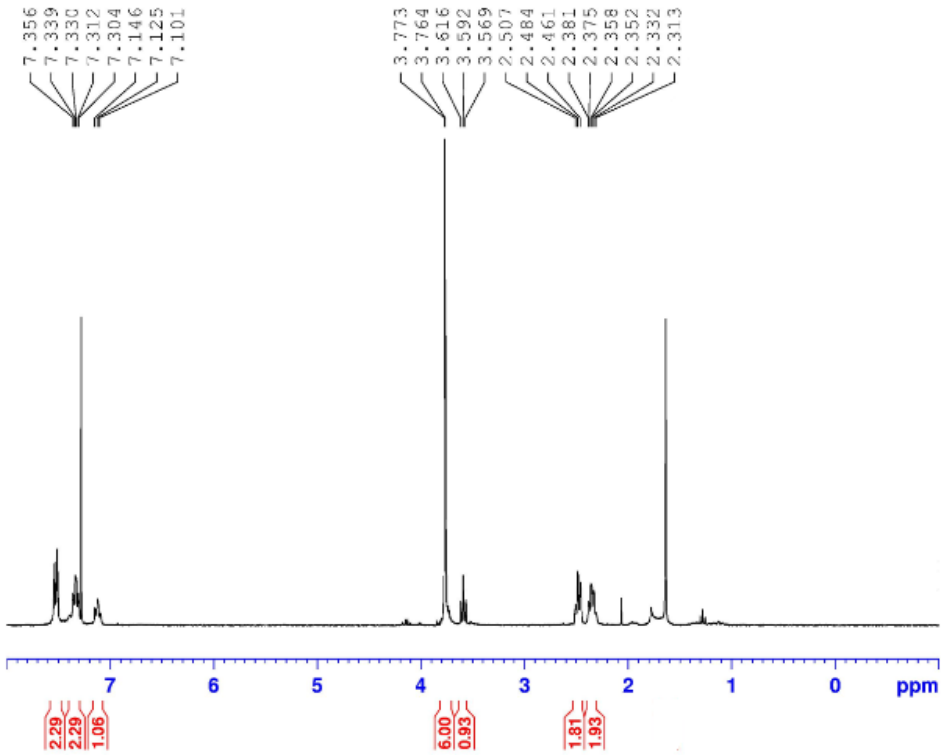

^{13}C NMR

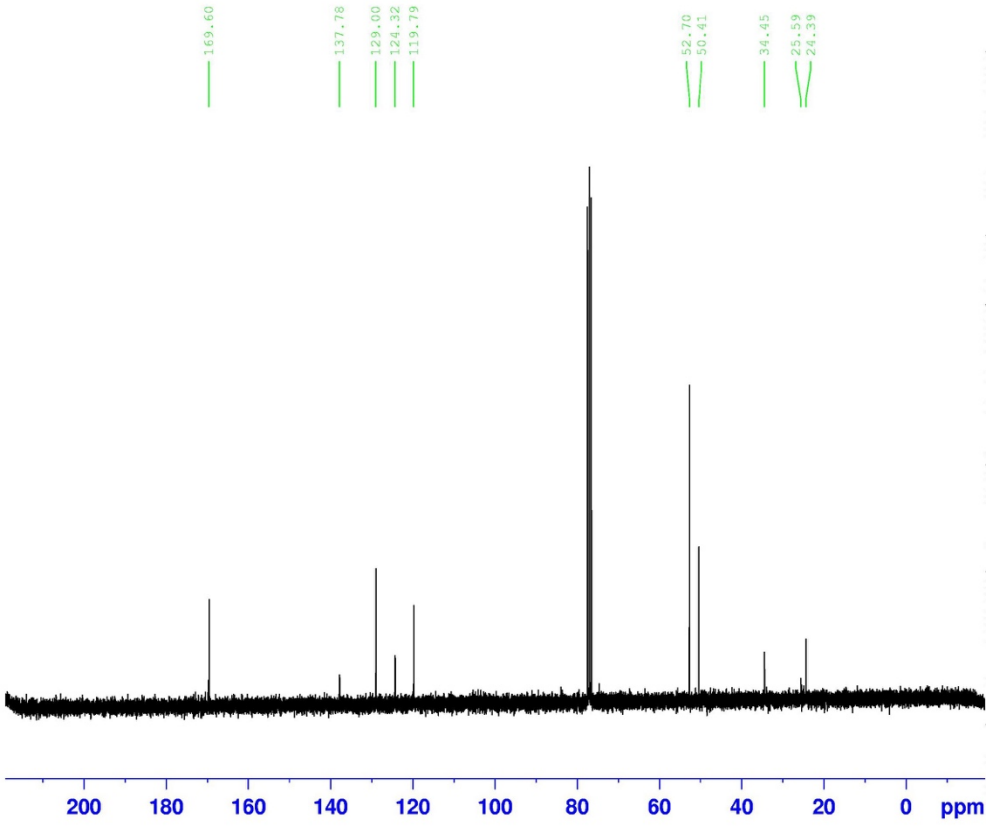
169.60
137.78
129.00
124.32
119.79
52.70
50.41
34.45
25.59
24.39
200
180
160
140
120
100
80
60
40
20
0
ppm

5-hydroxy-4-(hydroxymethyl)-*N*-phenylpentanamide 61

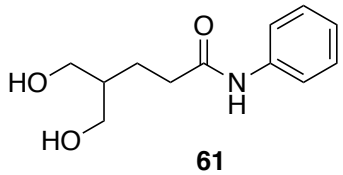

61

^{1}H NMR

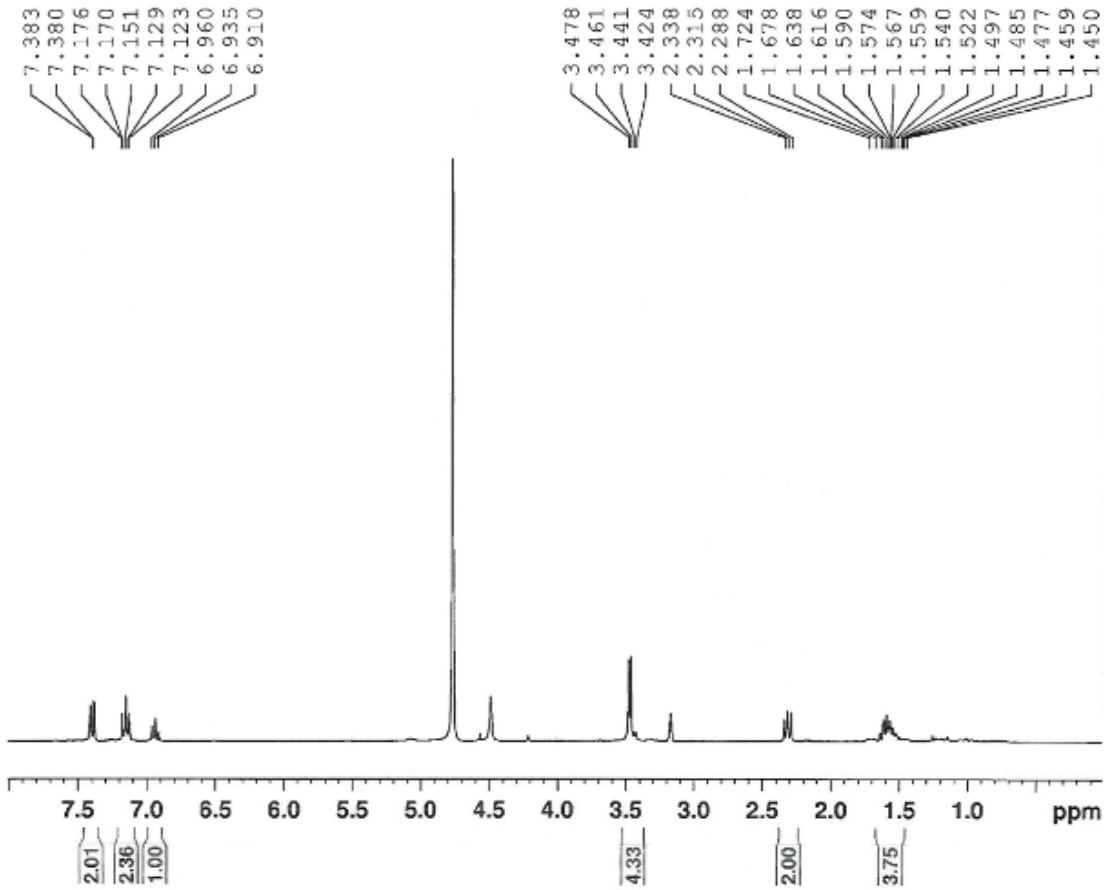

^{13}C NMR

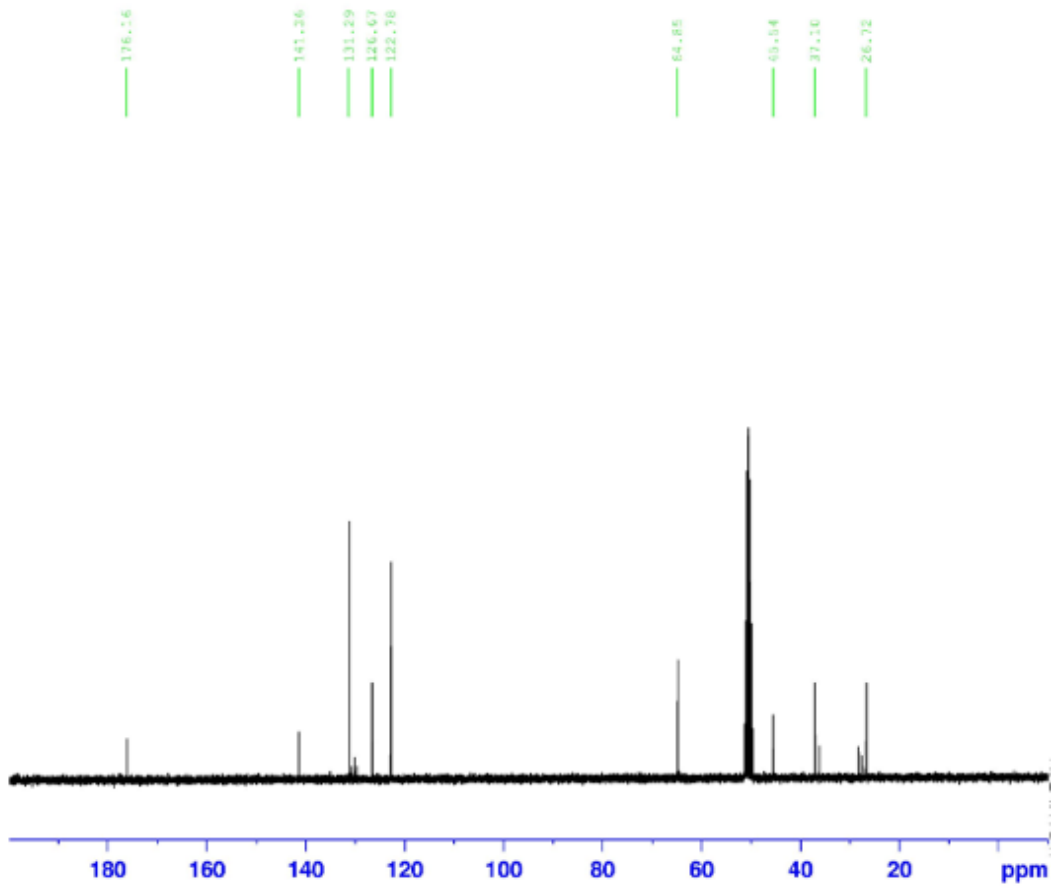
176.56
141.26
131.29
126.67
122.98
64.85
59.54
37.10
26.72
180
160
140
120
100
80
60
40
20
ppm

(+)-2-(hydroxymethyl)-5-oxo-5-(phenylamino)pentyl acetate 62

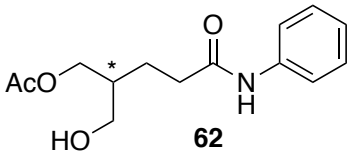

62

^{1}H NMR

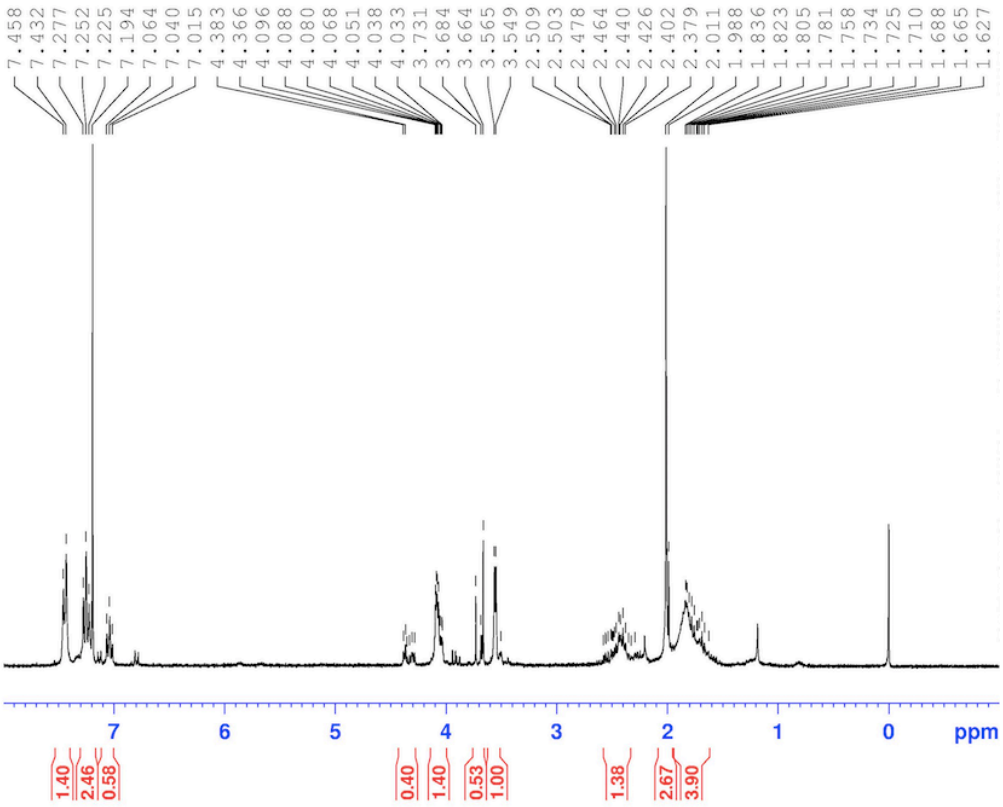

^{13}C NMR

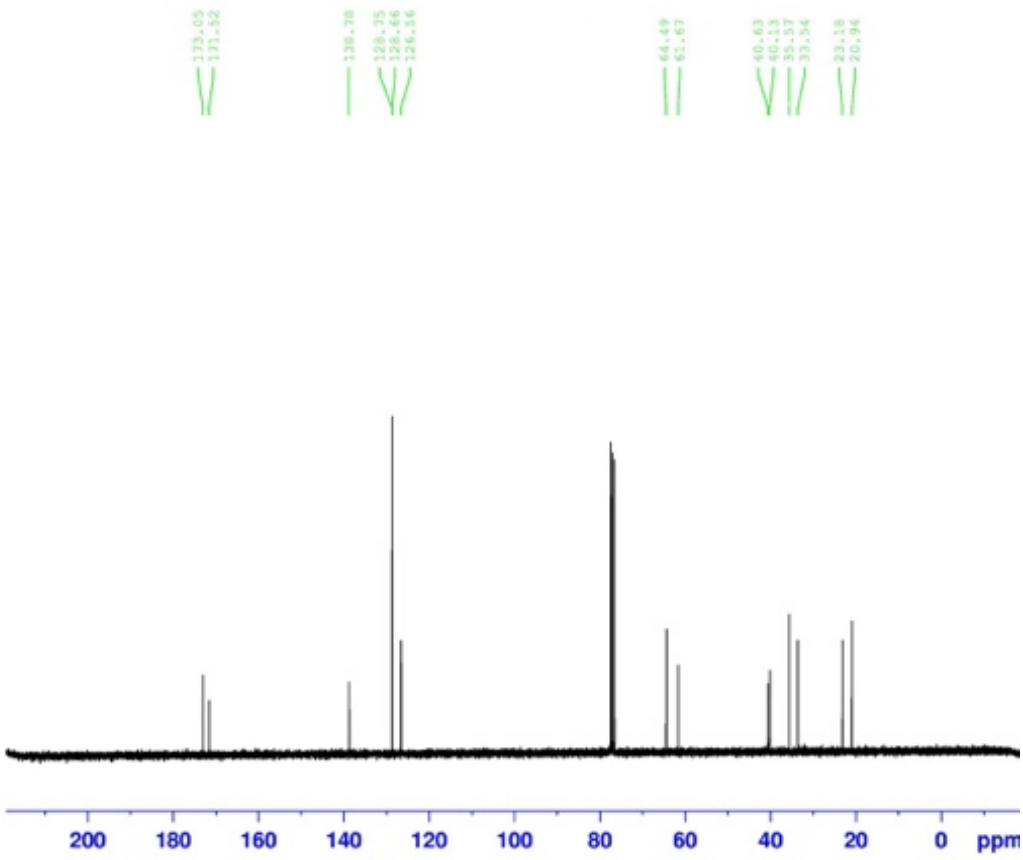
173.09
171.92
136.78
128.75
128.66
126.56
64.49
61.67
40.63
40.13
35.57
33.54
23.18
20.94
200
180
160
140
120
100
80
60
40
20
0
ppm

4-(hydroxymethyl)furan-2(5H)-one 64

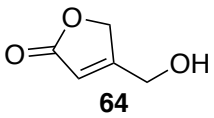

64

^{1}H NMR

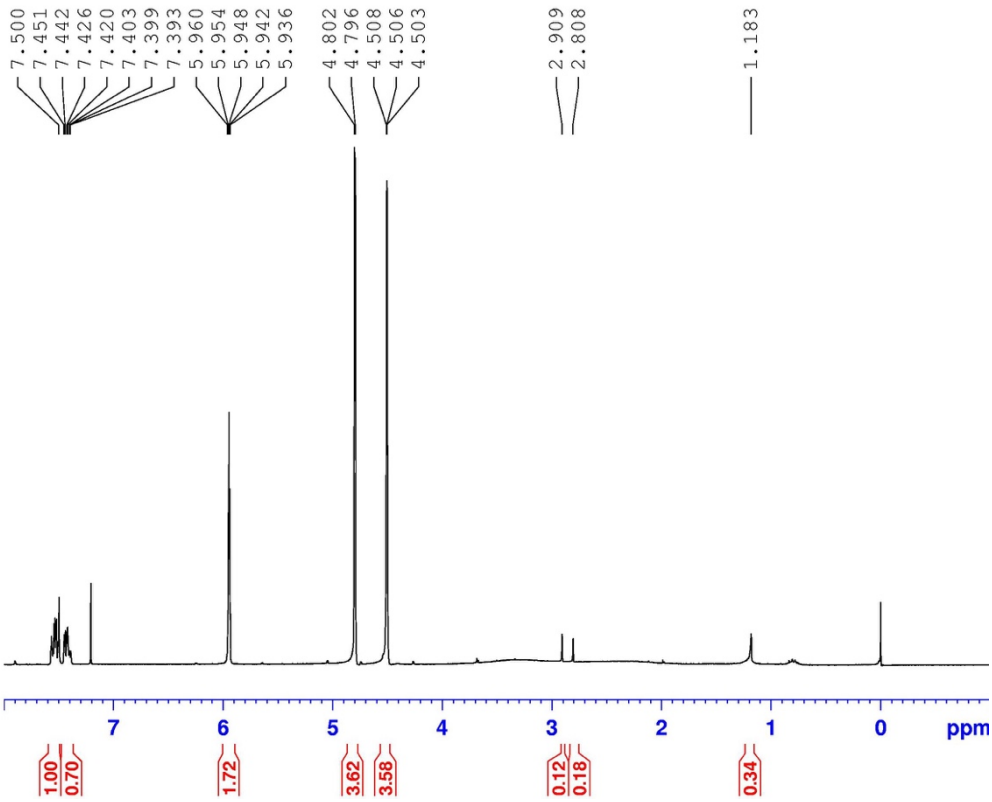

4-(hydroxymethyl)dihydrofuran-2(3H)-one 65

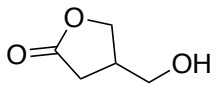

65

^{1}H NMR

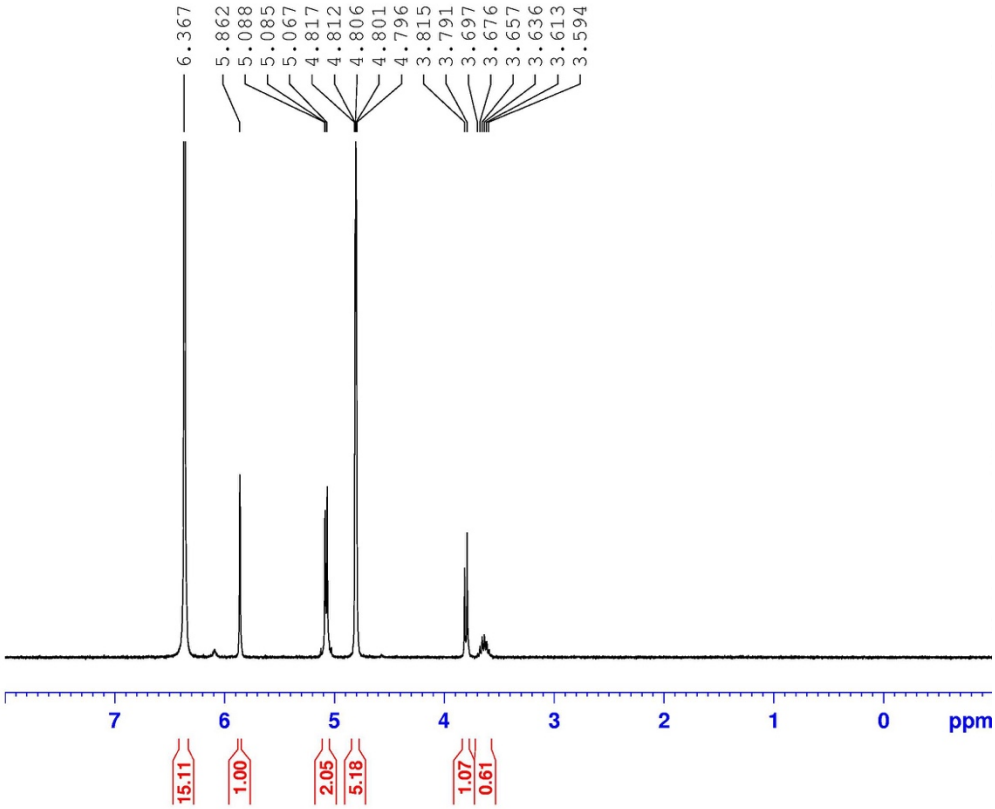

***N*-benzyl-4-hydroxy-3-(hydroxymethyl)butanamide 66**

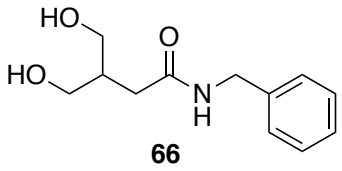

66

^{1}H NMR

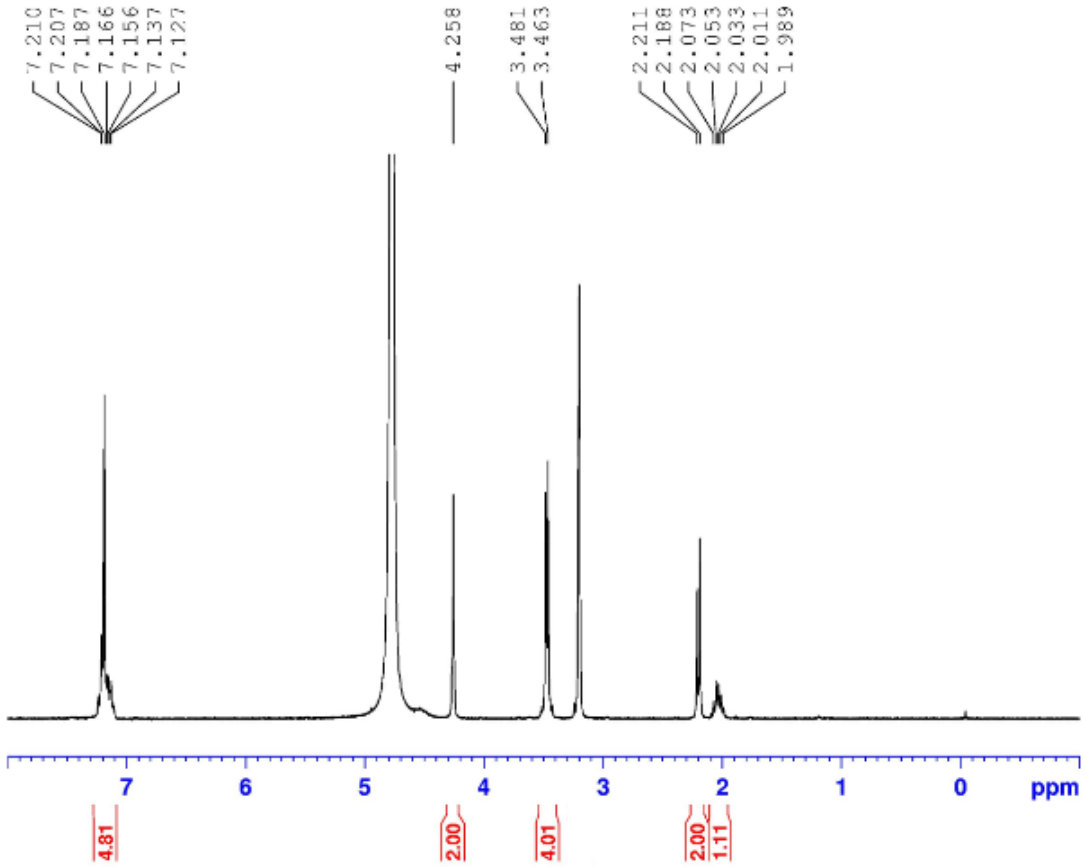

^{13}C NMR

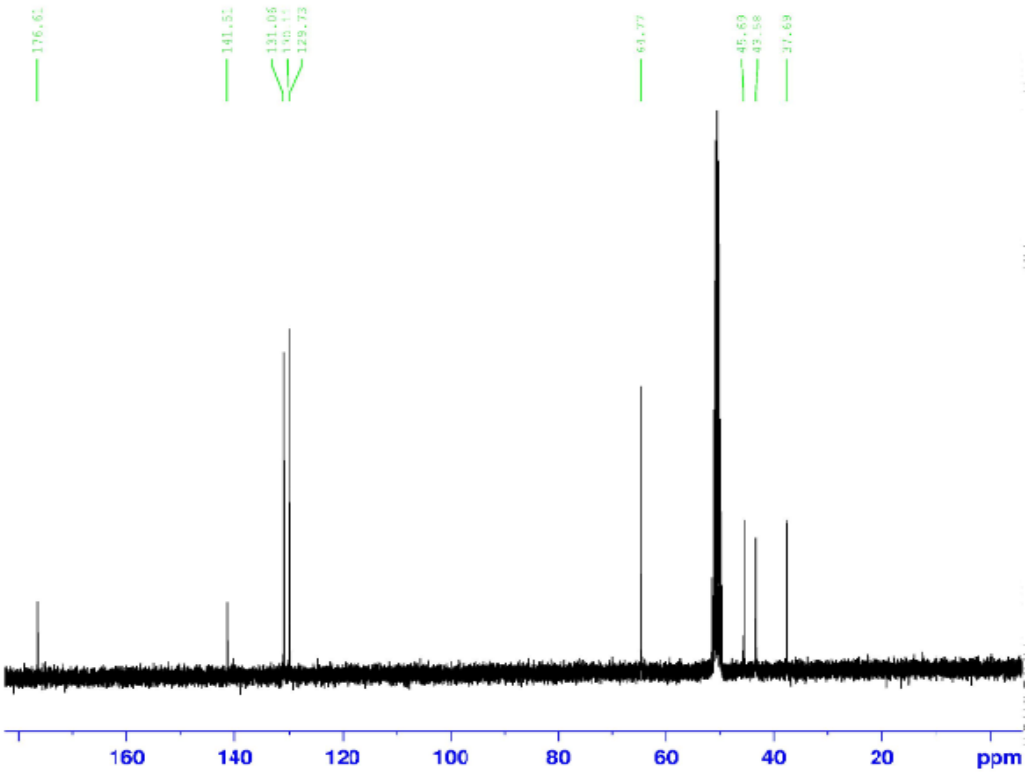
176.61
141.51
131.06
129.73
64.77
45.69
43.58
31.69
160
140
120
100
80
60
40
20
ppm

(-)-4-(benzylamino)-2-(hydroxymethyl)-4-oxobutyl acetate 67

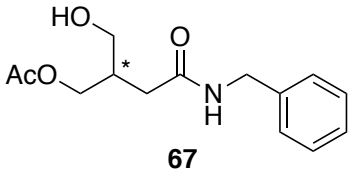

67

^{1}H NMR

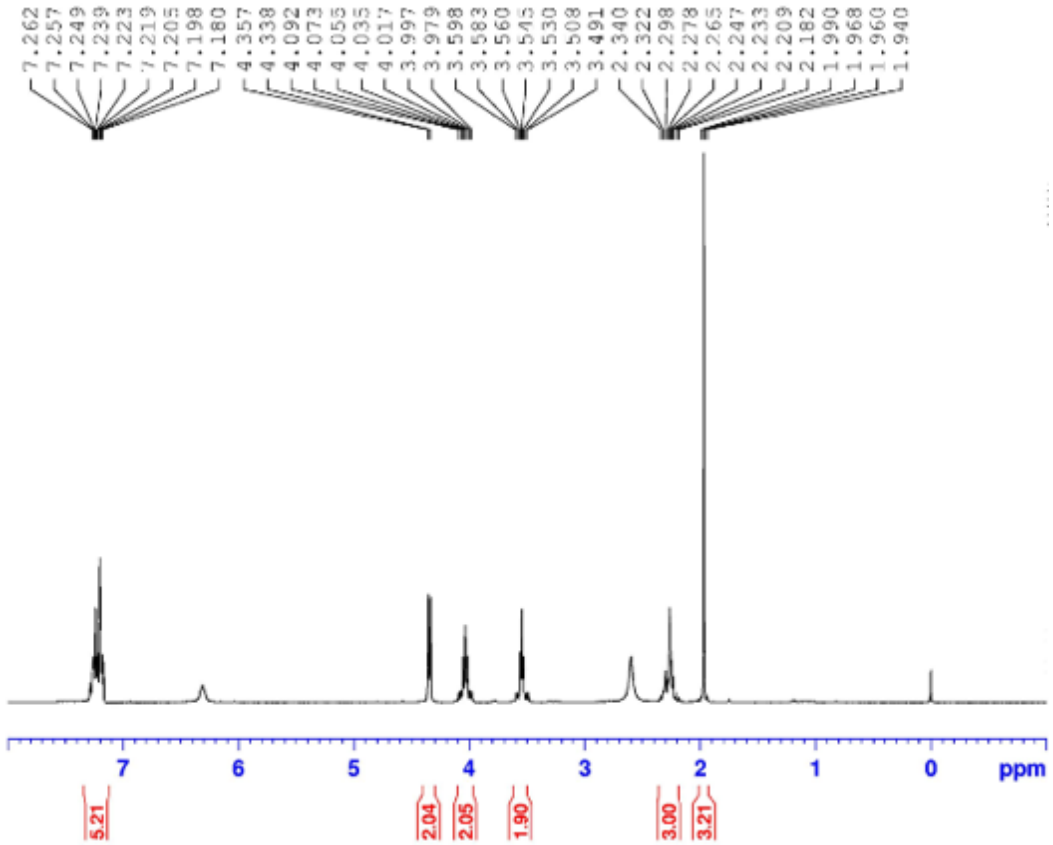

^{13}C NMR

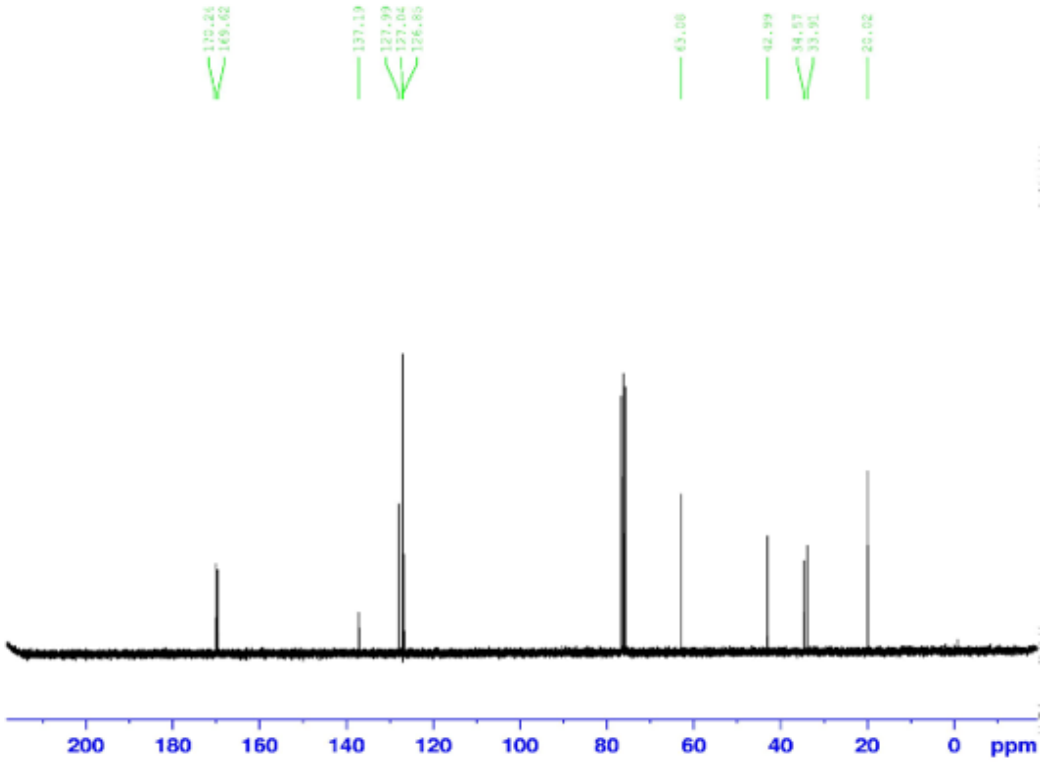
170.26
169.62
137.19
127.99
127.04
126.85
63.08
42.99
34.57
33.91
28.02
200
180
160
140
120
100
80
60
40
20
0
ppm

Dimethyl 2-(3-((4-methoxybenzyl)amino)-3-oxopropyl)malonate 69

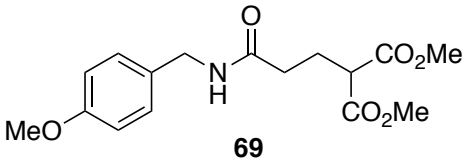

69

^{1}H NMR

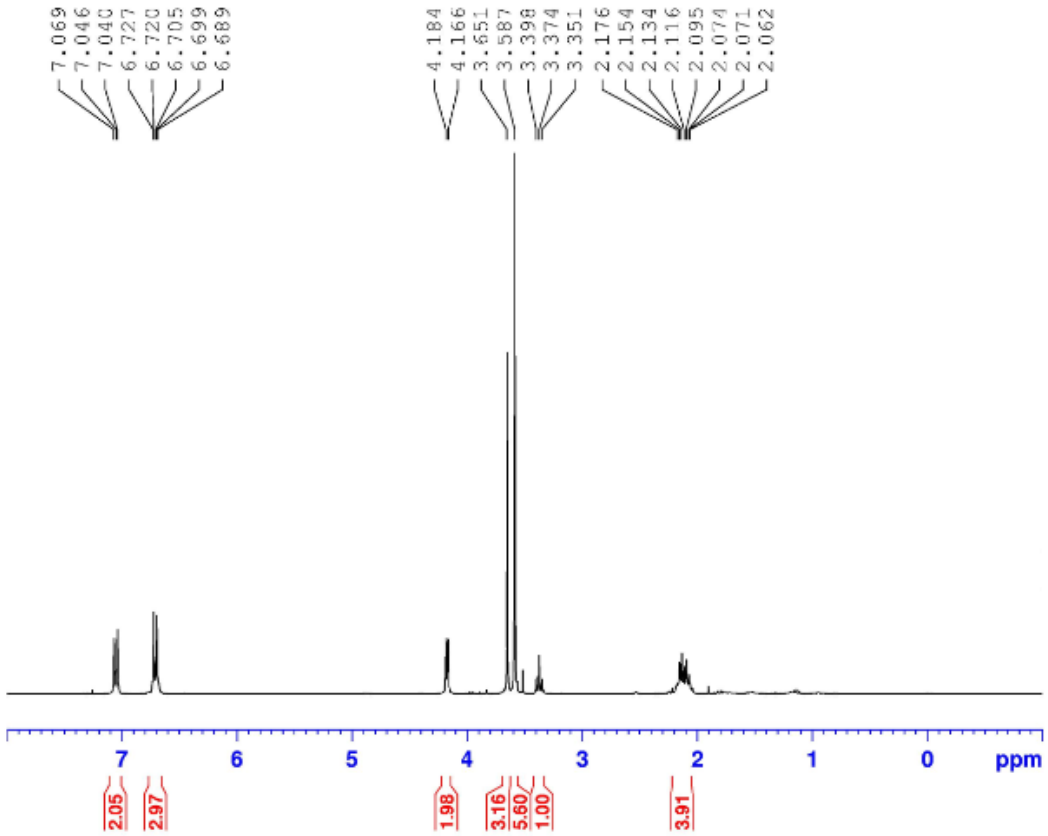

^{13}C NMR

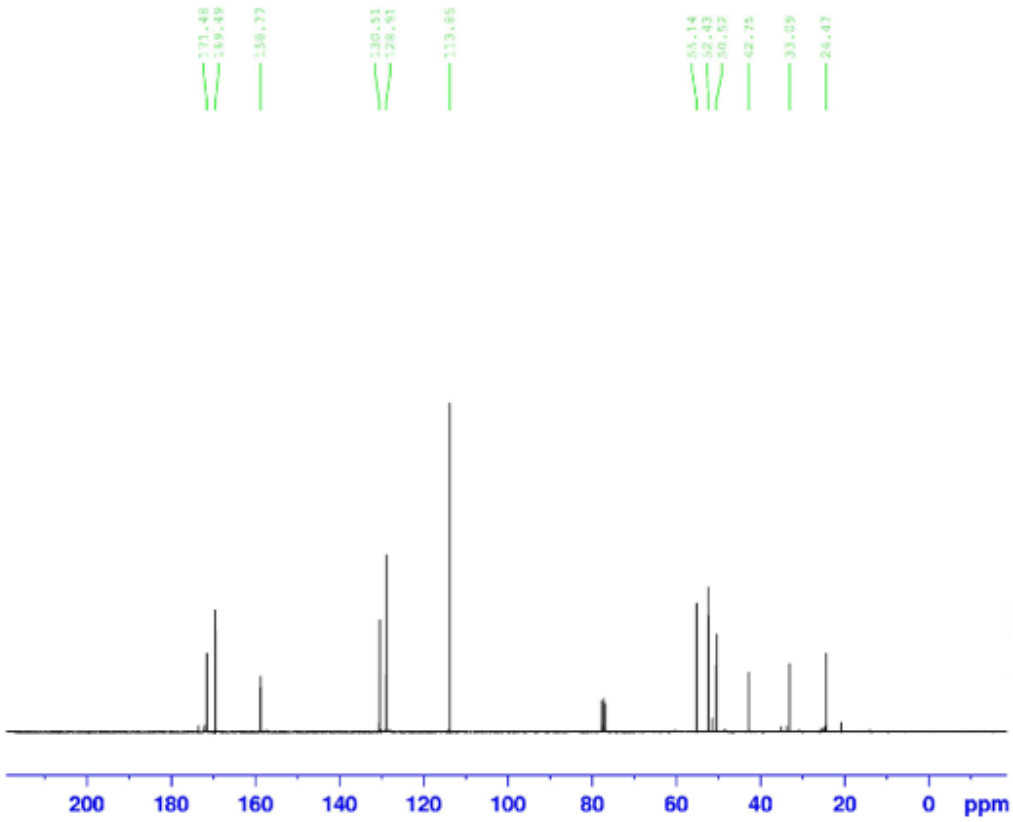
171.48
169.49
159.77
130.51
128.91
113.85
55.14
52.43
50.52
42.75
33.09
24.47
200
180
160
140
120
100
80
60
40
20
0
ppm

5-hydroxy-4-(hydroxymethyl)-N-(4-methoxybenzyl)pentanamide 70

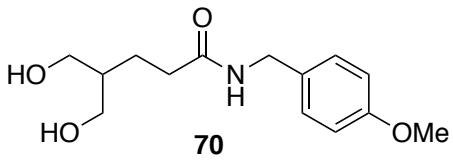

70

^{1}H NMR

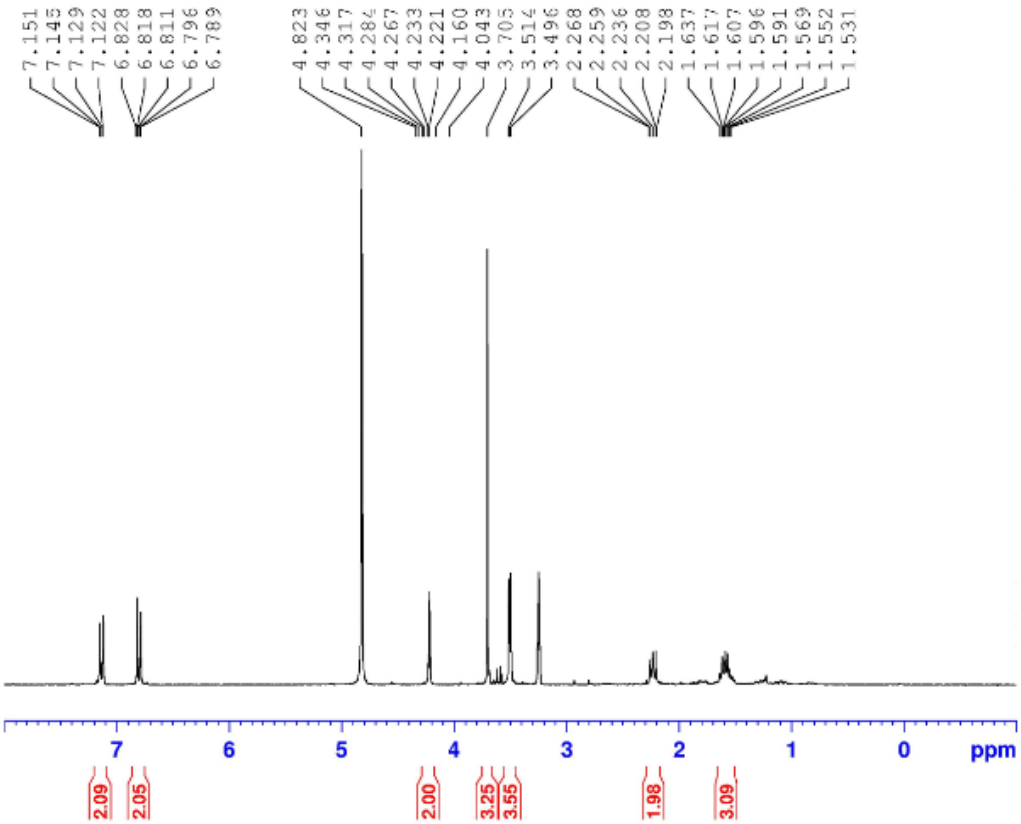

^{13}C NMR

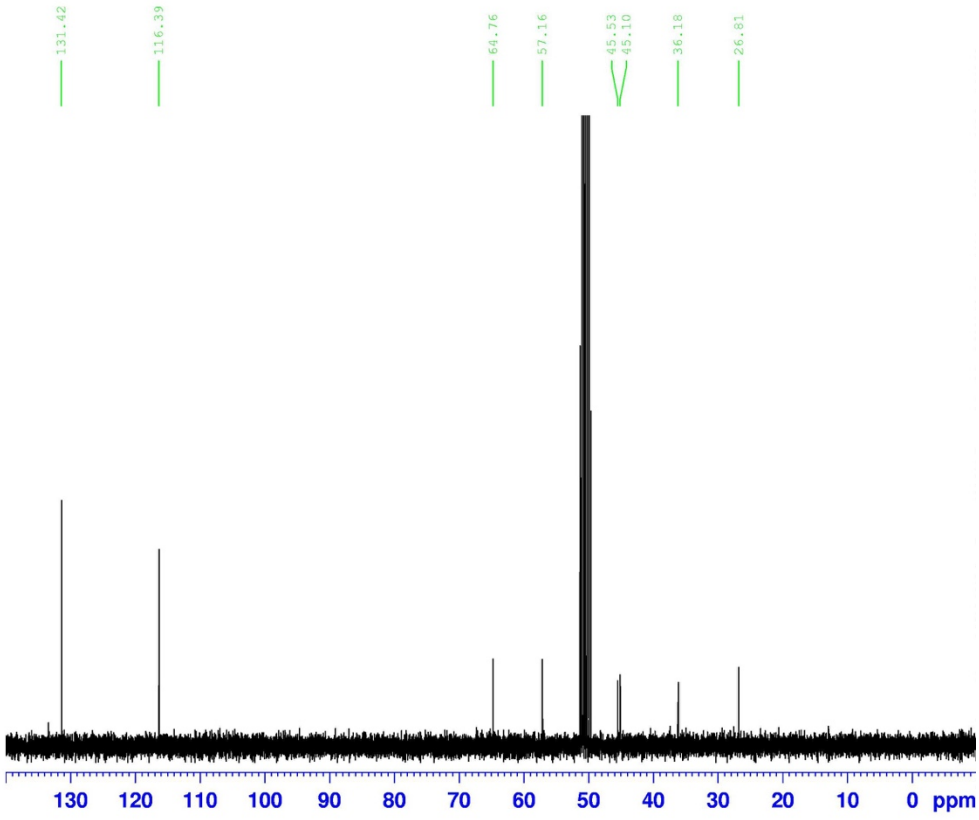
131.42
116.39
64.76
57.16
45.53
45.10
36.18
26.81
130
120
110
100
90
80
70
60
50
40
30
20
10
0 ppm

(+)-2-(hydroxymethyl)-5-((4-methoxybenzyl)amino)-5-oxopentyl acetate 71

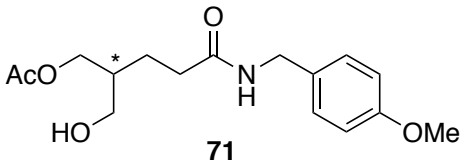

71

^{1}H NMR

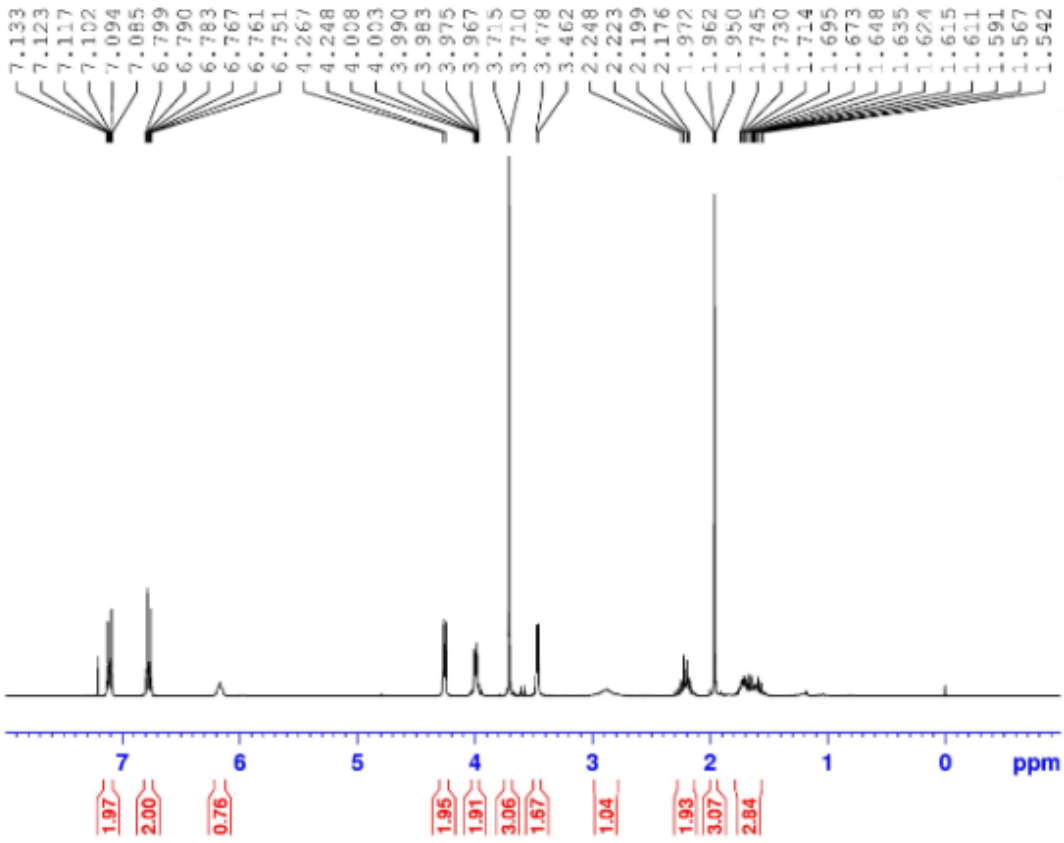

^{13}C NMR

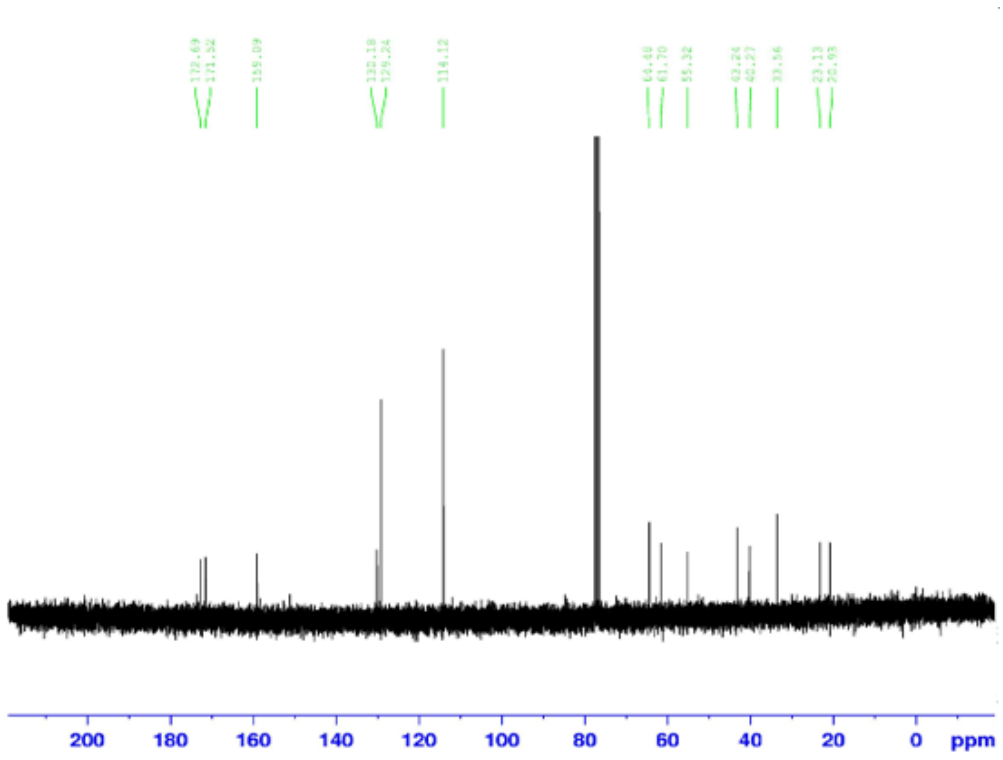
172.69
171.52
155.09
130.18
129.24
114.12
64.48
61.70
55.32
43.24
40.27
33.56
29.13
26.93
200
180
160
140
120
100
80
60
40
20
0
ppm

Dimethyl 2-(3-oxo-3-(phenethylamino)propyl)malonate 73

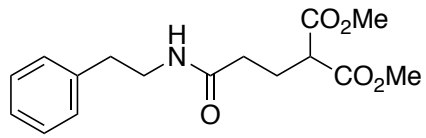

73

^{1}H NMR

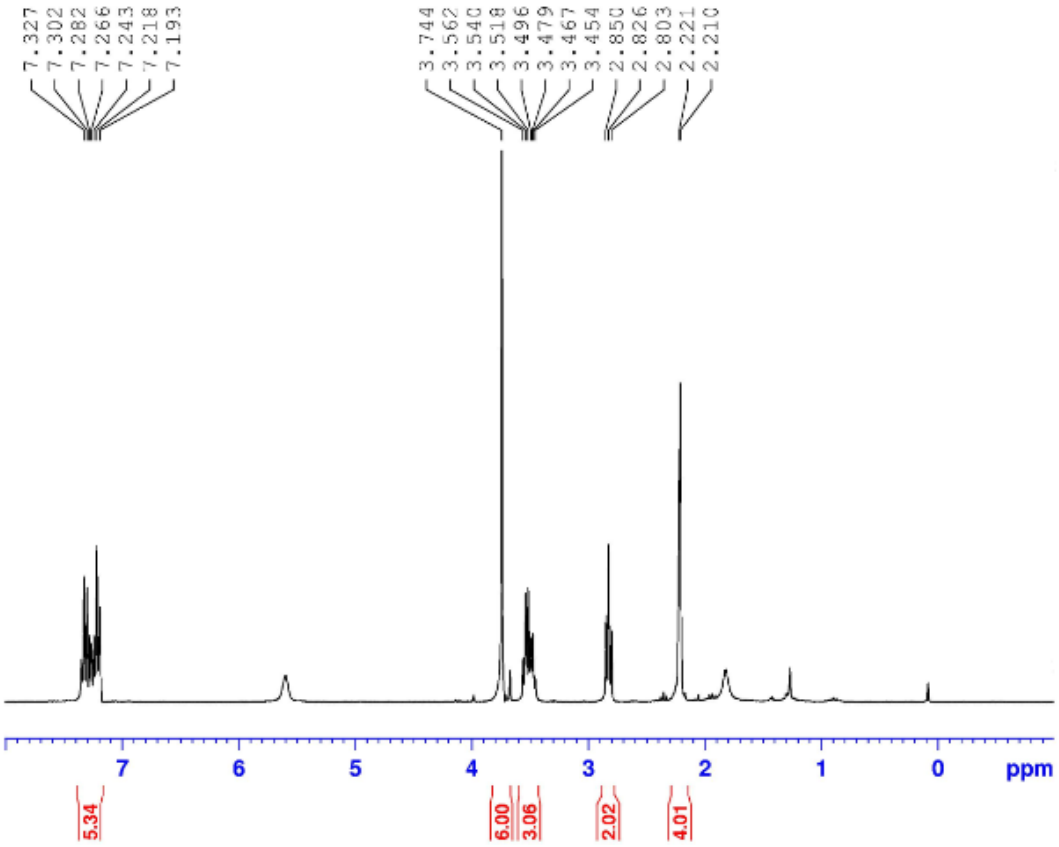

^{13}C NMR

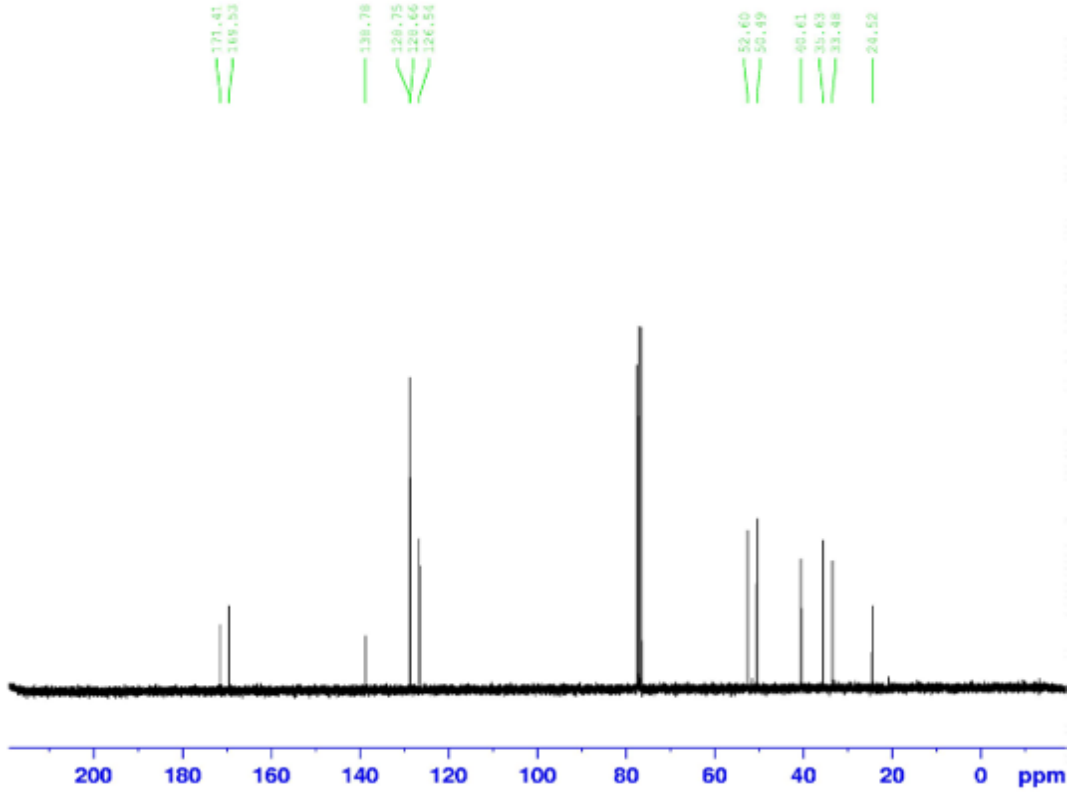
171.41
169.53
138.78
128.75
128.66
126.54
52.60
50.49
40.61
35.63
33.48
24.52
200
180
160
140
120
100
80
60
40
20
0
ppm

5-hydroxy-4-(hydroxymethyl)-N-phenethylpentanamide 74

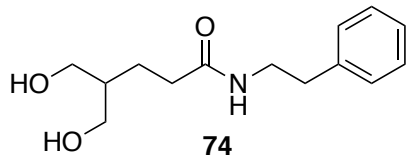

74

^{1}H NMR

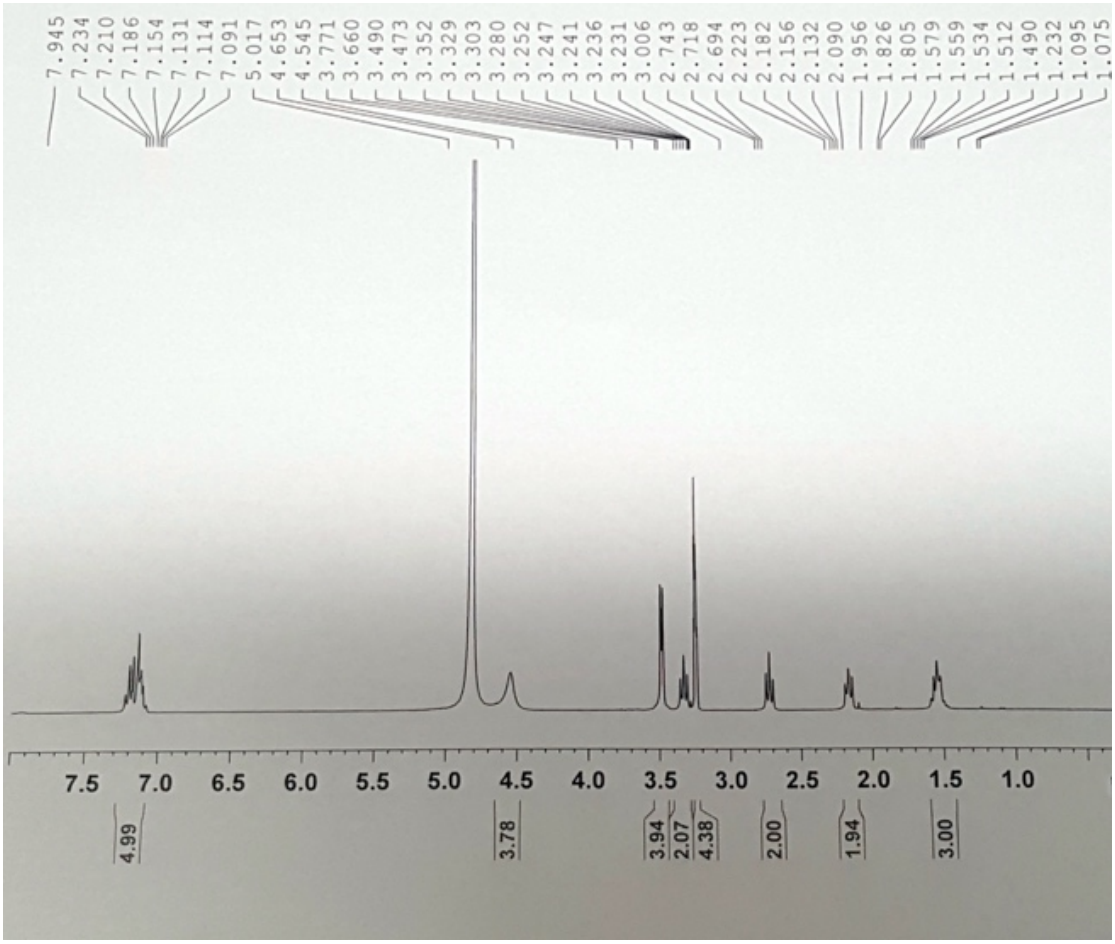

^{13}C NMR

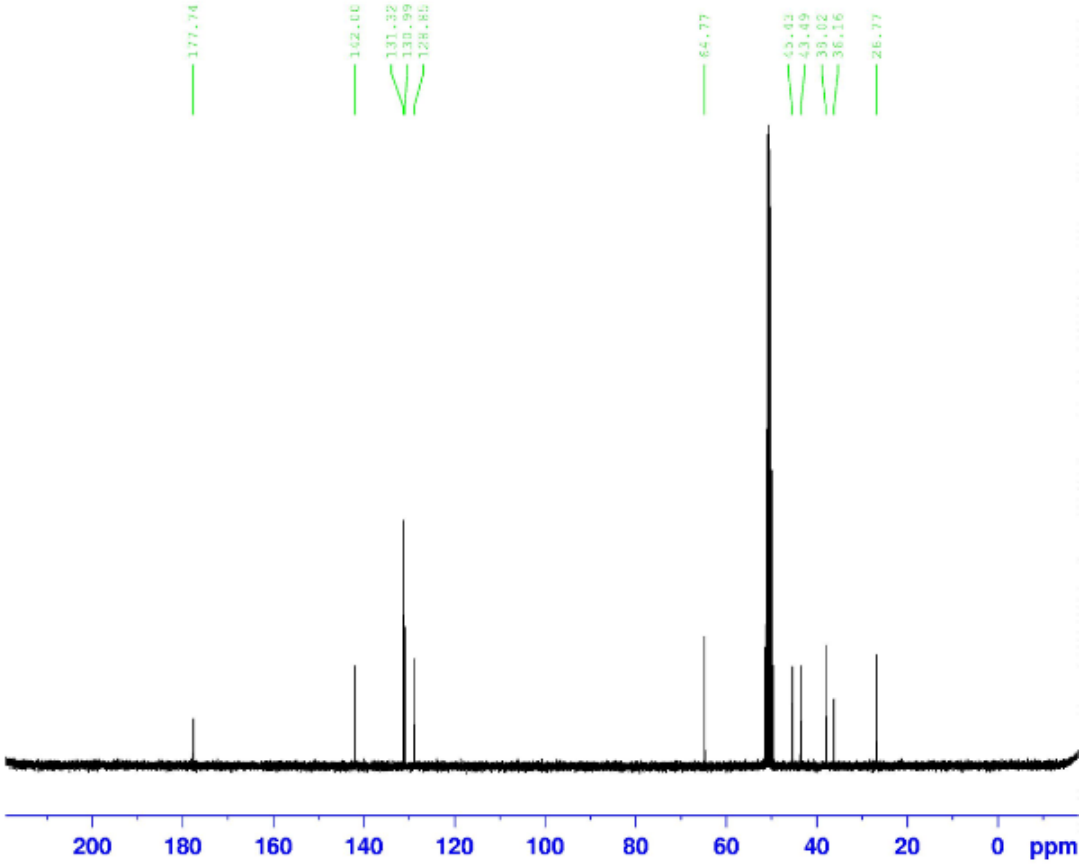
177.74
142.60
131.32
130.99
128.85
64.77
43.42
43.49
39.02
36.16
26.77
200
180
160
140
120
100
80
60
40
20
0
ppm

(+)-2-(hydroxymethyl)-5-oxo-5-(phenethylamino)pentyl acetate 75

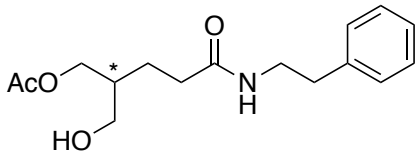

75

^{1}H NMR

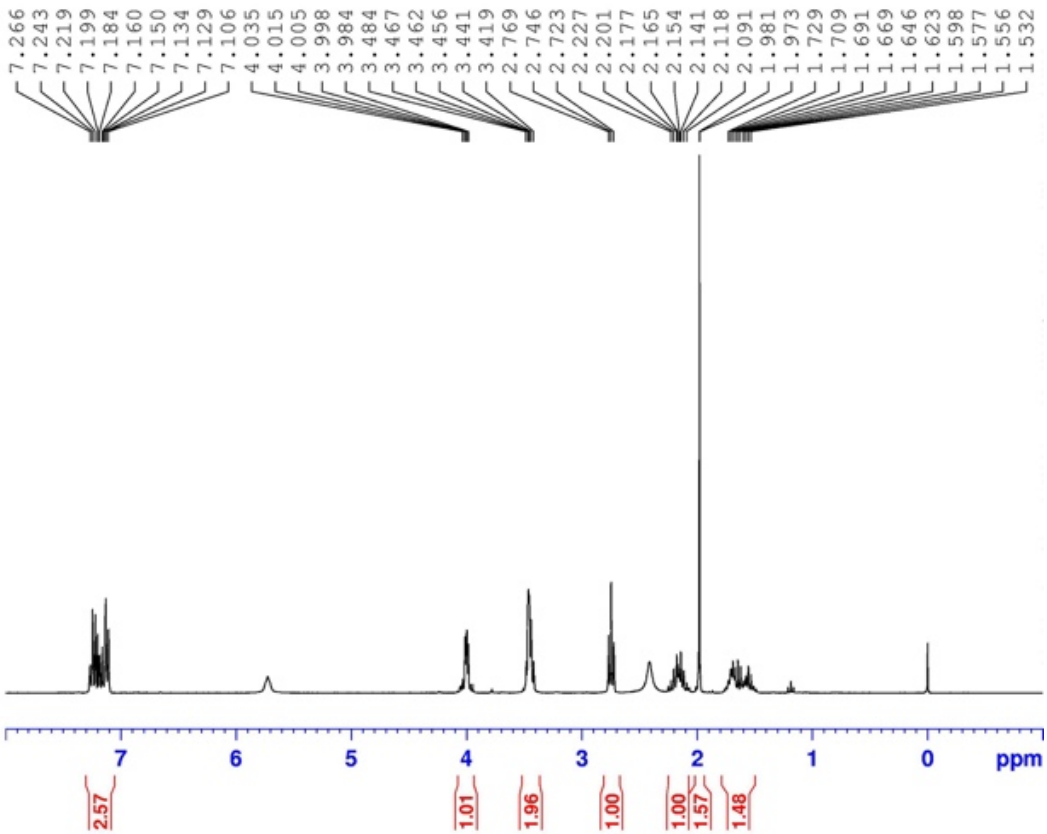

^{13}C NMR

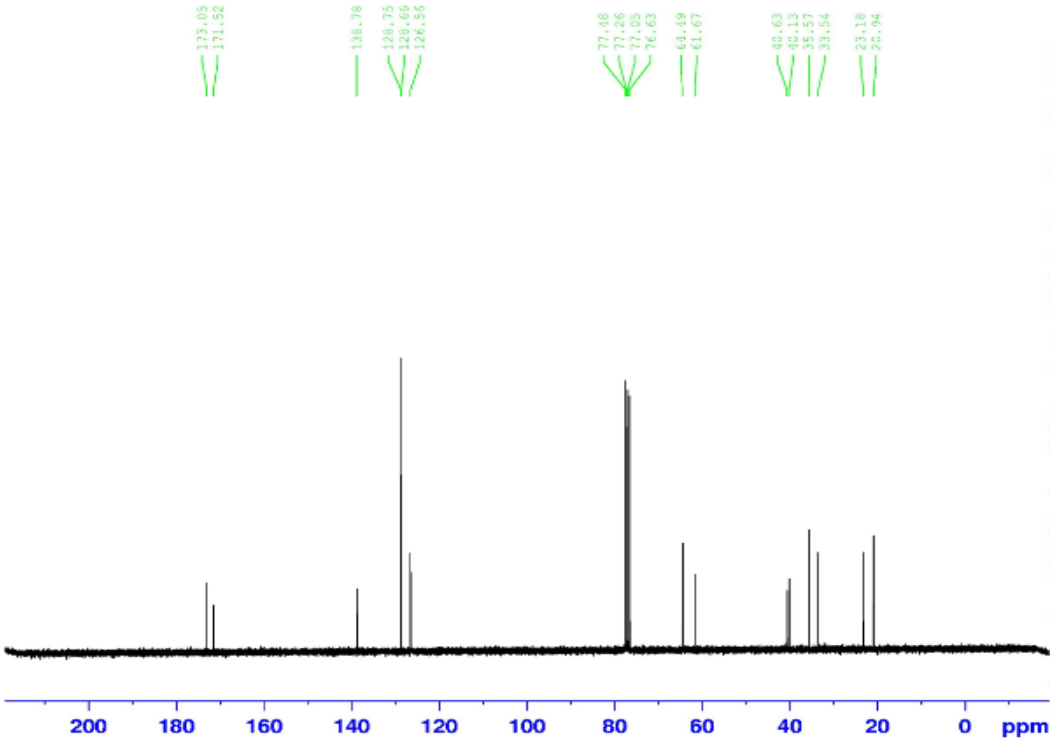
173.05
171.52
138.78
128.75
128.66
126.56
77.40
77.26
77.05
76.63
64.49
61.67
40.63
40.13
35.57
33.54
23.18
20.94
200
180
160
140
120
100
80
60
40
20
0
ppm

Dimethyl 2-(3-((3,4-dimethoxyphenethyl)amino)-3-oxopropyl)malonate 77

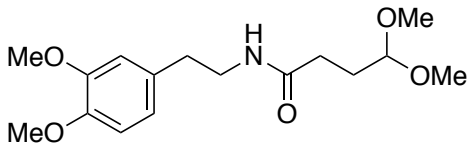

77

^{1}H NMR

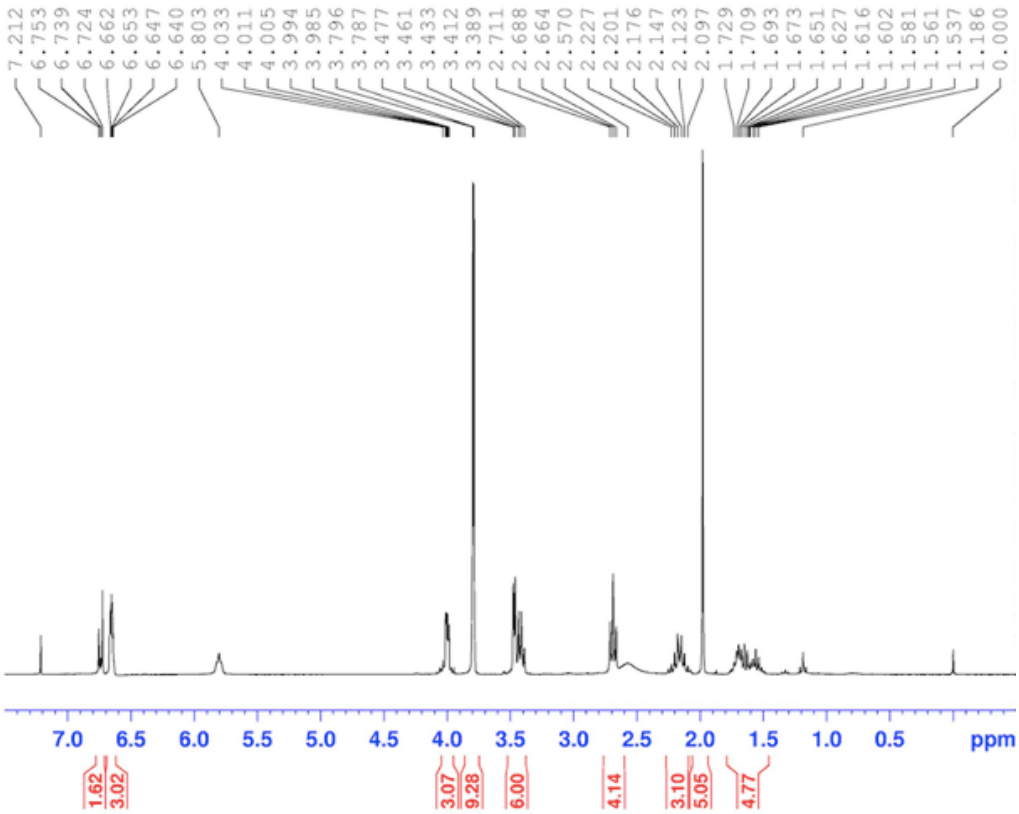

^{13}C NMR

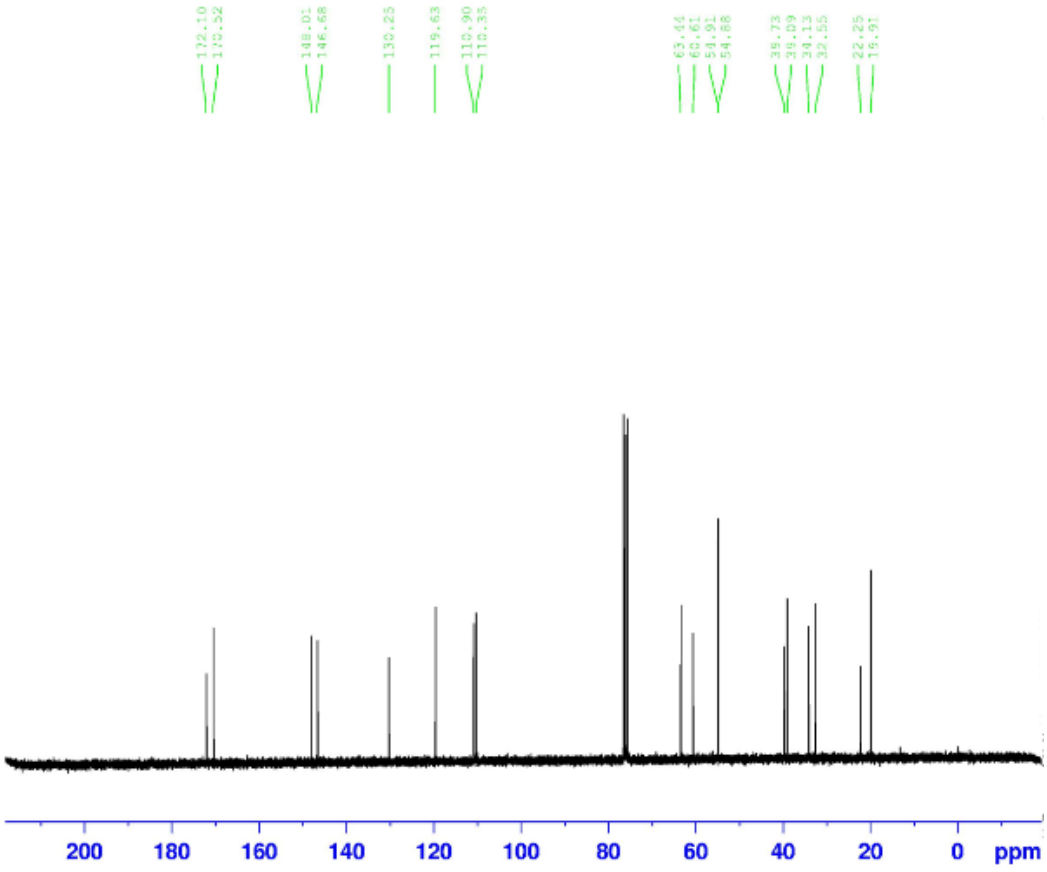
172.10
170.52
148.01
146.68
130.25
119.63
110.90
110.35
63.44
60.61
54.91
54.88
39.73
39.09
34.13
32.55
22.25
19.91
200
180
160
140
120
100
80
60
40
20
0
ppm

***N*-(3,4-dimethoxyphenethyl)-5-hydroxy-4-(hydroxymethyl)pentanamide 78**

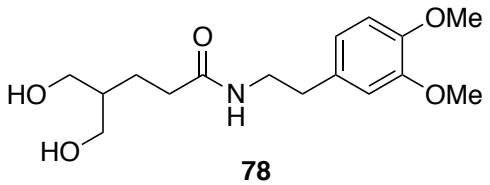

78

^{1}H NMR

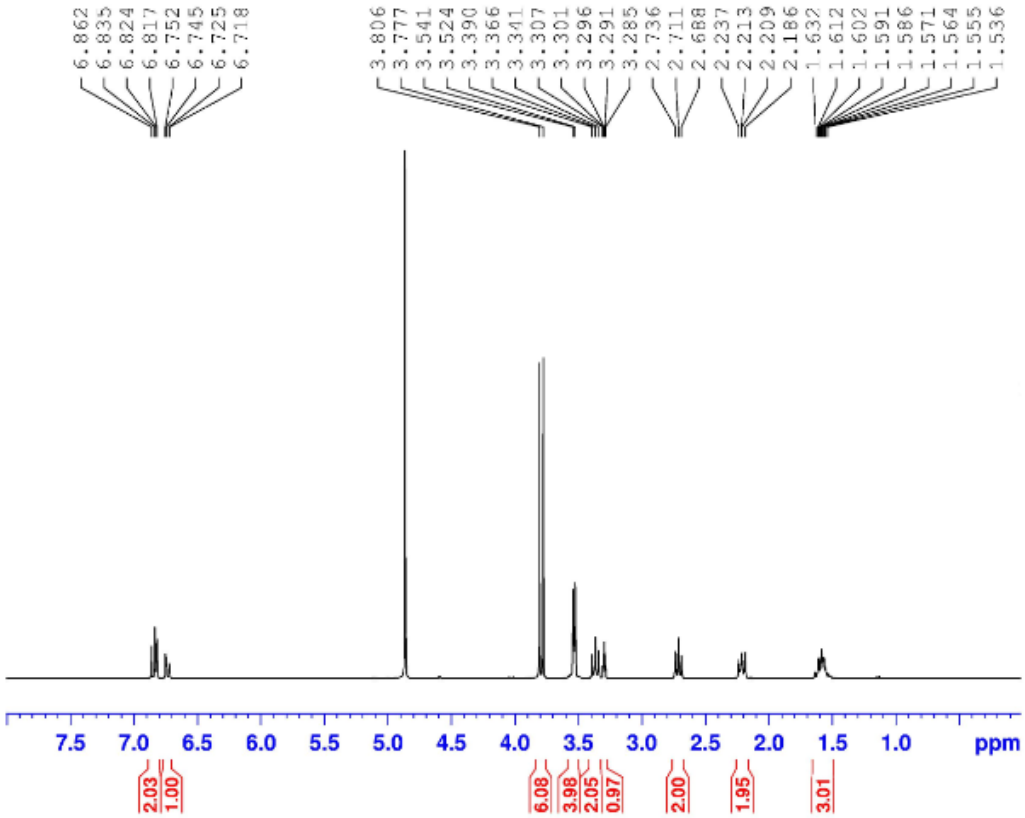

^{13}C NMR

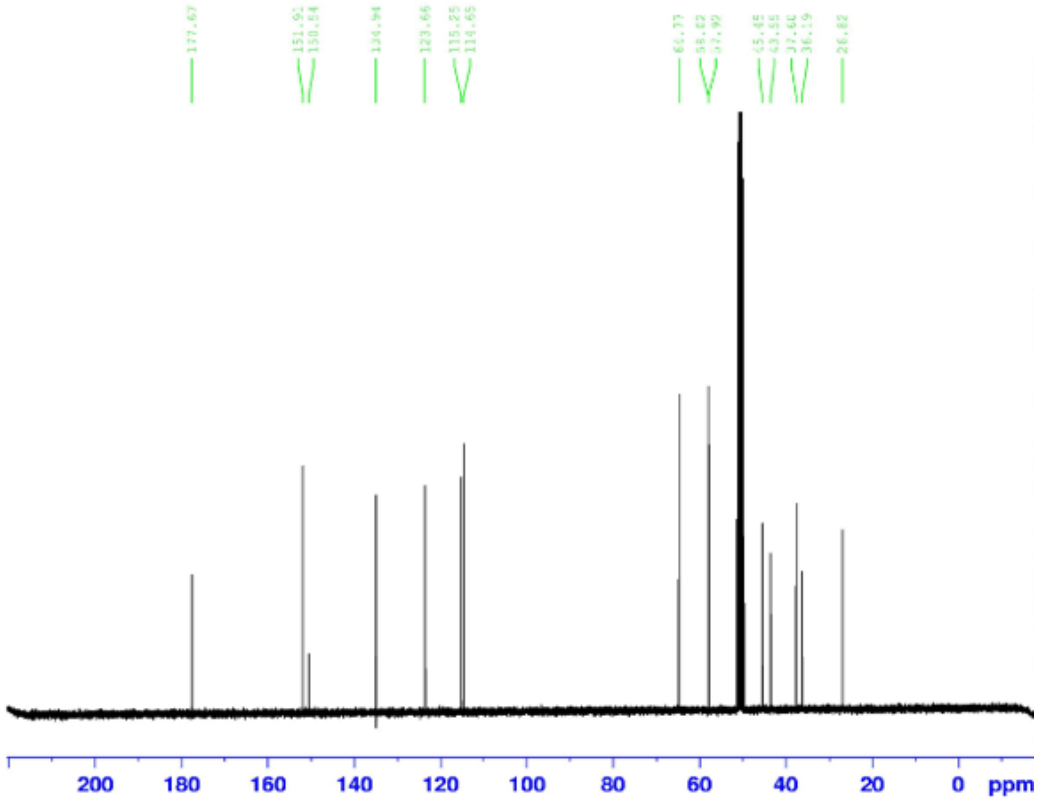
177.67
151.91
150.54
134.94
123.66
115.25
114.65
66.77
58.02
47.99
45.48
43.56
37.60
36.19
26.82
200
180
160
140
120
100
80
60
40
20
0
ppm

(+)-5-((3,4-dimethoxyphenethyl)amino)-2-(hydroxymethyl)-5-oxopentyl acetate 79

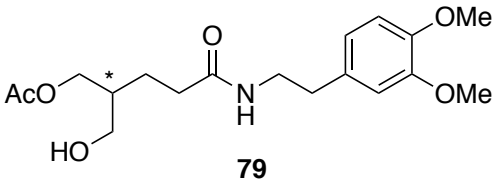

79

^{1}H NMR

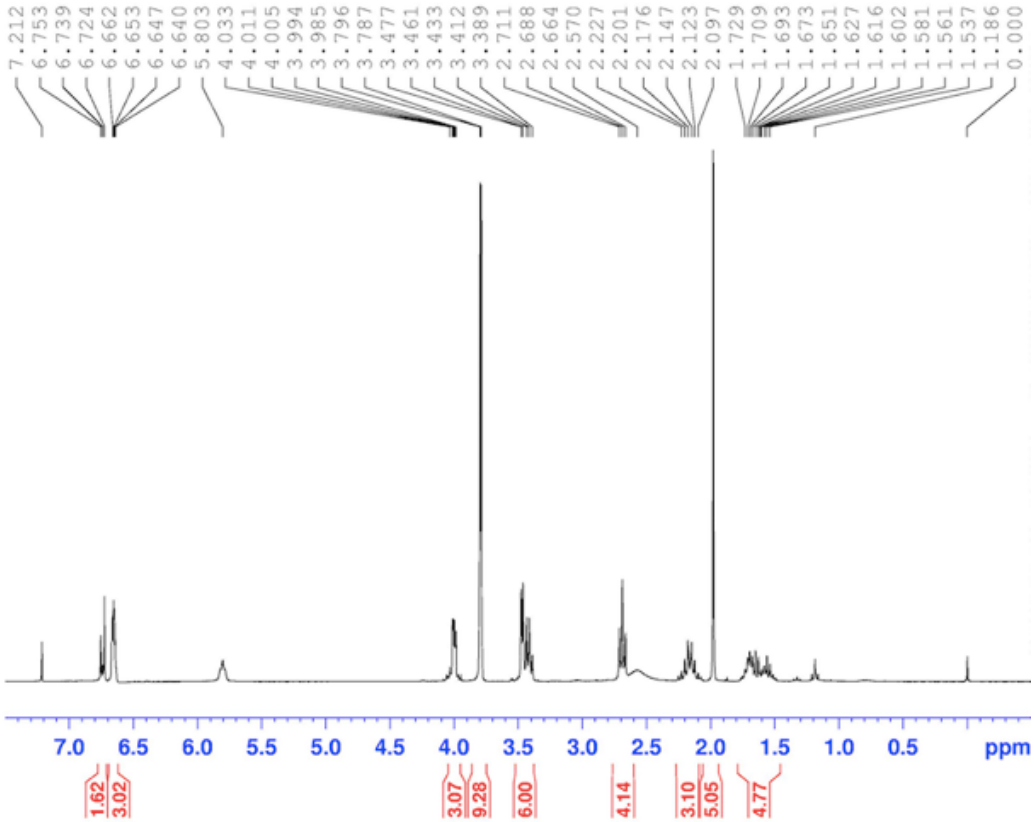

^{13}C NMR

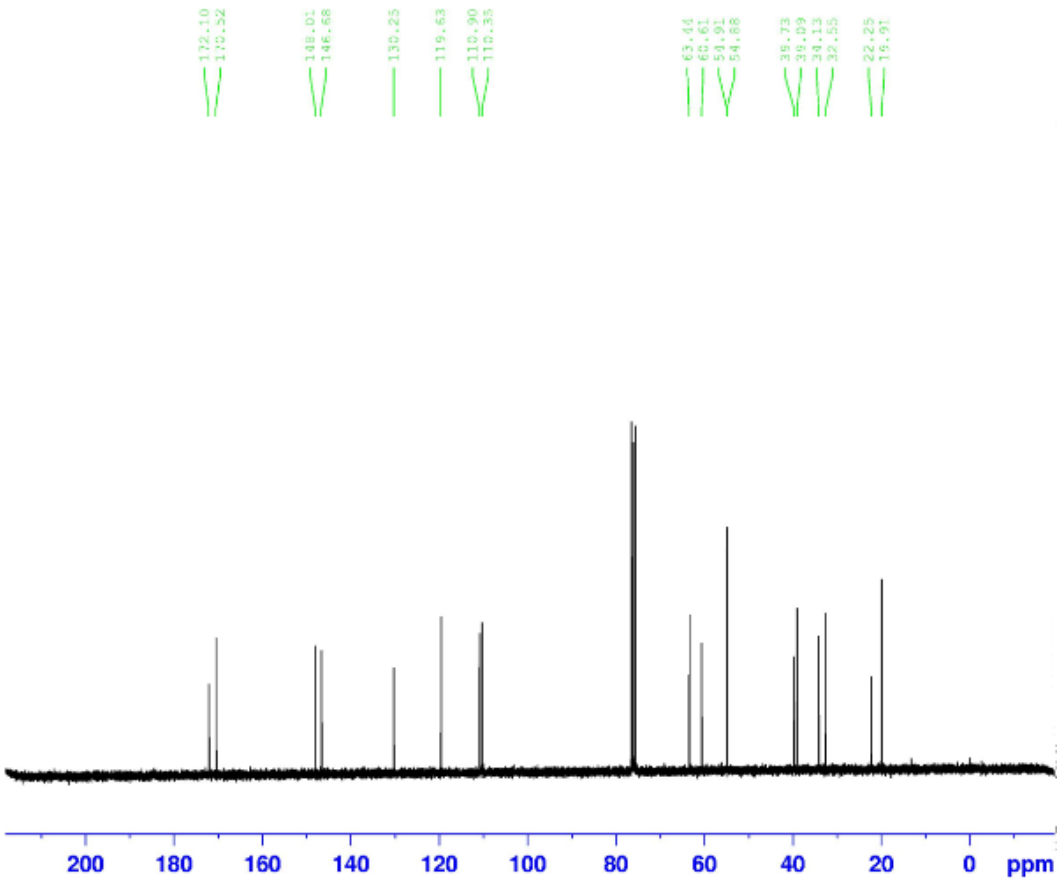
172.10
170.52
148.01
146.68
130.25
119.63
110.90
110.35
63.44
63.61
59.91
54.88
39.73
39.09
34.13
32.55
22.25
19.91
200
180
160
140
120
100
80
60
40
20
0
ppm

Preparation of 0.1 M Sodium phosphate buffer solutions

0.1 M sodium phosphate buffer solutions of various pH values were prepared using 1 M NaH_2PO_4 and 1 M Na_2HPO_4 solutions. To prepare 1 M sodium dihydrogen phosphate (NaH_2PO_4), 12 g of the salt was dissolved in 100 ml DI water. To prepare 1 M sodium hydrogen phosphate (Na_2HPO_4), 14.2 g of the salt was dissolved in 100 ml DI water.

Table 38: Volumes of 1 M NaH_2PO_4 and 1 M Na_2HPO_4 to be taken to obtain 0.1 M sodium phosphate buffer solution of corresponding pH

pH	Volume of 1 M NaH_2PO_4 solution (ml)	Volume of 1 M Na_2HPO_4 solution (ml)
6	4.4	0.6
6.5	3.42	1.58
7	2.12	2.88
7.5	0.8	4.2
8	0.34	4.66

1 M of NaH_2PO_4 and 1 M Na_2HPO_4 solutions were taken as per the volumes mentioned in Table 38, and dissolved in 45 ml of DI water to prepare 50 ml of 0.1 M sodium phosphate buffer of corresponding pH.

Bradford Standard Assay

The concentration of enzyme present in the buffer solution was determined by performing the Bradford assay for which the standard curves were plotted using bovine serum albumin (BSA) as a standard. Blank samples were run using 0.1 M sodium phosphate buffer solutions of the corresponding pH values. The assay reagent was obtained from Sigma Aldrich and was used as such without further

purification. The procedure was based on the work reported by Bradford. Standard solutions of one ml each were prepared using BSA as a standard at concentrations of 0 μg/ml, 250 μg/ml, 500 μg/ml, 1000 μg/ml, 1500 μg/ml and 2000 μg/ml. To one ml of Bradford assay reagent, 50 μl of the standard solution was added in a clean cuvette. The solution was left to incubate at room temperature for 15 min. Absorbance was noted at 595 nm using a UV-vis spectrophotometer with Bradford assay reagent (One ml) and 0.1 M sodium phosphate buffer of corresponding pH (50 μl) as blank and reference. Standard graphs were plotted with concentration of BSA on the x-axis and absorbance value at 595 nm on the y-axis. The analysis was done in triplicates and the average values are reported.

Bradford assay standard curves

Table 39: Absorbance values of BSA sample in pH 6 sodium phosphate buffer (0.1 M) using Bradford assay at 25 °C

Entry	Concentration of BSA (mg/ml)	Absorbance at 595 nm
1	0	0
2	0.25	0.2
3	0.5	0.402
4	1	0.769
5	1.4	0.972

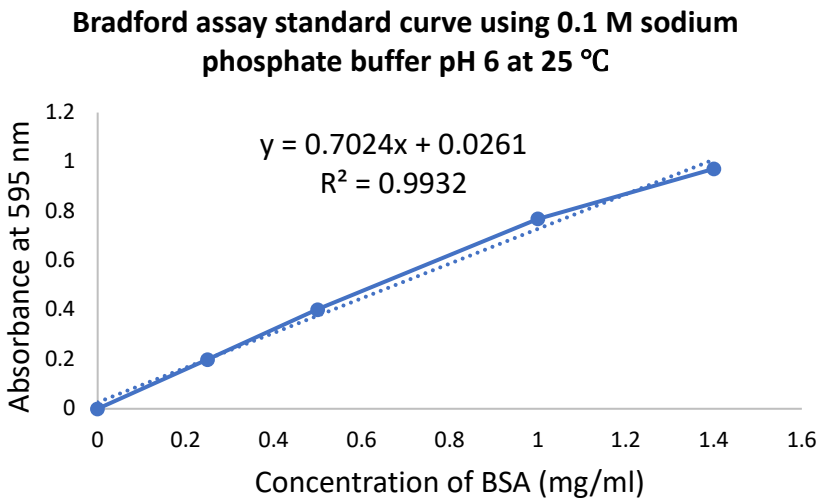

Figure 28: Bradford assay standard curve at 25 °C using 0.1 M sodium phosphate buffer pH 6

Table 40: Absorbance values of BSA sample in 0.1 M sodium phosphate buffer pH 6.5 using Bradford assay at 25 °C

Entry	Concentration of BSA (mg/ml)	Absorbance at 595 nm
1	0	0
2	0.25	0.191
3	0.5	0.368
4	1	0.762
5	1.4	0.985

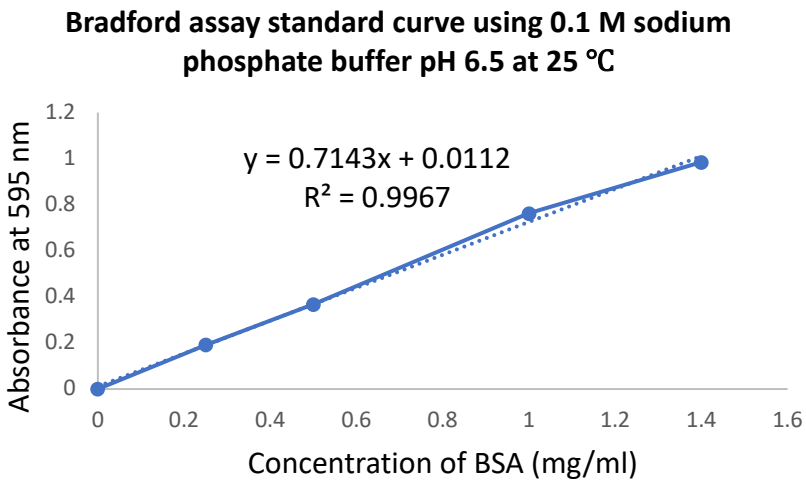

Figure 29: Bradford assay standard curve at 25 °C using 0.1 M sodium phosphate buffer pH 6.5

Table 41: Absorbance values of BSA sample in 0.1 M sodium phosphate buffer pH 7 using Bradford assay at 25 °C

Entry	Concentration of BSA (mg/ml)	Absorbance at 595 nm
1	0	0
2	0.25	0.191
3	0.5	0.377
4	1	0.769
5	1.4	0.996

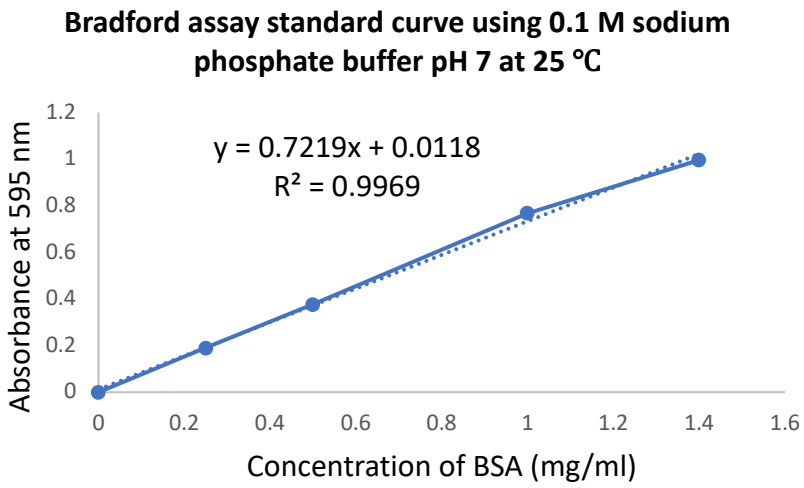

Figure 30: Bradford assay standard curve at 25 °C using 0.1 M sodium phosphate buffer pH 7

Table 42: Absorbance values of BSA sample in 0.1 M sodium phosphate buffer pH 7.5 at 25 °C

Entry	Concentration of BSA (mg/ml)	Absorbance at 595 nm
1	0	0
2	0.25	0.193
3	0.5	0.371
4	1	0.724
5	1.4	0.997

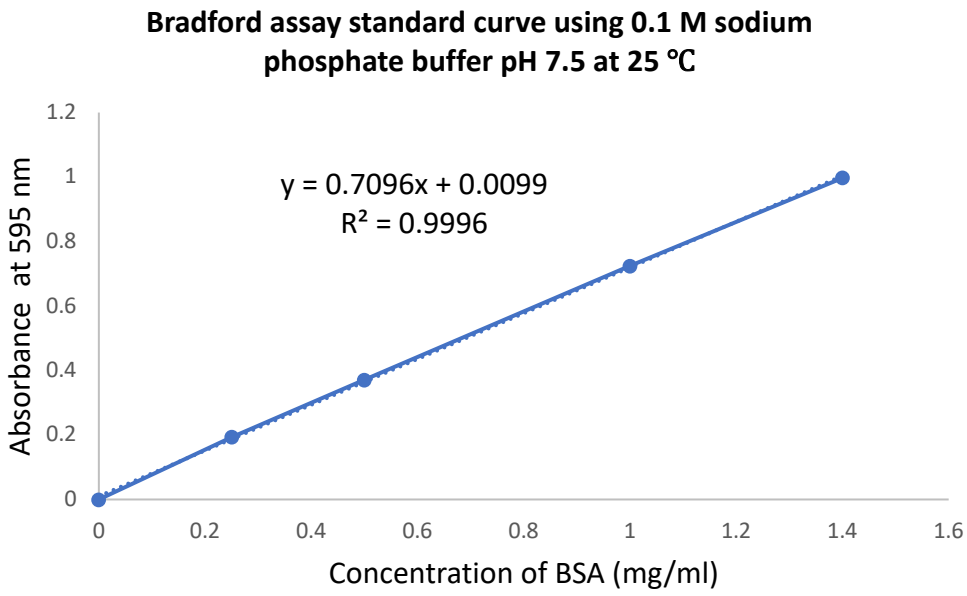

Figure 31: Bradford assay standard curve at 25 °C using 0.1 M sodium phosphate buffer pH 7.5

Table 43: Absorbance values of BSA sample in 0.1 M sodium phosphate buffer pH 8 using Bradford assay at 25 °C

Entry	Concentration of BSA (mg/ml)	Absorbance at 595 nm
1	0	0
2	0.25	0.169
3	0.5	0.331
4	1	0.651
5	1.4	0.783

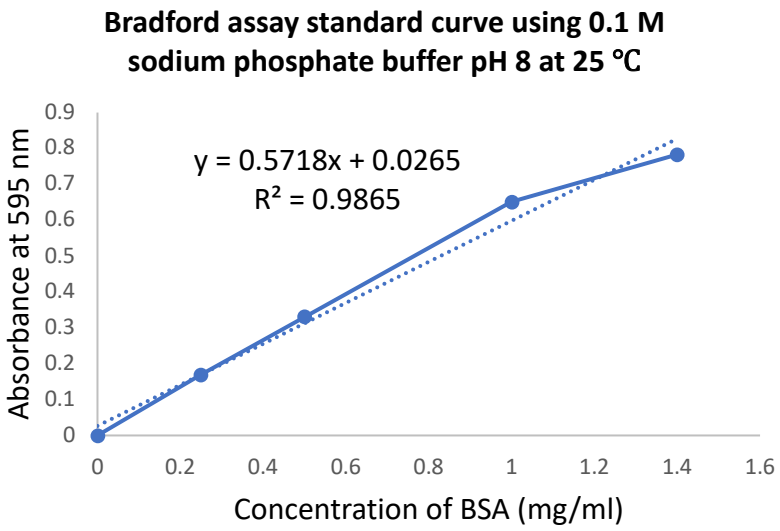

Figure 32: Bradford assay standard curve at 25 °C using 0.1 M sodium phosphate buffer pH 8

References

1. Tseng, S., et al., *Rediscovering thalidomide: a review of its mechanism of action, side effects, and potential uses.* Journal of the American Academy of Dermatology, 1996. **35**(6): p. 969-979.
2. Calcaterra, A. and I. D'Acquarica, *The market of chiral drugs: Chiral switches versus de novo enantiomerically pure compounds.* Journal of Pharmaceutical and Biomedical Analysis, 2018. **147**: p. 323-340.
3. Blaser, H.U., *The chiral pool as a source of enantioselective catalysts and auxiliaries.* Chemical reviews, 1992. **92**(5): p. 935-952.
4. Keith, J.M., J.F. Larrow, and E.N. Jacobsen, *Practical considerations in kinetic resolution reactions.* Advanced Synthesis & Catalysis, 2001. **343**(1): p. 5-26.
5. Porter, W.H., *Resolution of chiral drugs.* Pure and applied chemistry, 1991. **63**(8): p. 1119-1122.
6. Kitamura, M., et al., *Enantioselective addition of dialkylzincs to aldehydes promoted by chiral amino alcohols. Mechanism and nonlinear effect.* Journal of the American Chemical Society, 1989. **111**(11): p. 4028-4036.
7. Noyori, R., et al., *Stereoselective hydrogenation via dynamic kinetic resolution.* Journal of the American Chemical Society, 1989. **111**(25): p. 9134-9135.

8. Polshettiwar, V., et al., *Magnetically recoverable nanocatalysts.* Chemical reviews, 2011. **111**(5): p. 3036-3075.

9. Adlercreutz, P., *Immobilisation and application of lipases in organic media.* Chemical Society Reviews, 2013. **42**(15): p. 6406-6436.

10. García-Urdiales, E., I. Alfonso, and V. Gotor, *Enantioselective enzymatic desymmetrizations in organic synthesis.* Chemical reviews, 2005. **105**(1): p. 313-354.

11. Patel, R.N., *Enzymatic synthesis of chiral intermediates for drug development.* Advanced Synthesis & Catalysis, 2001. **343**(6-7): p. 527-546.

12. Sharma, S. and S.S. Kanwar, *Organic solvent tolerant lipases and applications.* The Scientific World Journal, 2014. **2014**.

13. Cherry, J.R. and A.L. Fidantsef, *Directed evolution of industrial enzymes: an update.* Current opinion in biotechnology, 2003. **14**(4): p. 438-443.

14. Schmid, R.D. and R. Verger, *Lipases: Interfacial Enzymes with Attractive Applications.* Angewandte Chemie International Edition, 1998. **37**(12): p. 1608-1633.

15. Stepankova, V., et al., *Strategies for stabilization of enzymes in organic solvents.* Acs Catalysis, 2013. **3**(12): p. 2823-2836.

16. Cantone, S., et al., *Efficient immobilisation of industrial biocatalysts: criteria and constraints for the selection of organic polymeric carriers and immobilisation methods.* Chemical Society Reviews, 2013. **42**(15): p. 6262-6276.

17. Azevedo, A.M., et al., *Stability of free and immobilised peroxidase in aqueous–organic solvents mixtures.* Journal of Molecular Catalysis B: Enzymatic, 2001. **15**(4-6): p. 147-153.

18. Villeneuve, P., et al., *Customizing lipases for biocatalysis: a survey of chemical, physical and molecular biological approaches.* Journal of molecular catalysis B: enzymatic, 2000. **9**(4-6): p. 113-148.

19. Palomo, J.M., et al., *Modulation of immobilized lipase enantioselectivity via chemical amination.* Advanced Synthesis & Catalysis, 2007. **349**(7): p. 1119-1127.

20. Brady, L., et al., *A serine protease triad forms the catalytic centre of a triacylglycerol lipase.* Nature, 1990. **343**(6260): p. 767.

21. Gupta, M.N., *Thermostability of enzymes*. 1993: Springer-Verlag.

22. Sheldon, R.A., *Enzyme immobilization: the quest for optimum performance.* Advanced Synthesis & Catalysis, 2007. **349**(8-9): p. 1289-1307.

23. Hartmeier, W., *Immobilized biocatalysts—from simple to complex systems.* Trends in biotechnology, 1985. **3**(6): p. 149-153.

24. Katchalski-Katzir, E., *Immobilized enzymes—learning from past successes and failures.* Trends in biotechnology, 1993. **11**(11): p. 471-478.

25. Mateo, C., et al., *Improvement of enzyme activity, stability and selectivity via immobilization techniques.* Enzyme and microbial technology, 2007. **40**(6): p. 1451-1463.

26. Clark, D.S., *Can immobilization be exploited to modify enzyme activity?* Trends in Biotechnology, 1994. **12**(11): p. 439-443.

27. Sheldon, R.A. and S. van Pelt, *Enzyme immobilisation in biocatalysis: why, what and how.* Chemical Society Reviews, 2013. **42**(15): p. 6223-6235.

28. Iyer, P.V. and L. Ananthanarayan, *Enzyme stability and stabilization—aqueous and non-aqueous environment.* Process biochemistry, 2008. **43**(10): p. 1019-1032.

29. Gottifredi, J.C. and E.E. Gonzo, *On the effectiveness factor calculation for a reaction–diffusion process in an immobilized biocatalyst pellet.* Biochemical engineering journal, 2005. **24**(3): p. 235-242.

30. Sengupta, S. and J.M. Modak, *Optimization of fed-batch bioreactor for immobilized enzyme processes.* Chemical engineering science, 2001. **56**(11): p. 3315-3325.

31. Kallenberg, A.I., F. van Rantwijk, and R.A. Sheldon, *Immobilization of penicillin G acylase: the key to optimum performance.* Advanced Synthesis & Catalysis, 2005. **347**(7-8): p. 905-926.

32. Wegman, M.A., et al., *Towards biocatalytic synthesis of β-lactam antibiotics.* Advanced Synthesis & Catalysis, 2001. **343**(6-7): p. 559-576.

33. Katchalski-Katzir, E. and D.M. Kraemer, *Eupergit® C, a carrier for immobilization of enzymes of industrial potential.* Journal of molecular catalysis B: enzymatic, 2000. **10**(1-3): p. 157-176.

34. Kirk, O. and M.W. Christensen, *Lipases from Candida a ntarctica: Unique Biocatalysts from a Unique Origin.* Organic Process Research & Development, 2002. **6**(4): p. 446-451.

35. Chibata, I. and T. Tosa, *T. Shibatani. 1992. The industrial production of optically active compounds by immobilized biocatalysts.* Chirality in industry: p. 351-370.

36. Tosa, T., et al., *Studies on continuous enzyme reactions. II. Preparation of DEAE-cellulose-aminoacylase column and continuous optical resolution of acetyl-DL-methionine.* Enzymologia, 1966. **31**(4): p. 225-238.

37. Krajewska, B., *Application of chitin-and chitosan-based materials for enzyme immobilizations: a review.* Enzyme and microbial technology, 2004. **35**(2-3): p. 126-139.

38. Lozinsky, V.I., et al., *Polymeric cryogels as promising materials of biotechnological interest.* TRENDS in Biotechnology, 2003. **21**(10): p. 445-451.

39. Bruns, N. and J.C. Tiller, *Amphiphilic network as nanoreactor for enzymes in organic solvents.* Nano letters, 2005. **5**(1): p. 45-48.

40. Diaz, J.F. and K.J. Balkus Jr, *Enzyme immobilization in MCM-41 molecular sieve.* Journal of Molecular Catalysis B: Enzymatic, 1996. **2**(2-3): p. 115-126.

41. Yan, A.-X., X.-W. Li, and Y.-H. Ye, *Recent progress on immobilization of enzymes on molecular sieves for reactions in organic solvents.* Applied biochemistry and biotechnology, 2002. **101**(2): p. 113-129.

42. Moelans, D., et al., *Using mesoporous silica materials to immobilise biocatalysis-enzymes.* Catalysis Communications, 2005. **6**(4): p. 307-311.

43. Takahashi, H., et al., *Immobilized enzymes in ordered mesoporous silica materials and improvement of their stability and catalytic activity in an organic solvent.* Microporous and Mesoporous Materials, 2001. **44**: p. 755-762.

44. Wang, P., et al., *Enzyme stabilization by covalent binding in nanoporous sol-gel glass for nonaqueous biocatalysis.* Biotechnology and Bioengineering, 2001. **74**(3): p. 249-255.

45. Petri, A., P. Marconcini, and P. Salvadori, *Efficient immobilization of epoxide hydrolase onto silica gel and use in the enantioselective hydrolysis of racemic para-nitrostyrene oxide.* Journal of Molecular Catalysis B: Enzymatic, 2005. **32**(5-6): p. 219-224.

46. Ivanov, A.E., et al., *Conjugation of Penicillin Acylase with the Reactive Copolymer of N-Isopropylacrylamide: A Step Toward a Thermosensitive Industrial Biocatalyst.* Biotechnology progress, 2003. **19**(4): p. 1167-1175.

47. Kim, K., O. Lee, and E. Lee, *Nano-immobilized biocatalysts for biodiesel production from renewable and sustainable resources.* Catalysts, 2018. **8**(2): p. 68.

48. Bezbradica, D., et al., *Enzymatic syntheses of esters-green chemistry for valuable food, fuel and fine chemicals.* Current Organic Chemistry, 2017. **21**(2): p. 104-138.

49. Palomo, J.M., *Modulation of enzymes selectivity via immobilization.* Current Organic Synthesis, 2009. **6**(1): p. 1-14.

50. Nelson, J. and E.G. Griffin, *ADSORPTION OF INVERTASE.* Journal of the American Chemical Society, 1916. **38**(5): p. 1109-1115.

51. Schulze, B. and M.G. Wubbolts, *Biocatalysis for industrial production of fine chemicals.* Current Opinion in Biotechnology, 1999. **10**(6): p. 609-615.

52. Lu, X., et al., *Catalytic Synthesis of Functional Silicon-Stereogenic Silanes through Candida antarctica Lipase B Catalyzed Remote Desymmetrization of Silicon-Centered Diols.* European Journal of Organic Chemistry, 2013. **2013**(26): p. 5814-5819.

53. Tsuji, T., et al., *Enzymatic desymmetrization of 2-amino-2-methyl-1, 3-propanediol: asymmetric synthesis of (S)-N-Boc-N, O-isopropylidene-α-methylserinal and (4R)-methyl-4-[2-(thiophen-2-yl) ethyl] oxazolidin-2-one.* Tetrahedron: Asymmetry, 2005. **16**(19): p. 3139-3142.

54. Lin, C., et al., *Comparison of the chiral recognition of prochiral substrates in the acetylation reaction by a novel lipase (CSL) from the yeast, Cryptococcus spp. S-2 with immobilized PPL: Enzyme-catalyzed desymmetrization and asymmetrization of prochiral 2-substituted 1, 3-*

propanediols by CSL and immobilized PPL. Journal of Molecular Catalysis B: Enzymatic, 2006. **38**(1): p. 1-10.

55. Busto, E., et al., *First desymmetrization of 1, 3-propanediamine derivatives in organic solvent. Development of a new route for the preparation of optically active Amines.* Organic letters, 2007. **9**(21): p. 4203-4206.

56. Patel, R.N., et al., *Preparation of a chiral synthon for an HBV inhibitor: enzymatic asymmetric hydrolysis of (1α, 2β, 3α)-2-(benzyloxymethyl) cyclopent-4-ene-1, 3-diol diacetate and enzymatic asymmetric acetylation of (1α, 2β, 3α)-2-(benzyloxymethyl) cyclopent-4-ene-1, 3-diol.* Tetrahedron: Asymmetry, 2006. **17**(2): p. 175-178.

57. Ozyilmaz, E., et al., *Improving catalytic hydrolysis reaction efficiency of sol–gel-encapsulated Candida rugosa lipase with magnetic β-cyclodextrin nanoparticles.* Colloids and Surfaces B: Biointerfaces, 2014. **113**: p. 182-189.

58. Sing, B., *Biotechnology Expanding Horizon*. 2007, Kalyani publishers, Ludhiana, India.

59. Britton, J. and T.F. Jamison, *The assembly and use of continuous flow systems for chemical synthesis.* nature protocols, 2017. **12**(11): p. 2423.

60. de la Hoz, A. and A. Díaz-Ortiz, *Nonconventional techniques in sustainable flow chemistry.* Sustainable Flow Chemistry: Methods and Applications, 2017.

61. Malet-Sanz, L. and F. Susanne, *Continuous flow synthesis. A pharma perspective.* Journal of medicinal chemistry, 2012. **55**(9): p. 4062-4098.

62. Porta, R., M. Benaglia, and A. Puglisi, *Flow chemistry: recent developments in the synthesis of pharmaceutical products.* Organic Process Research & Development, 2015. **20**(1): p. 2-25.

63. Watts, P., *The Application of Flow Chemistry in the Use of Highly Reactive Intermediates and Reagents.* Sustainable Flow Chemistry: Methods and Applications, 2017.

64. Liu, Z., et al., *Combined biosynthetic pathway for de novo production of UDP-galactose: catalysis with multiple enzymes immobilized on agarose beads.* ChemBioChem, 2002. **3**(4): p. 348-355.

65. Chen, P., et al., *A practical high through-put continuous process for the synthesis of chiral cyanohydrins.* The Journal of organic chemistry, 2002. **67**(23): p. 8251-8253.

66. Zhang, P., M.G. Russell, and T.F. Jamison, *Continuous flow total synthesis of rufinamide.* Organic Process Research & Development, 2014. **18**(11): p. 1567-1570.

67. Hartwig, J., et al., *Heating under High-Frequency Inductive Conditions: Application to the Continuous Synthesis of the Neurolepticum Olanzapine (Zyprexa).* Angewandte Chemie International Edition, 2013. **52**(37): p. 9813-9817.

68. Ing, H.R., *420. Cytisine. Part II.* Journal of the Chemical Society (Resumed), 1932: p. 2778-2780.

69. Partheil, A., *Über cytisin und ulexin.* Archiv der Pharmazie, 1894. **232**(3): p. 161-177.

70. Luetje, C.W. and J. Patrick, *Both alpha-and beta-subunits contribute to the agonist sensitivity of neuronal nicotinic acetylcholine receptors.* Journal of Neuroscience, 1991. **11**(3): p. 837-845.

71. Papke, R.L. and S.F. Heinemann, *Partial agonist properties of cytisine on neuronal nicotinic receptors containing the beta 2 subunit.* Molecular pharmacology, 1994. **45**(1): p. 142-149.

72. Giacobini, E., *Cholinergic receptors in human brain: effects of aging and Alzheimer disease.* Journal of neuroscience research, 1990. **27**(4): p. 548-560.

73. Wevers, A. and H. Schröder, *Nicotinic acetylcholine receptors in Alzheimer's disease.* Journal of Alzheimer's Disease, 1999. **1**(4-5): p. 207-219.

74. Martin-Ruiz, C., et al., *Nicotinic receptor abnormalities in Alzheimer's disease.* Biological psychiatry, 2001. **49**(3): p. 175-184.

75. Kawamata, J. and S. Shimohama, *Stimulating nicotinic receptors trigger multiple pathways attenuating cytotoxicity in models of Alzheimer's and Parkinson's diseases.* Journal of Alzheimer's disease, 2011. **24**(supplement2): p. 95-109.

76. Moser, P.C., et al., *The pharmacology of latent inhibition as an animal model of schizophrenia.* Brain Research Reviews, 2000. **33**(2-3): p. 275-307.

77. Ripoll, N., M. Bronnec, and M. Bourin, *Nicotinic receptors and schizophrenia.* Current medical research and opinion, 2004. **20**(7): p. 1057-1074.

78. Decker, M.W., L.E. Rueter, and R.S. Bitner, *Nicotinic acetylcholine receptor agonists: a potential new class of analgesics.* Current topics in medicinal chemistry, 2004. **4**(3): p. 369-384.

79. Rouden, J., et al., *(−)-Cytisine and derivatives: synthesis, reactivity, and applications.* Chemical reviews, 2013. **114**(1): p. 712-778.

80. Coe, J.W., *Total synthesis of (±)-Cytisine via the intramolecular Heck cyclization of activated N-alkyl glutarimides.* Organic letters, 2000. **2**(26): p. 4205-4208.

81. Govindachari, T., et al., *763. Synthesis of (±)-cytisine.* Journal of the Chemical Society (Resumed), 1957: p. 3839-3844.

82. Danieli, B., et al., *Total enantioselective synthesis of (−)-cytisine.* Organic letters, 2004. **6**(4): p. 493-496.

83. Honda, T., R. Takahashi, and H. Namiki, *Syntheses of (+)-cytisine,(−)-kuraramine,(−)-isokuraramine, and (−)-jussiaeiine A.* The Journal of organic chemistry, 2005. **70**(2): p. 499-504.

84. van Tamelen, E.E. and J.S. Baran, *The synthesis of dl-cytisine.* Journal of the American Chemical Society, 1955. **77**(18): p. 4944-4945.

85. van Tamelen, E.E. and J.S. Baran, *Total Synthesis of Oxygenated Lupin Alkaloids1.* Journal of the American Chemical Society, 1958. **80**(17): p. 4659-4670.

86. Gray, D. and T. Gallagher, *A Flexible Strategy for the Synthesis of Tri-and Tetracyclic Lupin Alkaloids: Synthesis of (+)-Cytisine,(±)-Anagyrine, and (±)-Thermopsine.* Angewandte Chemie International Edition, 2006. **45**(15): p. 2419-2423.

87. Botuha, C., C.M. Galley, and T. Gallagher, *A short synthesis of (±)-cytisine.* Organic & biomolecular chemistry, 2004. **2**(13): p. 1825-1826.

88. Pasikanti, S., et al., *An efficient synthesis of varenicline.* Tetrahedron Letters, 2010. **51**(1): p. 151-152.

89. Hirschhäuser, C., C.A. Haseler, and T. Gallagher, *Core Modification of Cytisine: A Modular Synthesis.* Angewandte Chemie, 2011. **123**(22): p. 5268-5271.

90. Takasu, K., et al., *Convenient synthesis of substituted piperidinones from α, β-unsaturated amides: formal synthesis of deplancheine, tacamonine, and paroxetine.* The Journal of organic chemistry, 2005. **70**(10): p. 3957-3962.

91. Kano, T., et al., *The first example of the direct asymmetric conjugate addition of aldehydes to a methylenemalonate promoted by an axially chiral amino diol catalyst.* Chemical Science, 2011. **2**(12): p. 2311-2313.

92. Samarat, A., et al., *An efficient synthetic route to functionalized δ-lactams.* Tetrahedron, 2008. **64**(40): p. 9540-9543.

93. Lerchner, A. and E.M. Carreira, *Synthesis of (±)-Strychnofoline via a Highly Convergent Selective Annulation Reaction.* Chemistry–A European Journal, 2006. **12**(32): p. 8208-8219.

94. Felluga, F., et al., *A chemoenzymatic approach to the synthesis of enantiomerically pure aza analogues of paraconic acid methyl ester and both enantiomers of methyl β-proline.* Tetrahedron: Asymmetry, 2001. **12**(23): p. 3241-3249.

95. Kim, M.-h., et al., *Synthesis of (−)-paroxetine via enantioselective phase-transfer catalytic monoalkylation of malonamide ester.* Organic letters, 2010. **12**(12): p. 2826-2829.

96. Kim, M.-h., et al., *The highly enantioselective phase-transfer catalytic mono-alkylation of malonamic esters.* Chemical Communications, 2009(7): p. 782-784.

97. Khong, D.T., et al., *Chemoenzymatic Synthesis of Chiral 1-Benzyl-5-(hydroxymethyl)-2-piperidone Enabled by Lipase AK-Mediated Desymmetrization of Prochiral 1, 3-Diol and Its Diacetate.* European Journal of Organic Chemistry, 2016. **2016**(18): p. 3084-3089.

98. Kojima, Y., M. Yokoe, and T. Mase, *Purification and characterization of an alkaline lipase from Pseudomonas fluorescens AK102.* Bioscience, biotechnology, and biochemistry, 1994. **58**(9): p. 1564-1568.

99. Atodiresei, I., C. Vila, and M. Rueping, *Asymmetric organocatalysis in continuous flow: opportunities for impacting industrial catalysis.* ACS Catalysis, 2015. **5**(3): p. 1972-1985.

100. Khan, S.A., et al., *Microfluidic synthesis of colloidal silica.* Langmuir, 2004. **20**(20): p. 8604-8611.

101. Exchangers, M., *Microreactors: New technology for modern chemistry*. 2000, Weinheim: Wiley/VCH. Google Scholar.

102. Szekely, L. and A. Guttman, *New advances in microchip fabrication for electrochromatography.* Electrophoresis, 2005. **26**(24): p. 4590-4604.

103. Ziaie, B., et al., *Hard and soft micromachining for BioMEMS: review of techniques and examples of applications in microfluidics and drug delivery.* Advanced drug delivery reviews, 2004. **56**(2): p. 145-172.

104. Fisher, K., et al., *Electro-enzymatic viologen-mediated substrate reduction using pentaerythritol tetranitrate reductase and a parallel, segmented fluid flow system.* Catalysis Science & Technology, 2013. **3**(6): p. 1505-1511.

105. Zaks, A. and A.M. Klibanov, *Enzyme-catalyzed processes in organic solvents.* Proceedings of the National Academy of Sciences, 1985. **82**(10): p. 3192-3196.

106. Ma, M., et al., *Preparation and characterization of magnetite nanoparticles coated by amino silane.* Colloids and Surfaces A: Physicochemical and Engineering Aspects, 2003. **212**(2): p. 219-226.

107. Das, S.K., et al., *Highly stable porous covalent triazine–piperazine linked nanoflower as a feasible adsorbent for flue gas CO2 capture.* Chemical Engineering Science, 2016. **145**: p. 21-30.

108. Polshettiwar, V., et al., *High-Surface-Area Silica Nanospheres (KCC-1) with a Fibrous Morphology.* Angewandte Chemie International Edition, 2010. **49**(50): p. 9652-9656.

109. Garcia-Galan, C., et al., *Potential of different enzyme immobilization strategies to improve enzyme performance.* Advanced Synthesis & Catalysis, 2011. **353**(16): p. 2885-2904.

110. Bassi, J.J., et al., *Interfacial activation of lipases on hydrophobic support and application in the synthesis of a lubricant ester.* International journal of biological macromolecules, 2016. **92**: p. 900-909.

111. Popat, A., et al., *Mesoporous silica nanoparticles for bioadsorption, enzyme immobilisation, and delivery carriers.* Nanoscale, 2011. **3**(7): p. 2801-2818.

112. Bayne, L., R.V. Ulijn, and P.J. Halling, *Effect of pore size on the performance of immobilised enzymes.* Chemical Society Reviews, 2013. **42**(23): p. 9000-9010.

113. Barbosa, O., et al., *Glutaraldehyde in bio-catalysts design: a useful crosslinker and a versatile tool in enzyme immobilization.* Rsc Advances, 2014. **4**(4): p. 1583-1600.

114. Baig, R.N., M.N. Nadagouda, and R.S. Varma, *Magnetically retrievable catalysts for asymmetric synthesis.* Coordination Chemistry Reviews, 2015. **287**: p. 137-156.

115. Kruger, N.J., *The Bradford method for protein quantitation*, in *The protein protocols handbook*. 2002, Springer. p. 15-21.

116. Winkler, U.K. and M. Stuckmann, *Glycogen, hyaluronate, and some other polysaccharides greatly enhance the formation of exolipase by Serratia marcescens.* Journal of bacteriology, 1979. **138**(3): p. 663-670.

117. Yamaura, M., et al., *Preparation and characterization of (3-aminopropyl) triethoxysilane-coated magnetite nanoparticles.* Journal of Magnetism and Magnetic Materials, 2004. **279**(2-3): p. 210-217.

118. Maity, D., et al. *Synthesis and studies of APTES functionalized magnetite nanoparticles*. in *Nanoscience and Nanotechnology (ICONN), 2010 International Conference on*. 2010. IEEE.

119. Todaka, Y., et al., *Synthesis of ferrite nanoparticles by mechanochemical processing using a ball mill.* Materials Transactions, 2003. **44**(2): p. 277-284.

120. Puthiaraj, P., et al., *Microporous covalent triazine polymers: efficient Friedel–Crafts synthesis and adsorption/storage of CO 2 and CH 4.* Journal of Materials Chemistry A, 2015. **3**(13): p. 6792-6797.

121. Zhao, H., et al., *Targeted synthesis of a 2D ordered porous organic framework for drug release.* Chemical Communications, 2011. **47**(22): p. 6389-6391.

122. Gunasekaran, S. and B. Anita, *Spectral investigation and normal coordinate analysis of piperazine.* 2008.

123. Secundo, F., *Conformational changes of enzymes upon immobilisation.* Chemical Society Reviews, 2013. **42**(15): p. 6250-6261.

124. Silva, G.S., et al., *Chitosan/siloxane hybrid polymer: synthesis, characterization and performance as a support for immobilizing enzyme.* Journal of the Brazilian Chemical Society, 2011. **22**(8): p. 1407-1417.

125. Zhang, R., et al., *Ordered Macro-/Mesoporous Anatase Films with High Thermal Stability and Crystallinity for Photoelectrocatalytic Water-Splitting.* Advanced Energy Materials, 2014. **4**(8): p. 1301725.

126. Dacquin, J.-P., et al., *An efficient route to highly organized, tunable macroporous− mesoporous alumina.* Journal of the American Chemical Society, 2009. **131**(36): p. 12896-12897.

127. He, J., et al., *Effect of surface hydrophobicity/hydrophilicity of mesoporous supports on the activity of immobilized lipase.* Journal of colloid and interface science, 2006. **298**(2): p. 780-786.

128. Dwivedee, B.P., et al., *Development of nanobiocatalysts through the immobilization of Pseudomonas fluorescens lipase for applications in efficient kinetic resolution of racemic compounds.* Bioresource technology, 2017. **239**: p. 464-471.

129. Lima, L.N., et al., *Immobilization of Pseudomonas fluorescens lipase on hydrophobic supports and application in biodiesel synthesis by transesterification of vegetable oils in solvent-free systems.* Journal of industrial microbiology & biotechnology, 2015. **42**(4): p. 523-535.

130. Salis, A., et al., *Role of the support surface on the loading and the activity of Pseudomonas fluorescens lipase used for biodiesel synthesis.* Journal of Molecular Catalysis B: Enzymatic, 2009. **57**(1-4): p. 262-269.

131. Santos, J., et al., *Pseudomonas fluorescens lipase immobilization on polysiloxane–polyvinyl alcohol composite chemically modified with*

epichlorohydrin. Journal of Molecular Catalysis B: Enzymatic, 2008. **52**: p. 49-57.

132. Dors, G., et al., *Transesterification of palm oil catalyzed by Pseudomonas fluorescens lipase in a packed-bed reactor.* Energy & Fuels, 2012. **26**(9): p. 5977-5982.

133. Xun, E.-n., et al., *Immobilization of Pseudomonas fluorescens lipase onto magnetic nanoparticles for resolution of 2-octanol.* Applied biochemistry and biotechnology, 2012. **168**(3): p. 697-707.

134. Ratledge, C. and B. Kristiansen, *Basic biotechnology*. 2006: Cambridge University Press.

135. Balevicius, Z., et al., *Crowding enhances lipase turnover rate on surface-immobilized substrates.* Colloids and Surfaces B: Biointerfaces, 2015. **131**: p. 115-121.

136. Arroyo, M., J. Moreno, and J. Sinisterra, *Alteration of the activity and selectivity of immobilized lipases by the effect of the amount of water in the organic medium.* Journal of Molecular Catalysis A: Chemical, 1995. **97**(3): p. 195-201.

137. Takabe, K., et al., *Reverse enantioselectivity in the lipase-catalyzed desymmetrization of prochiral 2-carbamoylmethyl-1, 3-propanediol derivatives.* Tetrahedron: Asymmetry, 2000. **11**(24): p. 4825-4829.

138. Ausseil, F., H. Biaudet, and P. Masson, *Hydrolase activity of Pseudomonas fluorescens lipase in organic media*, in *Progress in Biotechnology*. 1992, Elsevier. p. 593-600.

139. Umpierre, A.P., E. de Jesus, and J. Dupont, *Turnover numbers and soluble metal nanoparticles.* ChemCatChem, 2011. **3**(9): p. 1413-1418.

140. Jiménez-González, C., et al., *Key green engineering research areas for sustainable manufacturing: a perspective from pharmaceutical and fine chemicals manufacturers.* Organic Process Research & Development, 2011. **15**(4): p. 900-911.

141. Noël, T., et al., *Palladium-catalyzed amination reactions in flow: overcoming the challenges of clogging via acoustic irradiation.* Chemical Science, 2011. **2**(2): p. 287-290.

142. Allum, K., et al., *Supported transition metal complexes: V. Liquid phase catalytic hydrogenation of hexene-1, cyclohexene and isoprene under continuous flow conditions.* Journal of Catalysis, 1976. **43**(1-3): p. 331-338.

143. Tundo, P., G. Moraglio, and F. Trotta, *Gas-liquid phase-transfer catalysis: a new continuous-flow method in organic synthesis.* Industrial & engineering chemistry research, 1989. **28**(7): p. 881-890.

144. Mascia, S., et al., *End-to-end continuous manufacturing of pharmaceuticals: integrated synthesis, purification, and final dosage formation.* Angewandte Chemie, 2013. **125**(47): p. 12585-12589.

145. Baxendale, I.R., et al., *A flow process for the multi-step synthesis of the alkaloid natural product oxomaritidine: a new paradigm for molecular assembly.* Chemical Communications, 2006(24): p. 2566-2568.

146. Watari, R., et al., *Distinct Promotive Effects of 1, 8-Diazabicyclo [5.4. 0] undec-7-ene (DBU) on Polymer Supports in Copper-Catalyzed Hydrogenation of C= O Bonds.* ChemCatChem, 2017. **9**(24): p. 4501-4507.

147. Jaman, Z., et al., *Rapid On-Demand Synthesis of Lomustine under Continuous Flow Conditions.* Organic Process Research & Development, 2019.

148. Mori, K. and K. Yamane, *Synthesis of optically active forms of a-factor the inducer of streptomycin biosynthesis in inactive mutants of streptomyces griseus.* Tetrahedron, 1982. **38**(19): p. 2919-2921.